NOISE REDUCTION FOR VENTILATION SYSTEMS WITH HEAT EXCHANGERS

Mohammad Kojourimanesh

Graduation committee members:

Chairman and Director of PDEng program
Prof.dr.ir. G. Brem, University of Twente

Supervisors
Prof.dr.ir. A. de Boer, University of Twente
Dr.ir. A.P. Berkhoff, University of Twente

Members
Prof.dr.ir. G. Brem, University of Twente
Prof.dr.ir. A. de Boer, University of Twente
Dr.ir. A.P. Berkhoff, University of Twente
Dr.ir. Y.H. Wijnant, University of Twente
Ir. I. Cleine, Development Engineer R&D at Brink Climate Systems

NOISE REDUCTION FOR VENTILATION SYSTEMS WITH HEAT EXCHANGERS

PDEng Thesis

to obtain the degree of

Professional Doctorate in Engineering (PDEng) at the University of Twente,

on the authority of the rector magnificus,

Prof.dr. T.T.M. Palstra,

on account of the decision of the graduation committee,

to be defended

on Monday the 14th of May 2018 at 13:30 hours

by

Mohammad Kojourimanesh

born in 1985

in Shiraz, Islamic Republic of Iran

This PDEng Thesis has been approved by:

Thesis Supervisor:

                Prof.dr.ir. A. de Boer

Co-supervisor(s):

                Dr.ir. A.P. Berkhoff

Contents

f

Chapter 1

1. Introduction

1.1 Problem Statement

The significance of ventilation systems in today's modern world is evident. In some cold areas, these systems are used without cooling cycles with the main function to send fresh air inside the house. But for a lower energy consumption in winter, heat recovery technologies are applied to preheat the fresh air with exhausted air before being supplied to the residential space. An overview of the ventilation system is presented in Fig. 1.1.
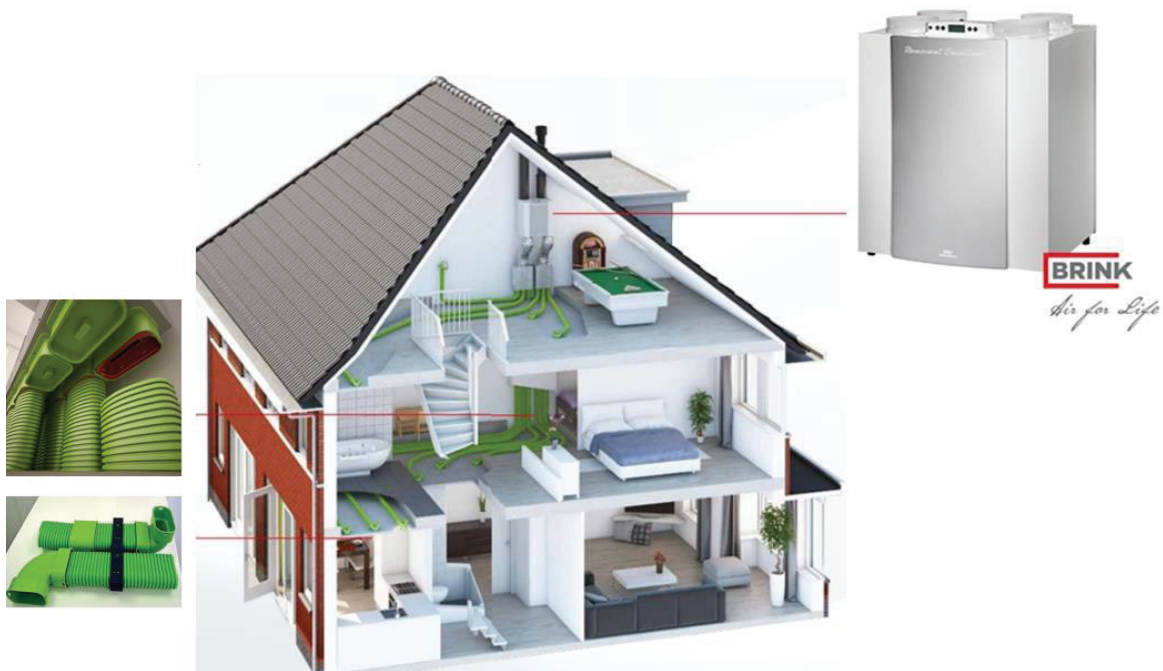
Figure 1.1: General view of a ventilation system in a house.

This ventilation system has two fans to blow the inlet and outlet air and produce sufficient pressure to overcome the pressure drops in inlet and outlet ducts. Besides breathing fresh air, customers have additional priorities. The important one is a low level of produced sound (noise). For low air flowrates, one of the best options is utilizing centrifugal fans. These fans,

however, are the primary source of the noise in the unit. The noise sources are mechanical vibrations due to the fan as the primary source, the acoustic pressure generated by the action of the impeller in air and the turbulence of the air in the ducts known as aeroacoustics noise. This acoustic pressure can become audible through the air supply vents. The level of the noise is crucial for the acceptance by the users. If the noise level is too high, many users reduce the amount of air flow. In some cases, this will lead to insufficient ventilation with possible consequences regarding health.

1.2 Objective

In this project, the goal is to reduce the noise radiated from the air supply vents. The dominant noise level is in the frequency range of 250 Hz to 2500 Hz. Because the standard acoustic dampers are big when they are to be effective at low frequencies, the objective of this project is to design small appliances which emit significantly lower noise levels. It should be mentioned that these appliances may produce pressure drops inside the duct, so the fan needs to work harder and more input power is consumed to blow the same amount of airflow.

1.3 Design challenge

The design challenges can be formulated as follows.
- How can the Sound Power Level of the ventilation system be reduced by 10 dB?
- Which type of noise reduction methods can be applied in this project?
- How much an input power of the unit will be increased?

1.4 Company

Brink Climate Systems is one of the leading manufacturers of ventilation systems. This company is active on the European market and in some Asian countries. Brink Climate Systems has approximately 180 employees and it is part of CENTROTEC Sustainable AG . CENTROTEC is a listed company with offices in 50 countries and nearly 3300 employees. Brink is one of the brands in the Climate Systems segment. With Brink's solutions in the fields of ventilation, heating, cooling and hot water generation, people live and work healthy, comfortable, and sustainable for a lifetime [1].

1.5 Design approach

Design science is a design of artifacts to interact with a problem context in order to meet desired goals [2]. The design and investigation process has two parts, i.e., design problems and knowledge questions. A design problem is a problem to (re)design an artifact and a knowledge question asks for the related knowledge [2]. The design quality depends on the quality of the design process. The design process is mostly presented in form of a phase-model which contains some steps that a designer should carry out [3]. Four main steps in this respect can be expressed as 1) an analysis and investigation of the problem, 2) a design of a solution or treatment, 3) an implementation of the treatment, and 4) an evaluation of the treatment. This model is called ADIE-model (Analysis, Design, Implementation, Evaluation) [3]. The more detailed design process can be seen in an engineering cycle. The engineering cycle is a rational process of solving the problem which is shown in Fig. 1.2 [2]. The first three design tasks, i.e., problem investigation, treatment design, and treatment validation are named a design cycle. The design cycle reduces uncertainty about the treatment and designs are validated before implemented. In the next steps of the engineering cycle, first it requires choice of a design results of the design cycle, and commitment to implement the design, then it will be applied in the real environment and evaluated there [2].
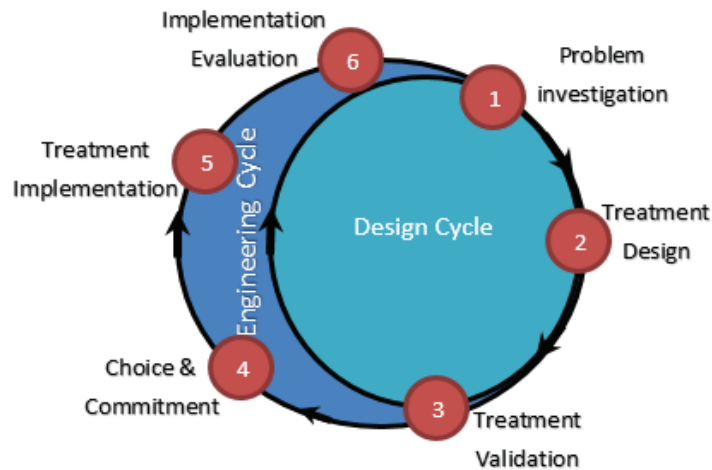

Figure 1.2: Design and Engineering cycles.

1.6 Outline of the PDEng thesis

Reducing the low frequency noise in ventilation systems can be considered as a main challenge for the manufacturers of these systems. The objective of this project is designing a

silencer as an accessory for the ventilation system to supply fresh air with 10 dB less Sound Power Level (SPL). This goal can be achieved by using various types of noise reduction methods. First of all, the noise can be reduced from the sound sources, i.e., the fans. Secondly, the so-called air-borne radiation, i.e., the aeroacoustics noise, can be absorbed after being emitted from the source. Thirdly, and in contrast with the second category, the so-called structure-borne radiation, i.e., the vibro-acoustic noise, can be absorbed from the structure of the unit itself. After a definition of the various noise reduction methods [4], the priority of each method is estimated using a Value Engineering procedure [5]. Based on the priorities, the best methods are selected. Next, upon finding and selecting the methods, the methods will be validated by design and simulation with SolidWorks, COMSOL, and MATLAB software. Furthermore, the detail design parameters will be defined. In Brink Climate Systems, subsequent development stages of a prototype are indicated with the designations Sample A to Sample D. In this project, Samples A to C will be developed, built, and tested. Next, the results are evaluated and if it is acceptable for the market, then Sample D of the new ventilation unit will be produced.

1.7 Thesis layout

In the second chapter of this study, the problem investigation, the stakeholders, and their goals are introduced. Then, the requirements are defined and the design approach is examined.

In the third chapter, after defining acoustic parameters and the ruling equations in this area, the analytical treatments are presented, subsequently knowledge based preliminary design is done.

The fourth chapter deals with the validation of each treatment by using the numerical software, i.e., SolidWorks, COMSOL, and MATLAB.

In the fifth chapter, based on the previous knowledge based preliminary design and the numerical results, the detail design of each treatment is presented.

The sixth chapter concerns preparing the test setup and implementing the treatments in the real environment. Then, this implementation is evaluated in the seventh chapter in which the Technical Performance Measures (TPMs) values are compared with each other.

Finally, the conclusion of the project is given and some suggestions for the future work are discussed.

Chapter 2

2. Problem investigation

2.1 Introduction

During the problem investigation step, it is necessary to define stakeholders, their needs, and goals. The next part of this step is determining the design framework, and mechanism. In addition, needs of stakeholders should be transformed into requirements. Then, available treatments might be found that attain the goals.

2.2 Stakeholders

A stakeholder is a group of people or institutions affected by the results of the project. Based on Alexander's list [2], the stakeholders in this project are:

• Normal operators: End users.
• Maintenance operators: Service technician of Brink Climate Systems.
• Functional beneficiaries: Company's managers, supervisors at the University of Twente.
• A financial beneficiary: Brink Climate Systems, University of Twente.
• A political beneficiary: Government.
• A negative stakeholder: Companies with the former technologies.
• A threat agent: Competitors of the company.
• The sponsor: Brink Climate Systems and the University directly and the government indirectly.
• The purchaser: R&D department's manager at Brink Climate Systems.
• Suppliers: Injection molding Companies.

2.3 Goals

Goals are desires of stakeholders. Some of the goals of each stakeholder are written as below however, the main goal is reducing the noise level of the ventilation system:

• End users: Less noise, less size of the ventilation unit and supplying enough airflow.
• Service technician: Increasing the maintenance interval and maintainability.
• Company managers: Gain a better market.

• Supervisors at the university: Solving the problem using noise reduction theories.

• University of Twente: Getting more reputation and more industrial projects.

• Government: Reducing a health problem in the society.

• R&D manager: Team working, make a patent, developing new technologies.

• Suppliers: Making the model with the Plastic injection molding technique.

2.4 Requirements

To define requirements, first it is needed to know more about the ventilation unit and its specification. A Flair 325 is a novel development with high-efficiency that it can supply the correct airflow rate in any situation. Fig. 2.1 shows the overall view of various entities of the Flair 325 and the description of the Fig. 1.2 is depicted in Table.2.1 [6].
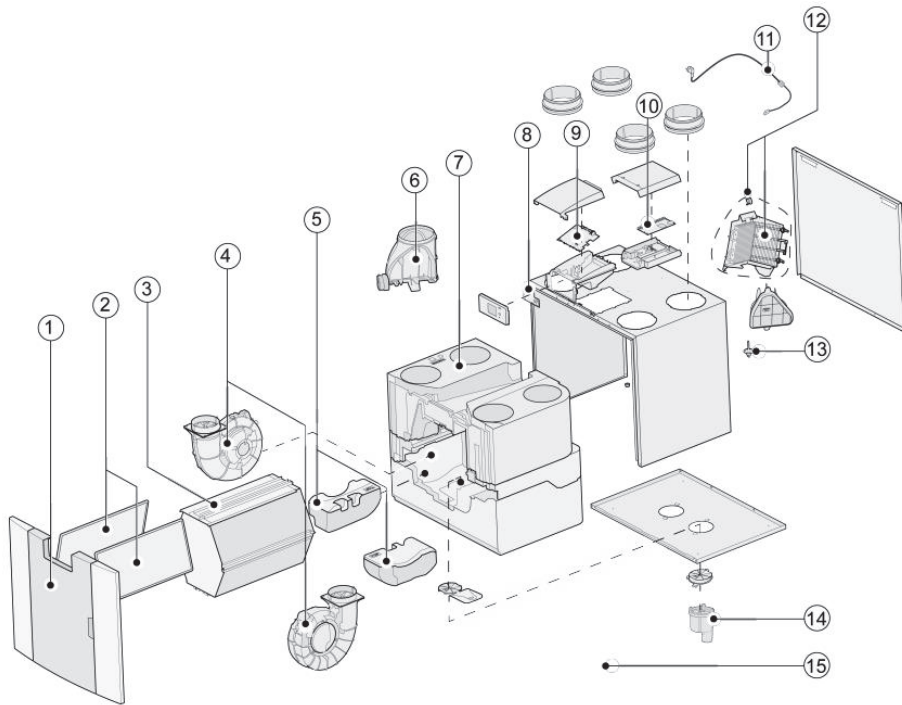
Figure 2.1: Overall view of various entities of the Flair 325 [6].

Table 2.1: Description of the Flair 325.

Flair 325			
1	Plastic front panel	9	Basic pcb UWA2-B
2	Filters (2 items) ISO Coarse 60%	10	Plus pcb UWA2-E
3	Heat exchanger	11	Mains plug and cable 230 V
4	Fan (1 item)	12	Internal preheater incl. maximum security
5	EPS assembly	13	Temperature sensor
6	Bypass valve with motor	14	Condensation discharge
7	EPP interior	15	Cable set
8	Display pcb UBP-2		

Hence, requirements for this project are defined as below:

1. Satisfy ISO 3741 standard.
2. Sound Power Level should be less than 60 dB at 325 m^3/h air flowrate and 150 Pa pressure differences between the inlet and outlet ducts of the unit.
3. External Muffler's size should be less than 1 m in length and 300 mm in outside diameter and more than 125 mm in inside diameter.
4. Size of the unit cannot be extended (dimensions (H x W x D): 650 x 750 x 560 mm^3).
5. Pressure drop of the appliance inside the duct should be less than 50 Pa.
6. Modifications should not have any drawbacks in terms of health issues.

2.5 Assumptions

1. Airflow range is 50 to 325 m^3/h.
2. Temperature range is 16 °C to 35 °C.
3. Humidity range is 30 to 90 %.
4. Ducts are smooth.
5. Air flow is turbulent after emitting from the fan.
6. The dust-particle size is negligible.

2.6 Framework

The conceptual framework can be used to frame a research problem, describe the phenomena, and analyze the structure. Architectural and statistical structures are two main types of structures. The architectural structure is useful in case-based research, while the statistical structure supports sample-based research. This project is case-based research, and architectural structure is a proper structure to consider.

2.7 Design Mechanism

There are many ways to investigate implementation and find the mechanism of the problems like Survey, Observational Case Studies, Single-Case Mechanism Experiments, and Statistical Difference-Making Experiments. The applicable methods in this project could be determined by literature study and talking with product developer R&D, R&D manager of the Company, supervisors at the university as experts in this field. So, the first mechanism is expert opinion. Afterwards, it is needed to use some limited models and compare the results, which can be considered as Statistical Difference-Making Experiments mechanism. Generally, in statistical difference-making experiments, an artifact is tested by using it to treat a sample of population elements [2]. Finally, the new appliance will be built and tested by considering Technical

Action Research mechanism i.e. a newly designed artifact is tested in the field by using it to help a client [2]. This stage will be the last stage in scaling up a technology from the laboratory to the real world which is called Scaling Up Mechanism.

2.8 Process model

We have three well-known process models as waterfall, spiral, and Vee models. To select which one is the best for a specific project, it is needed to study the literature and practice. In this project, due to technical tests in each step, the Vee model can be used effectively. Applicable criteria regarding the system should be expressed in terms of technical performance measures (TPMs) and exhibited at the system level. Technical performance measures are quantitative values (estimated, predicted and measured) that describe system performance. Some of the TPMs in this project are Sound Power Level (PL), Sound Pressure Level (SPL), Insertion Loss (IL), Transmission Loss (TL), size, airflow capacity. To ensure that all the requirements are met, the TPMs will be tracked throughout the design process and we use the scheduling formal design review. Also, the TPMs will be checked with all members of the group by sending an email or at face to face steering meetings and so on.

2.9 Design process algorithm

One of the reliable methods to get the treatment from requirements is depicted in Fig. 2.2 [7], which is labeled as design process algorithm. Synthesis, analysis, evaluation and modification are tasks that the designer should carry out to get the proper treatment [7].
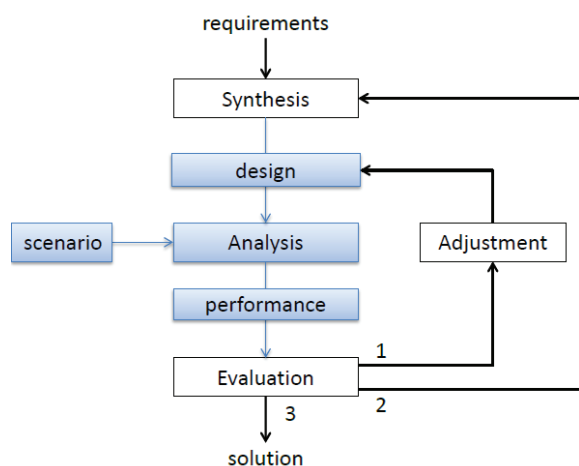

Figure 2.2: Design process algorithm.

16

The synthesis task transforms requirements into a possible solution. The performance of the solution can be calculated with the analysis task. Scenario parameters and design parameters play an important role in this step. The parameters which can be changed by the designer are named *design parameters* and the other parameters like environmental conditions or design limitations which affect the design, but cannot be changed by the designer are called *scenario parameters*. Then, the performance of the solution is evaluated and the accepted solution might be modified in the adjustment task [8]. The main part of the design process is shown in Fig. 2.1 with blue color, that is proposed *Design Process Unit* (DPU) [7]. The DPU has four sub-processes as synthesis, analysis, evaluation, and adjustment. Each part has its values, and they can be derived from various methods, but all of them should be applied in design process to obtain goals. Decomposition is one of the main parts of the DPU, and it creates smaller models from a big model. Regarding the decomposition, this project is divided into three sub-projects and each of them has its needs, requirements, designing, implementation, etc. Although these methods are independent from each other, they have interconnection between themselves due to the application in one unit.

2.10　Function Analysis System Technique

As mentioned before, the aim of this project is to find good ways to reduce the unit noise as much as possible without decreasing the system's efficiency. Based on a literature review [4], various methods of noise reduction and their functions have been defined. Next, these functions have been categorized by a Function Analysis System Technique (FAST) diagram, as depicted in Fig. 2.3.
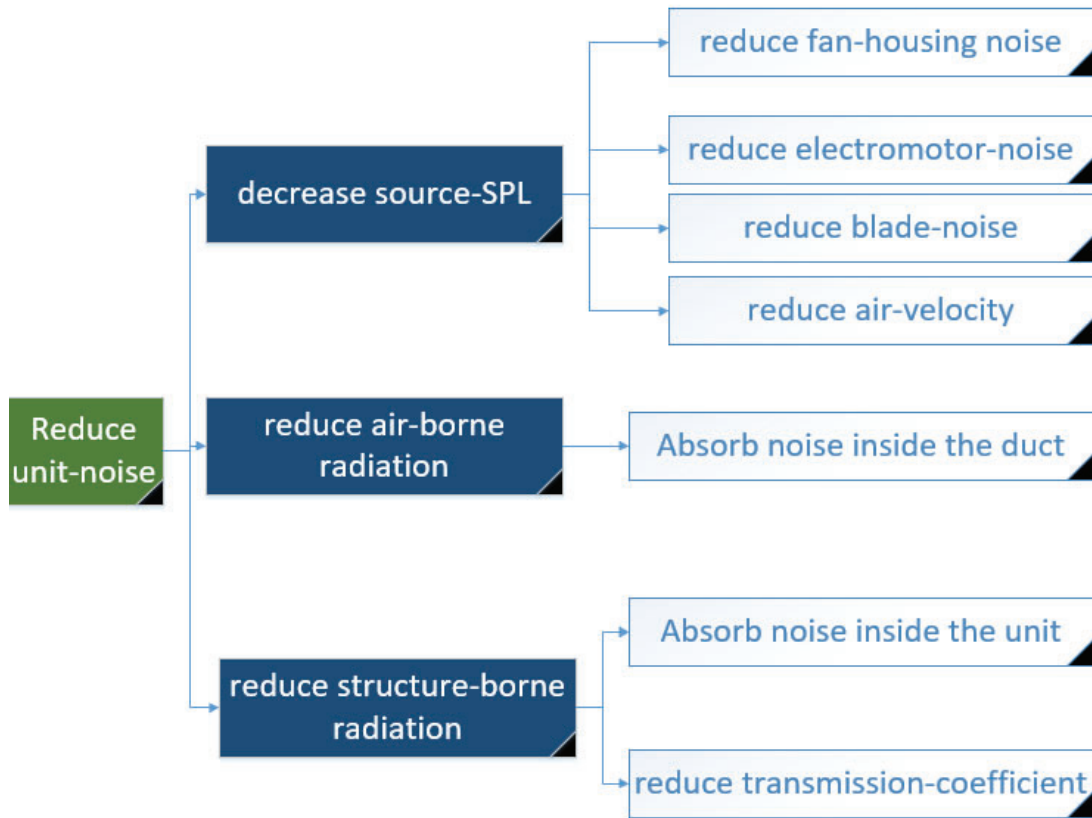
Figure 2.3: FAST diagram of the noise reduction methods.

2.11   Treatments overview

According to Fig. 2.3, different functions and solutions are taken into account to reach the final goal. For instance, some modifications can be made in order to have good flow streamlines inside the fan-housing such as adjusting the geometry of the volute tongue, changing the material of the fan-housing, using porous materials covered by thin layers, and last but not least installing a Helmholtz resonator at the volute tongue [4]. The purpose of these modifications is to reduce the noise source sufficiently. To following attributes can contribute in reducing structure-borne noise: the location of the fans, the correct selection of the unit body material, the size of the unit, the sizes of the inlet and outlet ducts, the position of the heat exchanger, the insulation joints, and finally the installment of a vibration absorber. The combination of the previously mentioned attributes can all be used in order to reduce the structure-borne radiation. Finally, by applying the various types of mufflers and resonators, the noise can be reduced in a significant way. In this case, various techniques in active and passive categories can be taken into account to attenuate the duct noise. Many manufacturers prefer to use passive techniques instead of active ones due to the cost and

necessary control systems. The passive techniques are divided into two parts, termed internal and external methods. Some of the internal passive techniques are the Internal Acoustic Black Hole muffler (IABH), the Helicoidal Resonator (HR), the Spiral Resonator (SR), and the Funnel Resonator (FR); also for the external methods, the hybrid muffler, the External Acoustic Black Hole muffler (EABH), the Cylinder Muffler (CM) could be considered.

Based on Value Engineering, the suggested methods have been evaluated in terms of the criteria listed below; each criterion is characterized by its own weighting factor (WF):

1. Power consumption by adding new entities for noise reduction (WF: 4)
2. Unit noise radiation (WF: 5)
3. Duct noise (WF: 5)
4. Lifetime (WF: 3)
5. Reliability (WF: 4)
6. Maintainability (WF: 3)
7. Maintenance interval (WF: 2)
8. Adjustment needed (WF: 1)
9. Clean air (WF: 5)
10. Volume (WF: 3)
11. Development time (WF: 2)
12. Development cost (WF: 2)
13. Cost (increasing the total price of the unit by adding a new entity) (WF: 4).

The comparison matrix is illustrated in Table. 2.2 where the values of each method are accordingly listed along with their priorities set by Brink Climate Systems, with A the highest priority and D the lowest priority.

Table. 2.2: Comparison matrix.

functions	methods	power consumption	unit noise radiation	duct noise	Lifetime	reliability	maintainability	maintainance interval	adjustment needed	clean air	volume	development time	development cost	cost	Value	BCS priority
	weighting factor:	4	5	5	3	4	3	2	1	5	3	2	2	4		
reducing noise from source	changing volute tongue shape	6	6	8	8	4	10	10	10	10	10	8	8	10	122	D
	changing housing shape	6	6	8	8	10	10	10	10	10	10	6	6	6	77	D
	using porous material with thin layer	10	6	6	8	6	8	10	10	10	8	8	8	8	99	C
	Helmholtz resonators at Volute tongue	10	8	10	8	8	6	8	6	10	8	8	8	8	106	B
	vibration analaysis of fan housing	10	8	6	10	8	10	10	10	10	10	6	6	8	108	C
	reduce the noise from electro motor	8	6	6	8	6	10	10	10	10	10	4	4	8	95	D
	adjust the noise from fan blades	8	8	8	10	8	10	10	10	10	10	4	6	8	107	D
	increase duct diamiter	8	4	6	10	4	10	10	10	10	4	8	8	8	90	D
reducing air-borne radiation	helicoidal resonators	6	6	10	8	10	10	10	10	10	8	6	8	8	106	A
	Using piezoelectric	8	6	8	8	6	8	8	8	10	10	8	6	6	73	B
	using active noise cancelation sys.	6	8	10	6	8	8	6	6	10	8	6	6	6	73	C
	hybrid muffler-helmholtz resonators	10	8	10	8	10	10	10	10	10	8	8	8	7	101	A
	hybrid muffler- (MPP) with layer	10	6	8	8	8	8	10	10	10	6	8	6	8	101	A
	hybrid muffler- extended inlet/outlet	6	4	6	10	4	10	10	10	10	8	10	10	10	118	B
	hybrid muffler- baffle plates	4	4	8	6	8	10	10	10	10	8	8	8	8	93	B
	hybrid muffler- dissipative units	6	8	10	10	10	8	10	10	8	4	10	10	8	106	A
reducing structure- borne radiation	changing the foam	10	6	4	10	6	10	10	10	10	10	8	8	10	126	A
	redesign the location of the parts	10	6	4	10	4	10	10	10	10	10	8	10	9	112	A
	noise wave absorber in cover of unit	10	8	6	8	6	10	10	10	10	10	8	10	9	120	A
	increasing reflect coeficient	8	8	10	6	6	6	8	10	10	8	6	9	8	100	A
	using vibration absorber	10	8	8	8	8	8	8	8	10	10	8	8	8	108	A
	using vibration insulation	10	10	6	10	6	10	10	10	10	10	8	10	10	140	A

Based on Table 2.2, some of the methods with larger values and highest priority (A) from the second category have been selected to design and develop the internal and external mufflers and resonators. This project has been divided into three sub-projects.

In the first sub-project, the internal resonators (inside the tube) are designed. The narrowband noise attenuation can be obtained by a properly designed, smart innovation, termed helicoidal resonator, which works as a passive acoustic filter inside the duct. Łapka [9] has simulated the HR inside the common ventilation duct size, 125 mm, and the lowest eigen-frequency that he achieved was 1282 Hz. Finding an analytical solution of the system would be a good way to gain a better understanding of the problem and seek the suitable treatment inside the duct afterwards. The analytical solution helps to develop the other innovative resonators, termed spiral resonator and funnel resonator, which work for frequencies lower than 1282 Hz which is not possible to achieve by the helicoidal resonator.

In the second sub-project, an Acoustic Black Hole muffler, which absorbs high amount of the incident wave energy, is considered as a passive treatment for low frequency noise reduction inside the duct while the External Acoustic Black Hole (EABH) is considered outside the duct. This absorption takes place by decreasing the velocity of wave propagation towards zero in finite length of the muffler. These mufflers will be installed after the fan to absorb the air noise.

In the third sub-project, in order to apply the treatment in the real environment, the selected method is designed such that it is possible to make it with the injection molding technique and install it inside the ventilation unit.

Chapter 3

3. Treatment design

Treatment design is a design of one or more artifacts that can treat the problem. The goal of treatment design is that some stakeholders are better off when the problem is treated. Treatment design consisted of a literature survey of the state of the art of requirements engineering, followed by the specification of a candidate solution [2]. In this chapter, first some acoustical terms are defined and then the possible analytical treatment will be determined. Based on the analytical treatment, some resonators are designed in the knowledge based preliminary design phase.

3.1 Definitions

3.1.1 Acoustics

The word acoustics is derived from the Greek word root Akuein meaning hearing. It was first used by Sauveur for this science. Acoustics as a science began with Pythagoras, who wanted to know why some musical sounds are more interesting than others which he found out in the numerical proportions. Aristoteles understood that sound is composed of air expansion and contraction. Galileo and Mersenne independently discovered and completed the law of vibrating strings that Pythagoras had started 2000 years ago [10]. Acoustics as a science may be defined as the generation, transmission, and reception of energy as vibrational waves in matter [11].

3.1.2　Acoustic Pressure

The difference between instantaneous pressure P and static (equilibrium) pressure p_0 is termed sound pressure or acoustic pressure p [12]:

$$p = P - p_0.$$

(3.1)

3.1.3　Acoustic Power

Acoustic power or sound power is the product of the sound pressure p and the component of the particle velocity, u_n, at a point on a surface in the direction normal to the surface, integrated over that surface [12] [13]:

$$w = \int p u_n dA.$$

(3.2)

3.1.4　Sound Pressure Level (SPL)

Sound Pressure Level is ten times the logarithm to the base 10 of the ratio of the square of the sound pressure p to the square of a reference value $p_0 = 20\mu Pa$ expressed in decibels (dB) [12]:

$$SPL = 10\log(\frac{p^2}{p^2_0}) = 20\log(\frac{p}{p_0}).$$

(3.3)

3.1.5　Power Level (PL)

Power Level is ten times the logarithm to the base 10 of the ratio of the sound power of a source w to a reference value $w_0 = 10^{-12}W$ expressed in decibels [12]:

$$PL = 10\log(\frac{w}{w_0}).$$

(3.4)

To define the efficiency and performance of the noise reduction systems, various types of methods can be used. The most important ones are expressed below.

3.1.6　Noise Reduction (NR)

The Noise Reduction (NR) parameter is the difference between the sound pressure levels at two arbitrary selected points like inlet and outlet of the duct [13]:

$$NR = SPL_{in} - SPL_{out}.$$

(3.5)

3.1.7　Insertion Loss (IL)

Insertion Loss difference between acoustic power level without any filter and with filter [13]:

$$IL = Power\, Level\, Out_{withoutFilter} - Power\, Level\, Out_{withFilter}.$$

(3.6)

3.1.8   Transmission Loss (TL)

The Transmission Loss (TL) describes the performance of the model by finding the differences between Sound Power Level before and after the model inside the tube [13]:

$$TL = Power\ Levl_{in} - Power\ Level_{out} = 10\log(\frac{Acoustic\ power_{in}}{Acoustic\ power_{out}}).$$

(3.7)

3.2   Analytical treatment design

3.2.1   Linear wave equation

When the fluid element with velocity *v(x, y, z, t)* at position *(x, y, z)* and time t moves to a new location *(x+dx, y+dy, z+dz)* at a later time $t + dt$, its new velocity is expressed by the leading terms of its Taylor expansion:

$$v = v(v_x, v_y, v_z, t) + \frac{\partial v}{\partial x} v_x dt + \frac{\partial v}{\partial y} v_y dt + \frac{\partial v}{\partial z} v_z dt + \frac{\partial v}{\partial t} dt.$$

(3.8)

Thus, the acceleration of the chosen element is:

$$a = \frac{\partial v}{\partial t} + (v.\nabla)v,$$

(3.9)

where $(v.\nabla) = v_x \frac{\partial}{\partial x} + v_y \frac{\partial}{\partial y} + v_z \frac{\partial}{\partial z}$.   By   considering $dm = \rho\, dV$, $df = a\, dm$ and $df = -\nabla p\, dV + g\, \rho\, dV$ it can be shown [11]:

$$-\nabla P + g\rho = \rho(\frac{\partial v}{\partial t} + (v.\nabla)v).$$

(3.10)

This nonlinear, inviscid force equation is Euler's equation with gravity. In the case of no acoustic excitation $\nabla P_0 = g\rho_0$ and thus $\nabla P = \nabla p + g\rho_0$ so it becomes:

$$-\frac{1}{\rho_0}\nabla p + gs = (1+s)(\frac{\partial v}{\partial t} + (v.\nabla)v)\,,\ s = \frac{\rho - \rho_0}{\rho_0}.$$

(3.11)

If we now make the assumptions that $|gs| << |\nabla p|/\rho_0$, $|s| << 1$, $|(v.\nabla)v| << \left|\frac{\partial v}{\partial t}\right|$ and take the divergence of the above equation, then:

$$\nabla.(\rho_0 \frac{\partial v}{\partial t}) = -\nabla^2 p,$$

(3.12)

where $\nabla.\nabla = \nabla^2$ is the three-dimensional Laplace operator. Next, take the time derivative of the continuity equation and use the facts that space and time are independent and that there are no large density variations over time:

$$\rho_0 \frac{\partial^2 s}{\partial t^2} + \nabla.(\rho_0 \frac{\partial v}{\partial t}) = 0.$$
(3.13)

By using these two equations, we obtain the linear lossless wave equation as [11]:

$$\nabla^2 p - \frac{1}{c_0^2} \frac{\partial^2 p}{\partial t^2} = 0,$$
(3.14)

where c_0 is the thermodynamic speed of sound defined as:

$$c_0^2 = \frac{\partial P}{\partial \rho}\bigg|_{adiabat} = \frac{\beta}{\rho_0}.$$
(3.15)

Hence, in cylindrical-coordinates an acoustic pressure p at each point (r, φ, z, t) inside the duct could be derived by solving wave equation below:

$$\nabla^2 p(r, \phi, z, t) - \frac{1}{c_0^2} \frac{\partial^2 p(r, \phi, z, t)}{\partial t^2} = 0,$$
(3.16)

where $\nabla^2 \equiv \frac{\partial^2}{\partial r^2} + \frac{1}{r} \frac{\partial}{\partial r} + \frac{1}{r^2} \frac{\partial^2}{\partial \varphi^2} + \frac{\partial^2}{\partial z^2}$. Using the separation of variables method, the general solution for wave equation could be expressed as [14]:

$$p(r, \phi, z, t) = R(r) \times \Phi(\phi) \times Z(z) \times T(t).$$
(3.17)

The expression for each term is written as [13],[14],[15]:

$$\begin{cases} \dfrac{d^2 T}{dt^2} + \omega^2 T = 0, \quad \omega = 2\pi f = c_0 k \\ \qquad T(t) = e^{i\omega t} \end{cases} \qquad \begin{cases} \dfrac{d^2 Z}{dz^2} + k_z^2 Z = 0 \\ Z(z) = A_{1z} e^{-ik_z z} + A_{2z} e^{ik_z z} \end{cases}$$
(3.18)

$$\begin{cases} \dfrac{d^2 \Phi}{d\phi^2} + m^2 \Phi = 0 \\ \Phi(\phi) = A_{1\phi} \cos(m\phi) + A_{2\phi} \sin(m\phi) \end{cases} \qquad \begin{cases} r^2(\dfrac{\partial^2 R}{\partial r^2} + \dfrac{1}{r} \dfrac{\partial R}{\partial r}) + \left[k_r^2 r^2 - m^2 \right] R = 0 \\ R(r) = \sum_m A_m J_m(k_r r) + B_m Y_m(k_r r) \end{cases}$$

where ω is the angular frequency, m is a separation constant, and the axial wave number k_z can be obtained from the wave number $k_0 = \dfrac{\omega}{c_0}$ and the radial wave number k_r as

$k_z = (k_0^2 - k_r^2)^{0.5} \ for \ \omega \geq 0 \,[13].$

26

3.2.2 Boundary Conditions

Three different types of boundary conditions are considered. At all the solid boundaries, sound hard (wall) boundary conditions are used [16]:

$$(-\frac{\nabla p}{\rho}).\hat{n} = 0 \, , \tag{3.19}$$

where $\hat{n}$ is a normal vector of the wall's surface. At the inlet boundary for the numerical solution, a combination of an incoming and an outgoing plane wave is assumed. This is explained in the Acoustics module User's Guide of the COMSOL Multiphysics 5.3 software [16], which is validated earlier in these papers [17], [18]:

$$(-\frac{\nabla p}{\rho}).\hat{n} = \frac{i\omega}{\rho c_0} p - \frac{2i\omega}{\rho c_0} p_0 \, . \tag{3.20}$$

In this equation, p_0 denotes the applied outer pressure, i.e., the emitted noise from the fan. At the outlet boundary, an outgoing plane wave radiation is set [16]:

$$(-\frac{\nabla p}{\rho}).\hat{n} = \frac{i\omega}{\rho c_0} p \, . \tag{3.21}$$

For the analytical solution, six boundary Conditions should be defined so that unknown parameters can be found.

Boundary conditions of the duct with the Open-Open Ends, i.e., Neumann BC's are expressed as below [14]:

$$\begin{cases} \dfrac{dZ(z=0)}{dz} = 0 \\ \dfrac{dZ(z=L)}{dz} = 0 \end{cases} \Rightarrow \begin{cases} Z(z) = \cos(k_z z) \\ k_z = 2n\pi / L \ , n = 1, 2, 3, ... \end{cases} \tag{3.21}$$
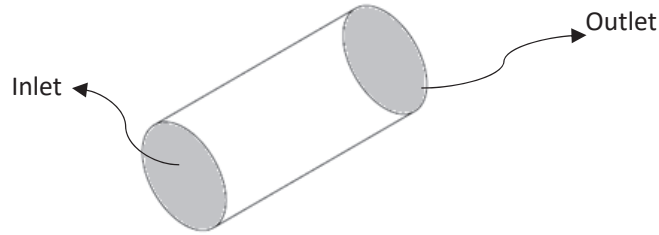
The axial boundary condition is shown in Fig. 3.1.

Figure 3.1: Axial boundaries at the simple duct.

Angular Boundary Conditions

For simple duct in Fig. 3.1, the angular boundary condition should be $\Phi(0) = \Phi(2\pi)$. In this state, *m* could be obtained as [15]:

$$\begin{cases} \Phi(0) = A_{1\varphi} \\ \Phi(2\pi) = A_{1\varphi} \cos(2m\pi) + A_{2\varphi} \sin(2m\pi) \end{cases} \Rightarrow \begin{cases} \sin(2m\pi) = 0 \\ \cos(2m\pi) = 1 \end{cases} \Rightarrow m = 0, \pm 1, \pm 2, \pm 3, ... \tag{3.22}$$

If the duct includes a blade like in Fig. 3.2 then *m* becomes $m = 0, \pm 0.5, \pm 1, \pm 1.5, \pm 2, ,...$ due to the following conditions [15]:

$$\begin{aligned} \dfrac{d\Phi}{d\phi}(0) = 0 \Rightarrow A_{2\phi} = 0 \\ \dfrac{d\Phi}{d\phi}(2\pi) = 0 \Rightarrow - A_{1\phi} * m * \sin(2\pi m) = 0 \end{aligned} \Rightarrow \begin{aligned} \Phi(\phi) = A_{1\phi} \cos(m\phi) \\ m = 0, \pm 0.5, \pm 1, \pm 1.5, \pm 2, ,... \end{aligned} \tag{3.23}$$
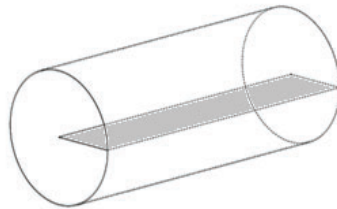

Figure 3.2: Angular boundaries at the duct.

It should be noted that the modes corresponding to $m = 0$ are axisymmetric.

Radial Boundary Conditions

If the duct includes no mandrel ($r_1 = 0$) shown in Fig. 3.3, the pressure at the center of the duct should be limited. Therefore, the coefficient of the second kind of the Bessel Function should be zero and the unknown parameter can be found as [15]:

$$\begin{cases} R_m(r_1 = 0) \ : finite \ \Rightarrow B_m = 0 \\ \dfrac{dR_m}{dr}(r_2) = 0 \Rightarrow J'_m(k_r r_2) = 0 \end{cases} . \tag{3.24}$$
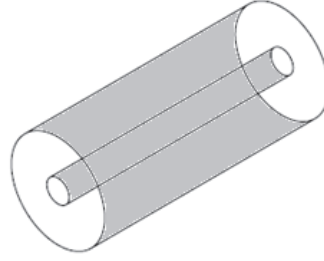

Figure 3.3: Radial boundaries at the duct.

Hence, the radial wave number $k_{r,m}$ will be obtained from the roots of the derivation of the first kind of the Bessel Function equation. The results for various *m* are written in Table 3.1 [15].

Table 3.1: Roots of the first kind of the Bessel Function.

Roots of the first kind of the Bessel Function ($k_{r,m} \times r_2$)	*m=0*	*m=0.25*	*m=0.5*	*m=1*
First root	0	0.7688	1.1650	1.8410
Second root	3.8310	4.2248	4.6040	5.3310
Third root	7.0150	7.4062	7.7890	8.5360

If the duct includes a mandrel or it is a co-axial cylindrical duct, then the pressure derivation at both radial boundaries should vanish [15]:

$$\begin{cases} \dfrac{dR_m}{dr}(r_1) = 0 \\ \dfrac{dR_m}{dr}(r_2) = 0 \end{cases} \Rightarrow \dfrac{dR_m}{dr}(r) = B_m[\dfrac{A_m}{B_m} J'_m(k_r r) + Y'_m(k_r r)]. \tag{3.25}$$

In this case, k_r should be obtained from the following [15]:

$$\begin{matrix} \dfrac{A_m}{B_m} J'_m(k_r r_1) + Y'_m(k_r r_1) = 0 \\ \dfrac{A_m}{B_m} J'_m(k_r r_2) + Y'_m(k_r r_2) = 0 \end{matrix} \Rightarrow \begin{matrix} \dfrac{A_m}{B_m} = -\dfrac{Y'_m(k_r r_1)}{J'_m(k_r r_1)} \\ \dfrac{A_m}{B_m} = -\dfrac{Y'_m(k_r r_2)}{J'_m(k_r r_2)} \end{matrix} \quad k_r r_2 = X, \dfrac{r_2}{r_1} = q$$

$$\Rightarrow \dfrac{A_m}{B_m} = -\dfrac{Y'_m(X/q)}{J'_m(X/q)} = -\dfrac{Y'_m(X)}{J'_m(X)} \Rightarrow J'_m(X) * Y'_m(X/q) - J'_m(X/q) * Y'_m(X) = 0 \tag{3.26}$$

Values of X for various m and q are given in Table 3.2.

Table 3.2: First and second roots of Eq. (3.26).

First and second Roots ($k_{r,m,q} \times r_2$)	m=0		m=1	
	First root	second root	First root	second root
q=2.0833	0	6.1531	1.3744	5.7297
q=4.1667	0	4.3975	1.6563	4.9844
q=6.25	0	4.0938	1.7494	4.9894
q=12.5	0	3.8994	1.8163	5.1938
q=31.2500	0	3.8400	1.8369	5.3069

By comparing the last row of Table 3.2 with the first and second rows of Table 3.1, it can be concluded that when the mandrel diameter approaches zero, the result of the wave number will approach the results without mandrel. This result also shows that by adding a mandrel inside the duct, lower eigen-frequencies will be obtained.

The pressure function becomes:

$$P(r,\phi,z,t) == \sum_{m=0}^{\infty} \sum_{n=0}^{\infty} \left[A_m J_m(k_{r,m,n}r) + B_m Y_m(k_{r,m,n}r) \right] \left[A_{1\phi} e^{-im\phi} + A_{2\phi} e^{im\phi} \right] \left[A_{1z} e^{-ik_{z,m,n}z} + A_{2z} e^{ik_{z,m,n}z} \right] e^{i\omega t}$$

where

$$k_{z,m,n} = (k_0{}^2 - k_{r,m,n}{}^2)^{0.5} \ for \ \omega \geq 0 \ , \tag{3.28}$$

and n is the index of the root of the Bessel function.

3.2.3   Inviscid moving air

If an inviscid moving air inside the duct is considered then the general solution will be[13]:

$$P(r,\phi,z,t) == \sum_{m=0}^{\infty} \sum_{n=0}^{\infty} \left[A_m J_m(k_{r,m,n}r) + B_m Y_m(k_{r,m,n}r) \right] \left[A_{1\phi} e^{-im\phi} + A_{2\phi} e^{im\phi} \right] \left[A_{1z} e^{-ik_{z,m,n}^+ z} + A_{2z} e^{ik_{z,m,n}^- z} \right] e^{i\omega t}$$

where $k_{z,m,n}^+$ and $k_{z,m,n}^-$ are governed by:

$$k_{z,m,n}^2 + k_{r,m,n}{}^2 = (k_0 + M k_{z,m,n})^2 . \tag{3.30}$$

Here, the mean-flow velocity is assumed to be constant in space and time, therefore, independent of all coordinates and M is the average Mach number of the mean flow.

3.3 Knowledge based preliminary design

3.3.1   Introduction

Scientific theories enhance our capability to describe, explain, and predict phenomena and to design artifacts that can be used to treat problems [2]. In design artifacts, one of the simple combination of above states is the half blade attaches to the mandrel shown in Fig. 3.4 and the radial wave number is written in Table 3.3.
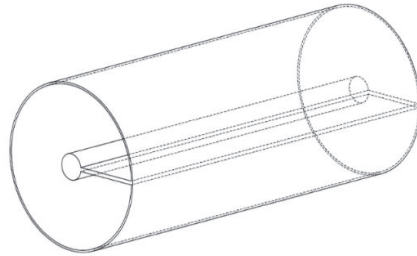

Figure 3.4: The half blade attached to the mandrel inside the duct.

Table 3.3: Radial wave number of the half blade attached to the mandrel.

First and second Roots ($k_{r,m,q} \times r_2$)	m=0.5	
	First root	*Second root*
q=2.0833	0.6565	5.6009
q=4.1667	0.8583	4.1781
q=6.25	0.9075	4.0006
q=12.5	1.0116	4.0260

3.3.2   Helicoidal Resonator (HR)

To decrease the wave number, one of the smart innovations is to install the helicoidal shape inside the duct shown in Fig. 3.5. The helicoidal shape is made by turning the blade by an axially dependent angle like $\varphi = \dfrac{2\pi}{L} z$.
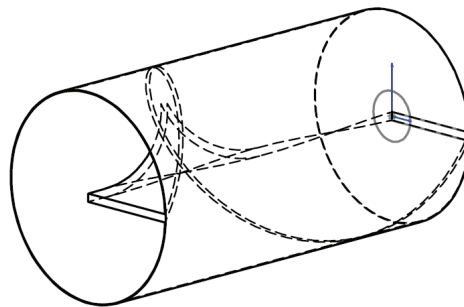
Figure 3.5: The helicoidal resonator.

The helicoidal resonator (HR) has a boundary condition at the combination of the axial and angular axes. The pressure gradient perpendicular to the helical surface should be zero:

$$\frac{\nabla \vec{P}}{\rho} . \hat{n} = 0 \Rightarrow \nabla \vec{P} . \hat{n} = 0 . \tag{3.31}$$

The pressure gradient in cylindrical coordinate could be written as below:

$$\nabla \vec{P} = \begin{pmatrix} \dfrac{\partial R}{\partial r} \cos(\phi) - \dfrac{1}{r} \dfrac{\partial \Phi}{\partial \phi} \sin(\phi) \\[2mm] \dfrac{\partial R}{\partial r} \sin(\phi) + \dfrac{1}{r} \dfrac{\partial \Phi}{\partial \phi} \cos(\phi) \\[2mm] \dfrac{\partial Z}{\partial z} \end{pmatrix} . \tag{3.32}$$

In addition, the helicoid surface and a normal vector of the surface are exposed in Fig. 3.6 and it can be expressed in Eq. (3.33):

$$Helicoid\ Surface = \begin{pmatrix} r\cos(\dfrac{2\pi}{L} z) \\[2mm] r\sin(\dfrac{2\pi}{L} z) \\[2mm] z \end{pmatrix} , \hat{n} = \begin{pmatrix} \sin(\dfrac{2\pi}{L} z) \\[2mm] -\cos(\dfrac{2\pi}{L} z) \\[2mm] \dfrac{2\pi r}{L} \end{pmatrix} . \tag{3.33}$$
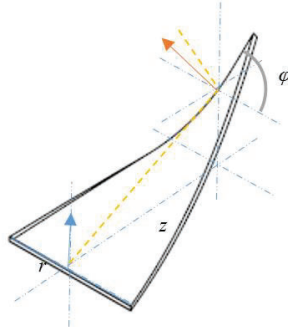
Figure 3.6: The helicoid surface.

More information can be found in Appendix A. Hence, the helicoid condition is:

$$\nabla \vec{P} . \hat{n} = -\frac{1}{r} \frac{\partial \Phi}{\partial \phi} + \frac{2\pi r}{L} \frac{\partial Z}{\partial z} = 0$$

$$\Rightarrow -\frac{m}{r} [-A_{1\phi} \sin(m\phi) + A_{2\phi} \cos(m\phi)] + \frac{2\pi r k_z i}{L} [-A_{1z} e^{-ik_z z} + A_{2z} e^{ik_z z}] = 0 \tag{3.34}$$

This helicoid condition is valid at $z = 0, \phi = 0$, so:

$$A_{2\phi} = \frac{2\pi r^2 k_z i}{mL} [-A_{1z} + A_{2z}], \ A_{1\phi r} = \sqrt{1 - A_{2\phi r}^2} . \tag{3.35}$$

Also, the helicoid condition is valid at $z = L, \phi = 2\pi$:

$$-\frac{m}{r}[-A_{1\phi}\sin(m2\pi) + A_{2\phi}\cos(m2\pi)] + \frac{2\pi r k_z i}{L}[-A_{1z}e^{-ik_z L} + A_{2z}e^{ik_z L}] = 0$$

$$\Rightarrow A_{1\phi}\sin(m2\pi) = \frac{2\pi r^2 k_z i}{mL}[-A_{1z}\cos(m2\pi) + A_{2z}\cos(m2\pi) + A_{1z}e^{-ik_z L} - A_{2z}e^{ik_z L}]$$

(3.36)

In Eq. (3.36), if $r = 0$ then m will be:

$$if\ r = 0 \Rightarrow \sin(m2\pi) = 0 \ \Rightarrow m = \pm 0.5, \pm 1, \dots. \tag{3.37}$$

By substituting m in Eq. (3.24), the radial wave number k_r will be determined which is depicted earlier in Table 3.1. Moreover, Eq. (3.36) is valid at $r = r_2$:

$$if\ r = r_2 \Rightarrow \frac{2\pi r_2^2 k_z i}{mL}[A_{1z}(1+e^{-ik_z L}) - A_{2z}(1+e^{ik_z L})] = 0 \Rightarrow \frac{A_{1z}}{A_{2z}} = \frac{1+e^{ik_z L}}{1+e^{-ik_z L}}. \tag{3.38}$$

To find the maximum TL, a below equation should be valid. Hence:

$$d(TL) = 0 \Rightarrow \frac{Z_0}{dZ_0} = \frac{Z_L}{dZ_L} \Rightarrow \frac{A_{1z} + A_{2z}}{-A_{1z} + A_{2z}} = \frac{A_{1z}e^{-ik_z L} + A_{2z}e^{ik_z L}}{-A_{1z}e^{-ik_z L} + A_{2z}e^{ik_z L}}. \tag{3.39}$$

So, the axial wave number for maximum TL will be derived by considering Eq. (3.38) and (3.39).

In short, the eigen-frequency of HR which has a maximum TL is $f = \frac{k_0 \times c_0}{2\pi}, k_0 = (k_z^2 + k_r^2)^{0.5}$ where the axial wave number is derived from Eq. (3.39) and the radial wave number can be obtained from Table. 3.1 and Table. 3.3.

3.3.3 Spiral Resonator (SR)

To absorb low frequency noise, another possibility is applying a spiral blade inside the duct as shown in Fig. 3.7.
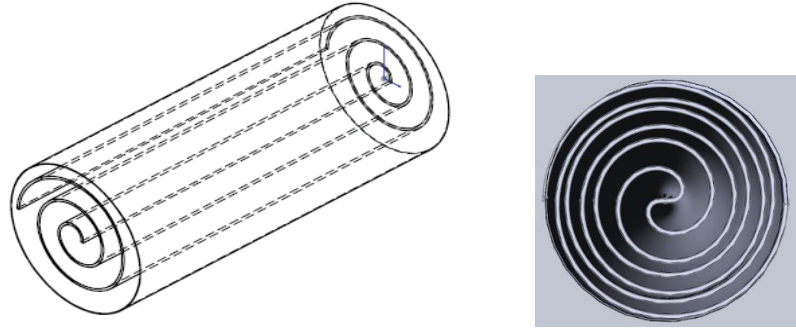
Figure 3.7: The Spiral Resonator (SR) and front view of the double spiral Resonator.

If we combine two spiral models together, the double spiral resonator presented in Fig. 3.7 is made. To find an analytical solution for the spiral resonator, it should be mentioned that the angular boundary condition will be changed and related to the function of the spiral curve. By considering the linear function, $\varphi(r) = 2n\pi \dfrac{r}{r_2}$, shown in Fig. 3.8, the solution can be derived.
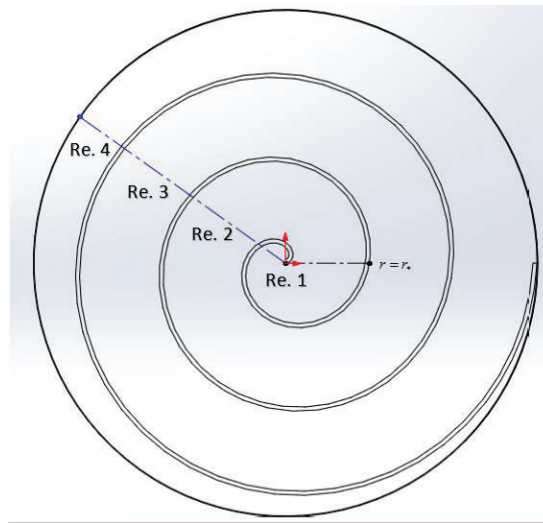
Figure 3.8: The front section view of the spiral resonator.

First, the function and normal vector of the spiral surface can be expressed (see Appendix A):

$$
Spiral\ Surface = \begin{pmatrix} \dfrac{r_2\phi}{2n\pi}\cos(\phi) \\[2mm] \dfrac{r_2\phi}{2n\pi}\sin(\phi) \\[2mm] z \end{pmatrix}, \hat{n} = \begin{pmatrix} \dfrac{r_2}{2n\pi}\sin(\phi) + \dfrac{r_2\phi}{2n\pi}\cos(\phi) \\[2mm] -\dfrac{r_2}{2n\pi}\cos(\phi) + \dfrac{r_2\phi}{2n\pi}\sin(\phi) \\[2mm] 0 \end{pmatrix}.
\tag{3.40}
$$

Second, the pressure gradient perpendicular to the spiral surface should be zero. Hence:

$$
\Rightarrow \frac{\partial R}{\partial r} * r\phi - \frac{\partial \Phi}{\partial \phi} = 0 \Rightarrow \begin{cases} k_r r\phi[A_m J'_m(k_r r)] - m[-A_{1\phi}\sin(m\phi) + A_{2\phi}\cos(m\phi)] = 0 & r \le r_* \\ k_r r\phi[A_m J'_m(k_r r) + B_m Y'_m(k_r r)] - m[-A_{1\phi}\sin(m\phi) + A_{2\phi}\cos(m\phi)] = 0 & r > r_* \end{cases}
$$

The spiral condition should be valid at $r = 0, \phi = 0$, so:

$$
\nabla \vec{P}.\hat{n}(r = 0, \varphi = 0) = 0 \Rightarrow A_{2\varphi} = 0, A_{1\varphi} = 1 \ .
\tag{3.42}
$$

From the radial boundary condition at the end of the first turn ($r = r_*, \varphi = 2\pi$), we have:

$$
\frac{dR_m}{dr}(r_*) = 0 \Rightarrow J'_m(k_r r_*) = 0 .
\tag{3.43}
$$

The spiral condition should be also valid at the end of the first turn ($r = r_*, \varphi = 2\pi$), hence:

$$
\nabla \vec{P}.\hat{n}(r = r_*, \varphi = 2\pi) = 0 \Rightarrow \sin(m2\pi) = 0 \Rightarrow m = (0, \pm 0.5, \pm 1, ...).
\tag{3.44}
$$

So, k_r can be obtained from $J'_{0.5}(k_r r_*) = 0$. Now based on spiral condition, Eq. (3.40), the coefficient of the radial functions for the first region, Re. 1 in Fig. 3.8, will be calculated as:

$$
A_{m1}(r) = -\frac{m\ \sin(m\dfrac{2\pi r}{r_*})}{k_r r\ \dfrac{2\pi r}{r_*}\ J'_m(k_r r)}, m = 0.5 \quad 0 < r \le r_* .
\tag{3.45}
$$

For the other regions, i.e., 2, 3 and 4, it can be found in Appendix A.

If both ends of the spiral resonator are opened, $Z(z) = \cos(k_z z)$, the pressure at the inlet will be the same as at the outlet and no noise reduction will be obtained. To overcome this difficulty, one of the solutions is to close a part of each of the ends like in Fig. 3.9:
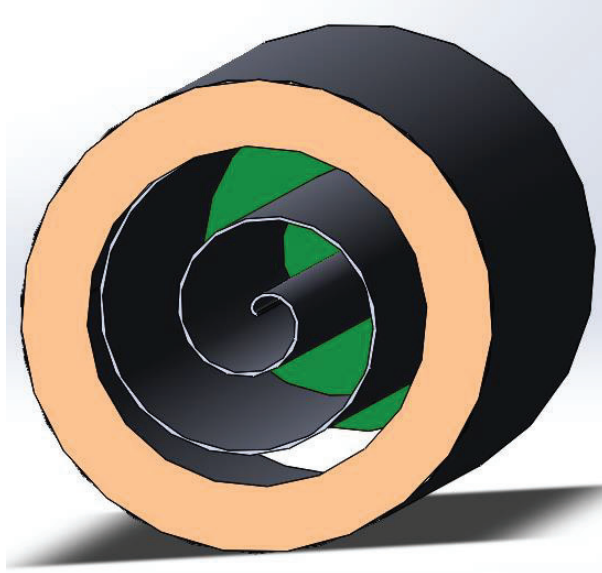
Figure 3.9: The spiral resonator with half closed ends.

In this case, the axial boundary condition will be changed at the closed end parts, so:

$$\begin{cases} Z(z=L)=0 \Rightarrow A_{1z}e^{-ik_zL} + A_{2z}e^{ik_zL} = 0 & r \le r_0 \quad (half\ outlet\ is\ closed) \\ Z(z=0)=0 \Rightarrow A_{1z}e^{-ik_z0} + A_{2z}e^{ik_z0} = 0 & r > r_0 \quad (half\ inlet\ is\ closed) \end{cases} . \tag{3.46}$$

3.3.4 Funnel Resonator (FR)

The other method to reduce the low frequency noise is using a funnel inside the tube which is demonstrated in Fig. 3.10. The axial and radial wave number will be derived from below formula.
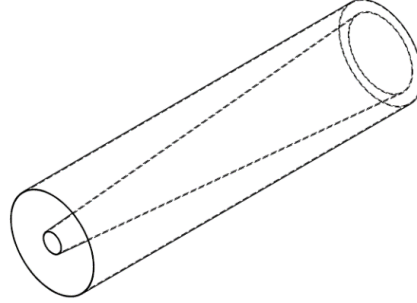
Figure 3.10: The funnel resonator inside the duct.

The funnel surface and normal vector of the surface can be expressed:

$$Funnel\ Surface = \begin{pmatrix} (r_1 + \frac{r_2 - r_1}{L} z)\cos(\phi) \\ (r_1 + \frac{r_2 - r_1}{L} z)\sin(\phi) \\ z \end{pmatrix}, \hat{n} = \begin{pmatrix} (\frac{L}{r_2 - r_1} r_1 + z)\cos(\phi) \\ (\frac{L}{r_2 - r_1} r_1 + z)\sin(\phi) \\ -(\frac{L}{r_2 - r_1} r_1 + z) \end{pmatrix}. \tag{3.47}$$

The pressure gradient perpendicular to the funnel surface should be zero, hence:

$$\nabla \vec{P}.\hat{n} = (\frac{L}{r_2 - r_1} r_1 + z)[\frac{\partial R}{\partial r} - \frac{\partial Z}{\partial z}] = 0 \Rightarrow \frac{\partial R}{\partial r} - \frac{\partial Z}{\partial z} = 0. \tag{3.48}$$

The funnel condition should be valid at funnel surface inside and outside of the funnel for $z = 0\ and\ z = L$:

$$inside\ of\ the\ funnel \Rightarrow \begin{cases} J'_m(k_{r01}r_{01}) = \frac{ik_{z01}}{k_{r01}}[-A_{1z}e^{-ik_{z01}0} + A_{2z}e^{ik_{z01}0}]\ , \ k^2_{z01} = k^2 - k^2_{r01} \\ J'_m(k_{rL1}r_{L1}) = \frac{ik_{zL1}}{k_{rL1}}[-A_{1z}e^{-ik_{zL1}L} + A_{2z}e^{ik_{zL1}L}]\ , \ k^2_{zL1} = k^2 - k^2_{rL1} \end{cases}. \tag{3.49}$$

By solving above 2 equations, 2 unknown parameters k_{r01}, k_{rL1} can be found. The funnel condition should also be valid at the outside region of the funnel for $z = 0\ and\ z = L$:

$$outside\ of\ the\ funnel \Rightarrow \begin{cases} [A_{m1}J'_m(k_{r02}r_{01})+B_{m1}Y'_m(k_{r02}r_{01})] = \dfrac{ik_{z02}}{k_{r02}}[-A_{1z}e^{-ik_{z02}0}+A_{2z}e^{ik_{z02}0}] \\ [A_{m2}J'_m(k_{rL2}r_{L1})+B_{m2}Y'_m(k_{rL2}r_{L1})] = \dfrac{ik_{zL2}}{k_{rL2}}[-A_{1z}e^{-ik_{zL2}L}+A_{2z}e^{ik_{zL2}L}] \end{cases} . \quad (3.50)$$

The duct Boundary condition will give:

$$Duct\ B.C. \Rightarrow \begin{cases} [A_{m1}J'_m(k_{r02}r_{02})+B_{m1}Y'_m(k_{r02}r_{02})] = 0 , \quad A^2{}_{m1}+B^2{}_{m1}=1 \\ [A_{m2}J'_m(k_{rL2}r_{L2})+B_{m2}Y'_m(k_{rL2}r_{L2})] = 0 , \quad A^2{}_{m2}+B^2{}_{m2}=1 \end{cases} \qquad (3.51)$$

By solving the above 6 equations, 6 unknown parameters $2\,k_r$, $A_{m1}, B_{m1}, A_{m2}, B_{m2}$ can be found. It means that when the acoustic pressure field can be obtained by these parameters then the transmission loss is derived. For instance, consider that a FR with 0.6 m length is installed in a duct with 0.125 m diameter and $d_0 = 0.03\,m, d_L = 0.055\,m$, this model will be compared in next chapters, based on written MATLAB code the first five frequencies are 287, 578, 858, 1147, 1455 Hz.

3.3.5   Spiral-Helicoidal Resonator (SHR)

The combination of spiral and helicoidal resonators will give a new resonator, shown in Fig. 3.11, which has lower eigen-frequencies whereas, with the helicoidal resonator, these frequencies cannot be achieved.
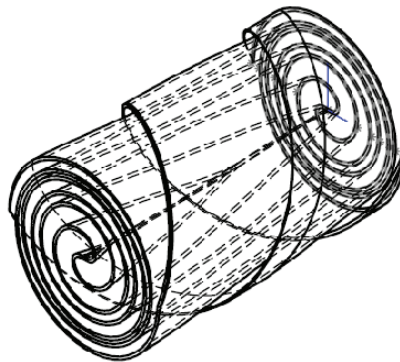
Figure 3.11: The Spiral-Helicoidal Resonator (SHR).

One of the advantages of SHR is that by rotating only 61 ° instead of 360 °, displayed in Fig. 3.12, the desired eigen-frequencies could be achieved with less pressure drop.
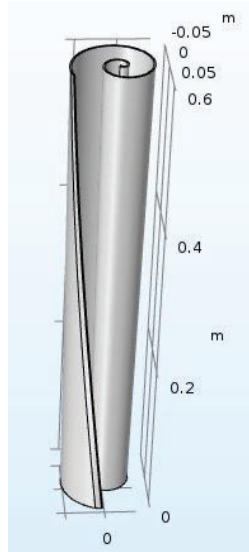
Figure 3.12: The spiral-helicoidal resonator with 61 ° helical rotation.

3.3.6 Funnel-Spiral-Helicoidal Resonator (FSHR)

The other combination of these three resonators termed Funnel-Spiral-Helicoidal Resonator (FSHR) is shown in Fig. 3.13. Based on the simulation results, this model has more eigen-frequencies lower than 1000 Hz and it has less pressure drop while the making process will become more complicated.
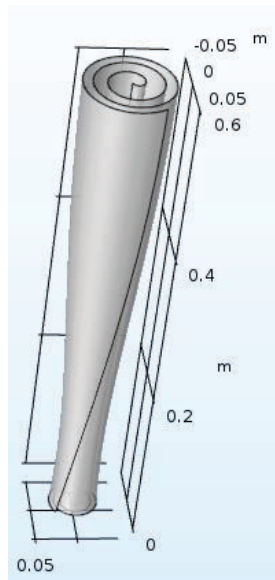

Figure 3.13: The funnel-spiral-helicoidal resonator.

3.3.7 Acoustic Black Hole effect

The Acoustic Black Hole (ABH) can be considered as a passive treatment for low frequency noise reduction inside the duct. A smooth decrease in the velocity of wave propagation in finite length is the main principle of the ABH. The ABH includes a specified number of tapered edges with particular distances from each other assembled inside a tube. The plates could be set on parallel form termed Normal Acoustical Black Hole (NABH) and a spiral tapered edge could also be used which is termed Spiral Acoustic Black Hole (SABH). These tapered edges should be smooth enough to cause no reflection by itself; also, the sound propagation inside the ABH will take extremely long time to reach the other part of the ABH, which is causing zero reflection therefore. The function of the inner diameter of the blades might be linear or quadratic, which are termed LABH and QABH respectively [19]. As mentioned before, the linear Euler's equation is [11]:

$$-\nabla p = (\rho_0 \frac{\partial V}{\partial t}),$$
(3.52)

where $V(x, y, z)$ is the fluid velocity at position *(x, y, z)*. In case of a narrow, axially symmetric waveguide of varying cross section, this equation can be written as:

$$-\frac{\partial p}{\partial z} = (\rho_0 \frac{\partial u}{\partial t}),$$
(3.53)

where u is the velocity component on the z axis. For varying cross section, the equation of continuity can be written as [19]:

$$d(\rho_0 Su) + (2\pi r v \rho_0)dz + \frac{\partial \rho}{\partial t} Sdz = 0,$$
(3.54)

where $S = S(z)$ and v is the projection of the velocity of fluid near the walls the perpendicular to the symmetry axis. The boundary admittance is defined as the quotient of the relative particle velocity and the sound pressure at the boundary [20], i.e.,

$$Y(z) = \frac{v_{rel}(z)}{p(z)},$$
(3.55)

where the relative particle velocity is defined as the difference between the particle velocities of the fluid and the structure. The reciprocal value is well known as the boundary impedance, defined as:

$$Z(z) = \frac{p(z)}{v_{rel}(z)} = \frac{1}{Y(z)} .$$

(3.56)

For many applications, it is useful to introduce dimensionless boundary admittances and impedances defined as [20]:

$$\tilde{Y}(z) = \rho c Y \quad and \quad \tilde{Z}(z) = \frac{Z}{\rho c} = \frac{1}{\tilde{Y}(z)} .$$

(3.57)

Substituting wall admittance in the equation of continuity, we obtain [19]:

$$-\frac{1}{\rho_0} \frac{\partial \rho}{\partial t} = u(\ln S)'_z + \frac{\partial u}{\partial z} + \frac{2Yp}{r} .$$

(3.58)

Taking into account the equality $\frac{\partial \rho}{\partial t} = \frac{1}{c^2} \frac{\partial p}{\partial t}$, the wave equation for the pressure will be [19]:

$$-\frac{1}{c^2} \frac{\partial^2 p}{\partial t^2} + \frac{2Y\rho_0}{r} \frac{\partial p}{\partial t} = \frac{\partial^2 p}{\partial z^2} + \frac{\partial p}{\partial z} (\ln S)'_z .$$

(3.59)

Assuming a time harmonic dependence of the acoustic pressure, $p(r,\phi,z,t) = p(r,\phi,z)e^{j\omega t}$, the equation reads in the frequency domain:

$$\frac{\partial^2 p}{\partial z^2} + \frac{\partial p}{\partial z} \frac{\partial (\ln S)}{\partial z} + p \left[k_0^2 + j\omega \frac{2Y}{r} \right] = 0 ,$$

(3.60)

where $k_0 \equiv \frac{\omega}{c_0}$ is a wave number. It should be noted that for zero-valued admittance Y, this equation transforms to the Webster equation. By considering the linear Euler's equation, the fluid particle velocity is related to the sound pressure by [20]:

$$v = \frac{\nabla p}{j\rho_0 \omega} .$$

(3.61)

3.3.8 Acoustic Black Hole muffler

The first model of Acoustic Black Hole muffler shown in Fig. 3.14 is proposed by Mironov [19].
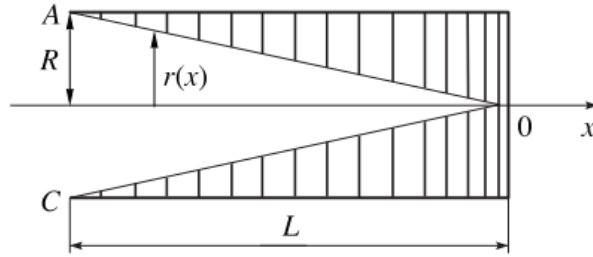
Figure 3.14: Acoustic Black Hole muffler.

In this model the linear radius function is expressed as:

$$r_{2x} = -\frac{R}{L}x \ \ and \ \ R = r_1 \ .$$ (3.62)

Hence, if the losses are neglected, the admittance in cylindrical coordinate would be [19]:

$$Y(r = r_z, \varphi, z) = (-j\omega)\frac{1}{\rho_0 c^2}\frac{R^2 - r_z^2}{2 \ r_z} \ .$$ (3.63)

Substituting the above equation into the wave equation for the pressure, and taking into account that $S = \pi r^2$, result in [19]:

$$\frac{\partial^2 p}{\partial z^2} + 2\frac{\partial p}{z \ \partial z} + p\left[\frac{k_0^2 R^2}{r^2}\right] = 0 \ .$$ (3.64)

For the linear Acoustic Black Hole muffler, this equation has a set of exact particular solutions in the form of power-law functions [19]:

$$p(z) = A_\alpha (z/L)^\alpha \ \ and \ \ \alpha_{1,2} = -\frac{1}{2} \pm \sqrt{\frac{1}{4} - (k_0 L)^2} \ .$$ (3.65)

Due to the closed end of the ABH muffler, it cannot be used inside the duct directly and it requires some modifications to be suitable for applying in the ventilation systems. For instance, the ABH muffler could be easily installed inside the T-joint to absorb the incident wave energy of the flow which is shown in Fig. 3.15. The size of the ABH muffler is suitable to apply in any bend pipe, elbows, and it has a negligible pressure drop. If the air flows into the ABH muffler, it might cause turbulences which results in no absorption. Therefore, the appropriate solution can include a membrane in front of the ABH muffler to allow only the

sound waves go into the ABH muffler. In short, this method is as a reliable way to get rid of the low frequency noise inside the duct with low investment.
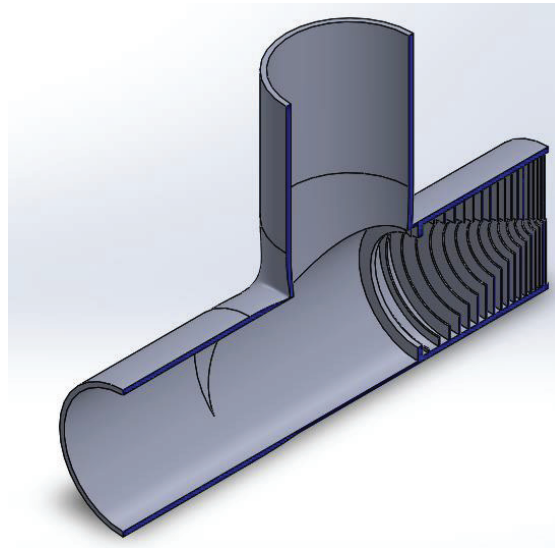
Figure 3.15: Section view of the Acoustic Black Hole muffler installing inside the T-joint.

3.3.9 External Acoustic Black Hole muffler

The second model of Acoustic Black Hole muffler, shown in Fig. 3.16, is termed External Acoustic Black Hole (EABH) muffler [19].
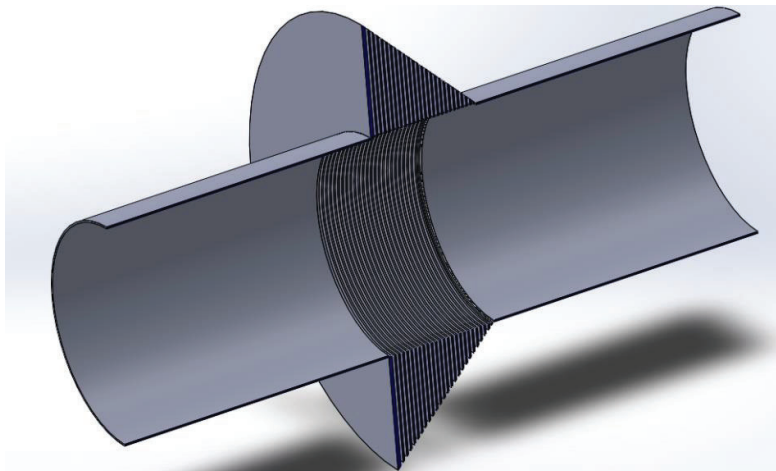

Figure 3.16: Section view of External Acoustic Black Hole muffler.

As mentioned before, the pressure could be written as $P(r,\varphi,z,t) = R(r)\Phi(\varphi)Z(z)T(t)$. So, the dimensionless admittance could be expressed as [21]:

$$\widetilde{Y}(r=r_1) = \frac{\rho c}{j\rho_0\omega} \frac{J'_m(k_r r_1) - \dfrac{J'_m(k_r r_2)}{Y'_m(k_r r_2)} Y'_m(k_r r_1)}{J_m(k_r r_1) - \dfrac{J'_m(k_r r_2)}{Y'_m(k_r r_2)} Y_m(k_r r_1)},$$ (3.66)

where $m=0$ due to the axisymmetric mode. In this model the linear radius function is expressed as:

$$r_{2x} = r_1 + \alpha * x \ .$$ (3.67)

Hence, if the losses are neglected, assuming $k_r r_1 \ll 1 \ and \ k_r r_2 \ll 1$ and making use of Taylor's expansions of Bessel function for $m=0$, see Appendix A, the wall admittance equation in cylindrical coordinate is simplified to the previous formula in Acoustics Black Hole as below, and then the solution is the same as mentioned before:

$$Y(r=r_1) = \frac{\rho c k_r r_1}{j\rho_0\omega} \frac{(\frac{r_2}{r_1})^2 - 1}{2}.$$ (3.68)

In summary, various resonators and mufflers are introduced and governing equations are derived. The differences between HR, SR, and FR are only on their boundary conditions, i.e., the surface which installs inside the tube. These differences shift the axial and radial wave numbers that causes noise absorption at the defined frequencies. In mufflers, the length of channels are important. Moreover, the function of increasing the length of channels has a strong effect on the transmission loss of mufflers. In this chapter to find the analytical solution, models are simplified and main equations are just expressed. However, it is possible to work on the detail of each resonator and muffler. Also, it should be noted that more time is needed to adapt the solution and results with a practical result which will be discussed in next chapters.

Chapter 4

4. Treatment Validation

4.1 Introduction

In the third task of the design cycle, treatment validation phase, the noise reduction systems are designed and simulated by commercial software SolidWorks, COMSOL, and MATLAB. COMSOL Multiphysics is a simulation software and in this project pressure acoustic and solid mechanics modules of COMSOL are used. In some simulations, it is needed to solve the coupled acoustic-structure equations so a multiphysics module is applied for an acoustic-structure interaction (ASI). Moreover, for taking into account losses in mufflers, a poroacoustics module with Delany-Bazley-Miki model has been applied [16]. A flow resistivity of $80\,Pa.\sec/m^2$ was used. The performance of the numerical results will determine the development of the first samples. This will result in the detail design and development phase where prototypes will be built and tested.

4.2 Helicoidal Resonator

The first model is the helicoidal resonator similar to the Łapka's model (involves the helicoidal resonator with a muffler) shown in Fig. 4.1:
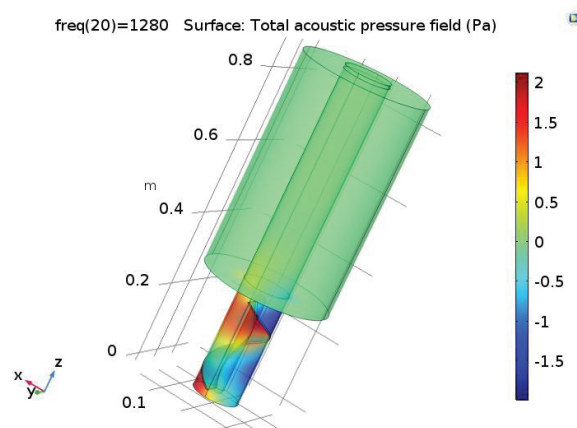
Figure 4.1: The helicoidal resonator with the muffler.

The transmission loss of three combinations of the HR and the muffler are depicted in Fig. 4.2. To compare and validate the simulation model, the transmission loss of the Łapka's model [22] is also presented in Fig. 4.3.
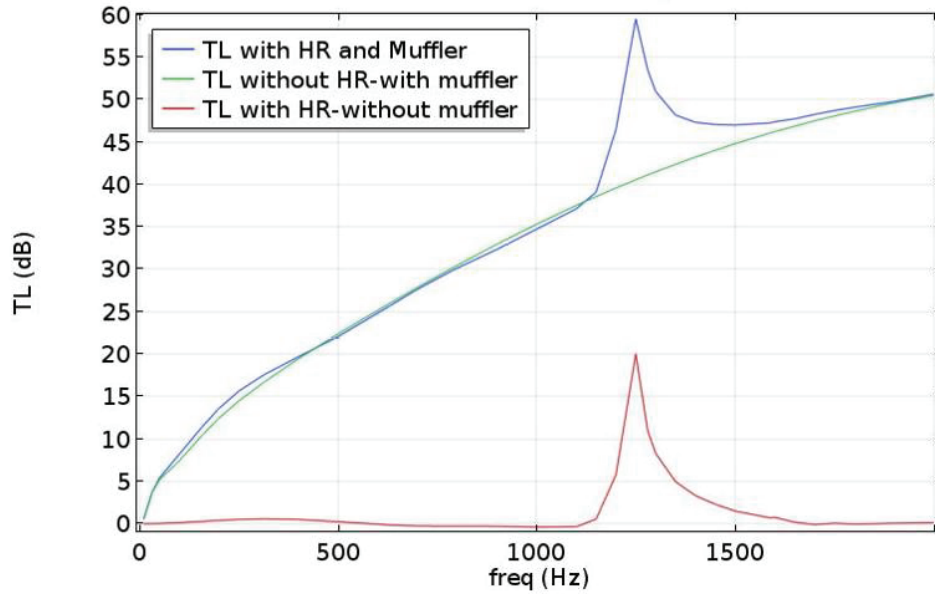
Figure 4.2: Transmission loss of the helicoidal resonator combine with a muffler.
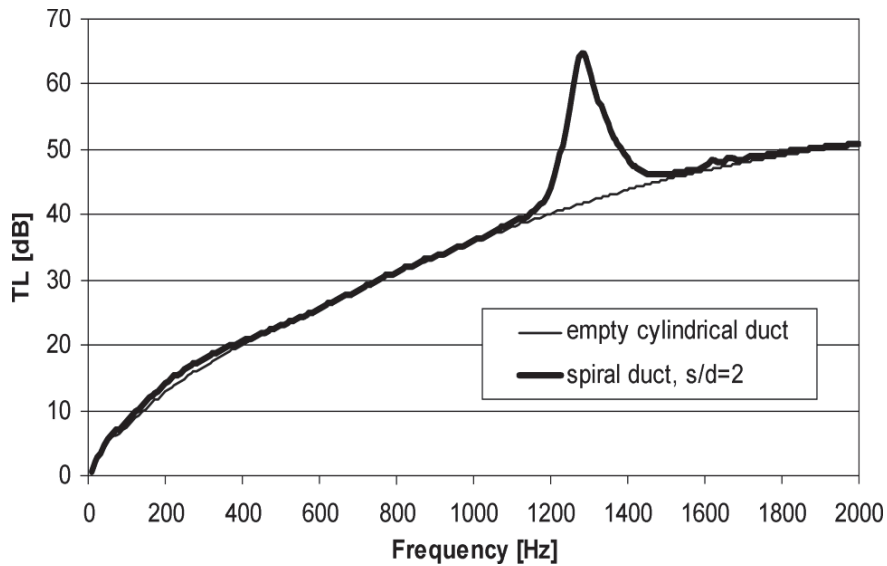
Figure 4.3: Transmission loss of the Lapka's model for the helicoidal resonator with a muffler [22].

By comparing Fig. 4.2, with Fig. 4.3, it can be concluded that the simulation models are similar which results in using this model of simulation for the other resonators.

To find out the performance of the helicoidal resonator, the pressure acoustics of two models i.e. flat plate and helicoidal resonator inside the ducts at their first eigen-frequencies are depicted in Fig. 4.4.
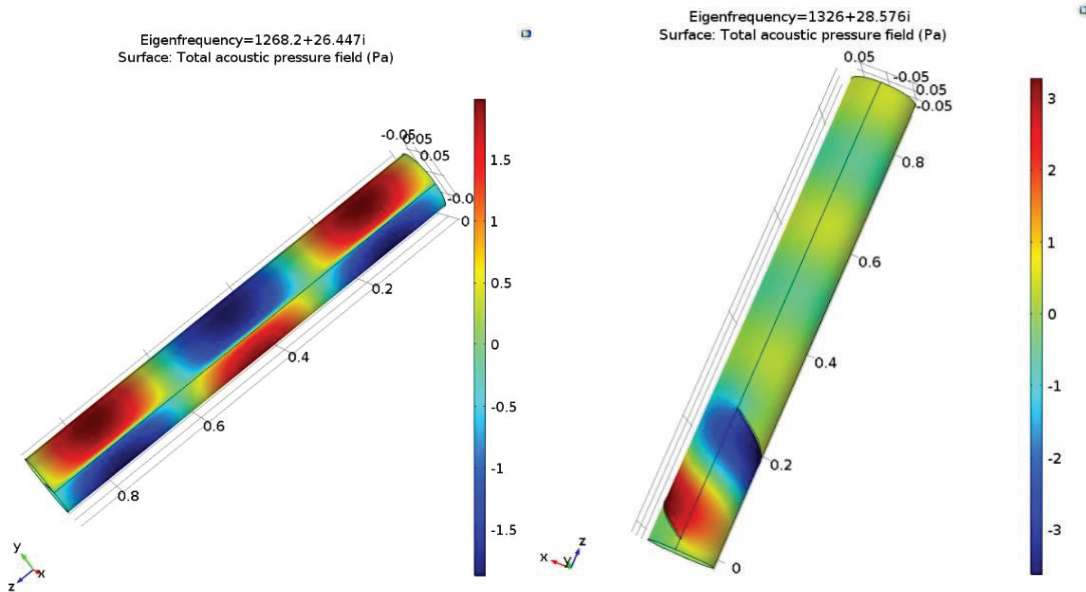
Figure 4.4. The numerical solution of inserting a flat blade and helicoidal resonator inside the duct.

As can be seen in Fig. 4.4 unlike the flat plate inside the duct, the positive pressure region of the air with the negative pressure region after the helicoidal resonator are mixed which causes noise attenuation at that first eigen-frequency. The advantage of the helicoidal resonator is to tune the noise and it cancels the noise at the first eigen-frequency. The MATLAB code based on analytical solution is written and the comparison of the COMSOL simulation's result with the analytical solution is demonstrated in Table 4.1:

Table 4.1: First eigen-frequency determined with analytical and numerical solutions.

Resonator	Specification	Numerical result	Analytical Result
Helicoidal resonator Without mandrel	Length: 0.247 m, R=0.0625 m Thickness: 5 mm	1331 Hz	1335 Hz
Helicoidal resonator Without mandrel	Length: 0.5 m, R=0.0625 m Thickness: 1 mm	1108 Hz	1102 Hz
Helicoidal resonator Without mandrel	Length: 0.7 m, R=0.0625 m Thickness: 1 mm	1066 Hz	1060 Hz
Plate inside the duct Without mandrel	Length: 0.254 m, R=0.0625 m Thickness: 1 mm	1244 Hz	1221 Hz
Helicoidal Resonator with mandrel	Length: 0.254 m, R=0.0625 m Thickness: 1 mm	1130 Hz	1129 Hz

4.3 Spiral Resonator

One of the spiral resonators with three spiral turns and the length of 0.5 m which is possible to put inside the ventilation duct is simulated in this section. As mentioned before, to force the air to have spiral rotation, half part of the one ends is closed (see. Fig. 3.9). The acoustic pressure field at the first eigen-frequency of this model, 430 Hz, is displayed in Fig 4.5:
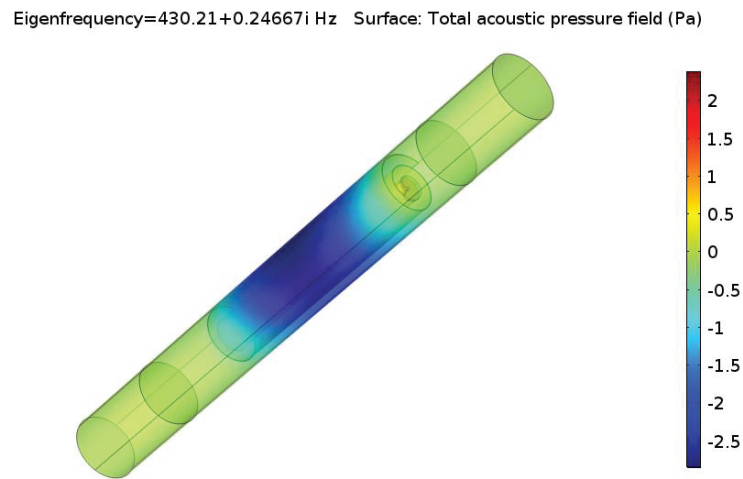

Figure 4.5: Acoustic pressure filed of the spiral resonator at first eigen-frequency.

The transmission loss of the mentioned spiral resonator at 400 Hz to 1150 Hz is shown in Fig. 4.6.
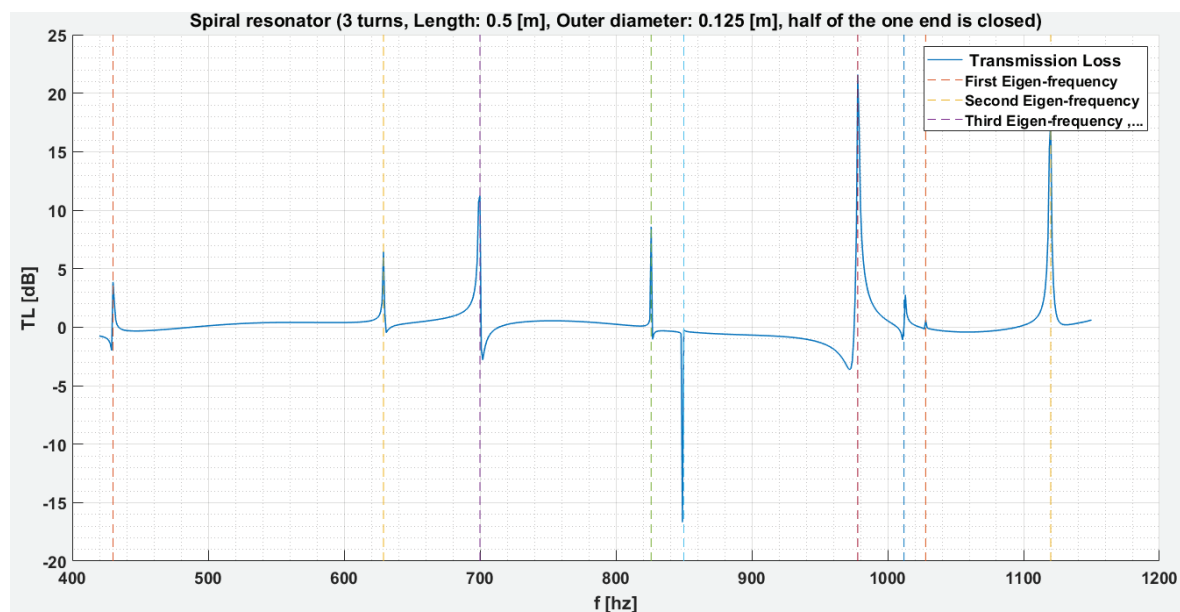
Figure 4.6: Transmission loss of the spiral resonator with three spiral turns.

As can be seen in Fig. 4.6 the eigen-frequencies are 430, 629, 700, 826, 850, 978, 1012, 1028 Hz. If the length of spiral resonator decreases to 0.254 m and half of the both ends are closed, then the first and second eigen-frequencies are shifted to the right which is shown in Fig. 4.7:
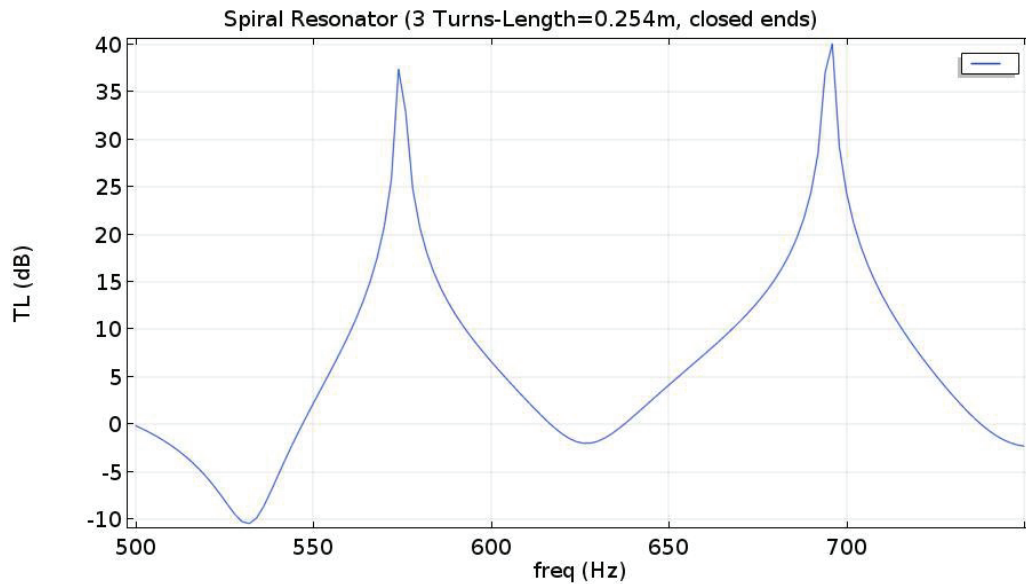
Figure 4.7: Transmission loss of the spiral resonator at the first to the second eigen-frequencies.

It should be mentioned that, using the helicoidal resonator with the same length the first eigen-frequency which caused noise attenuation was 1273 Hz while using the spiral resonator, it drops to 578 Hz that cannot be achieved by the helicoidal one anymore.

If the double spiral resonator with three spiral turns and 0.8 m length is used, then the TL will become as Fig. 4.8:
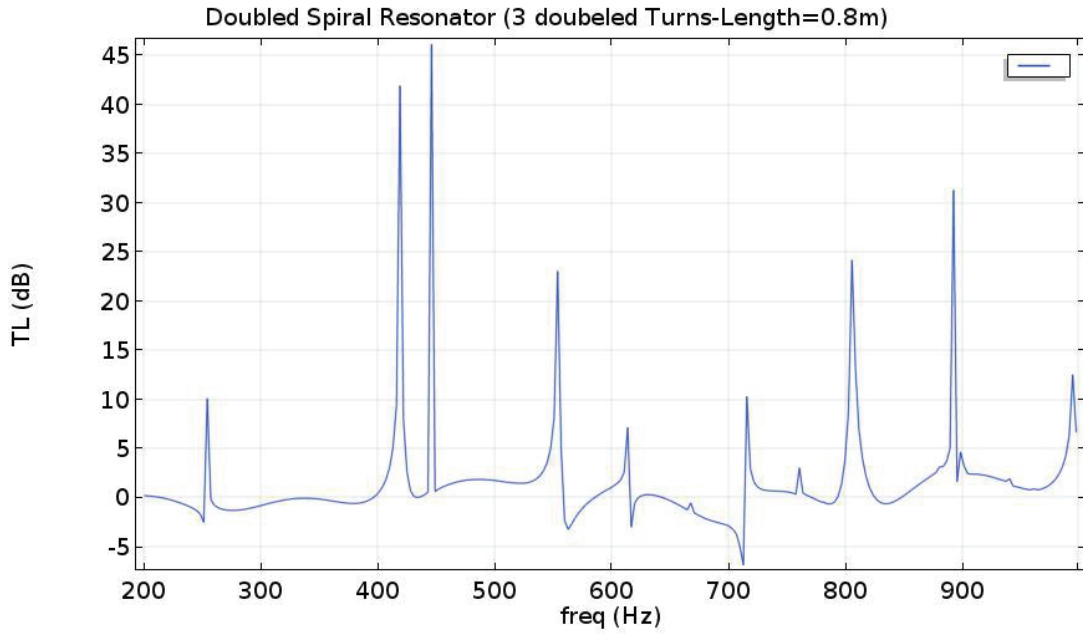
Figure 4.8: Transmission loss of the double spiral resonator.

4.4 Funnel Resonator

The next resonator is the funnel resonator, this resonator has simple shape, and it can absorb the noise at its low eigen-frequencies. The transmission loss of the funnel resonator with 0.5 m length is demonstrated in Fig. 4.9:
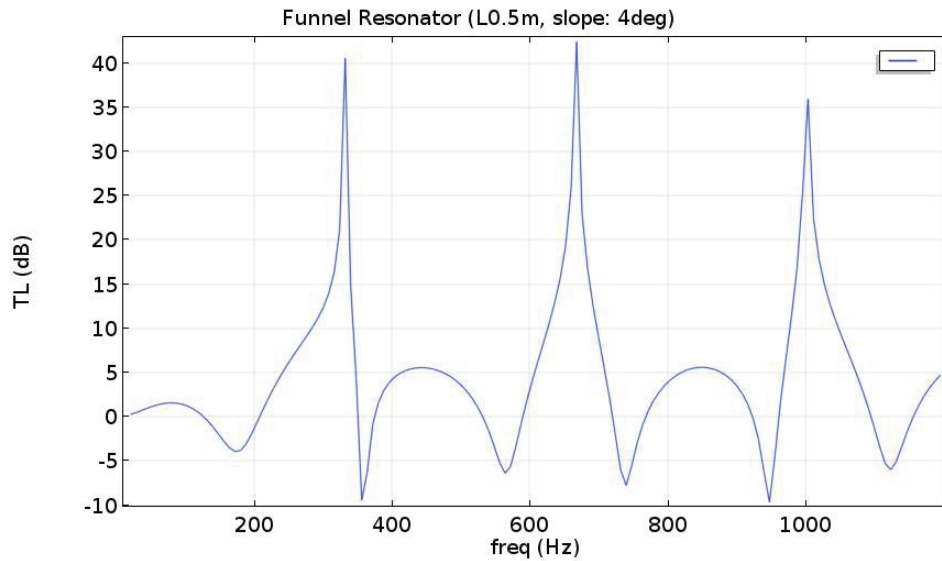
Figure 4.9: Transmission loss of the funnel resonator.

If the length of the funnel increases up to the 0.6 m and decreases the slope to the 2.36 degree, then the first eigen-frequency would be 272 Hz, i.e., the critical frequency of the fan,

50

which is our desired frequency. The acoustic pressure field of the FR at the first eigen-frequency and TL of this resonator are plotted in Fig. 4.10 and Fig. 4.11 respectively.
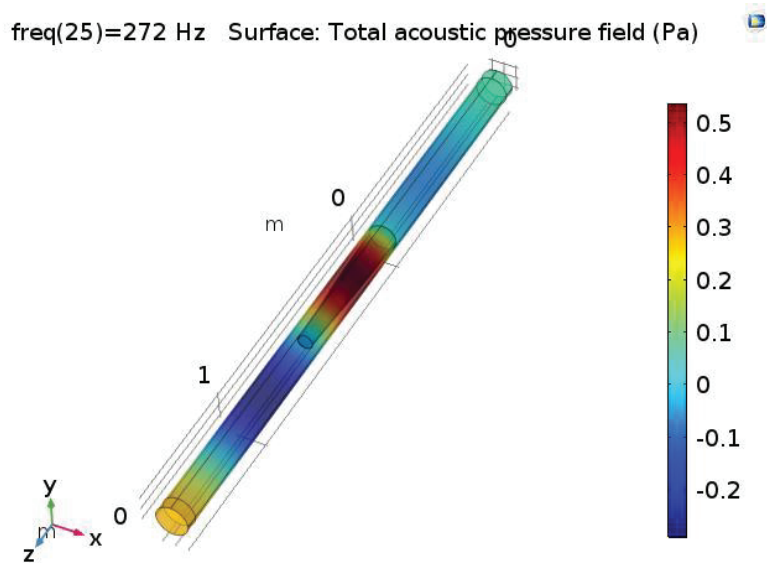
Figure 4.10: Acoustic pressure filed of the funnel resonator at the first eigen-frequency.
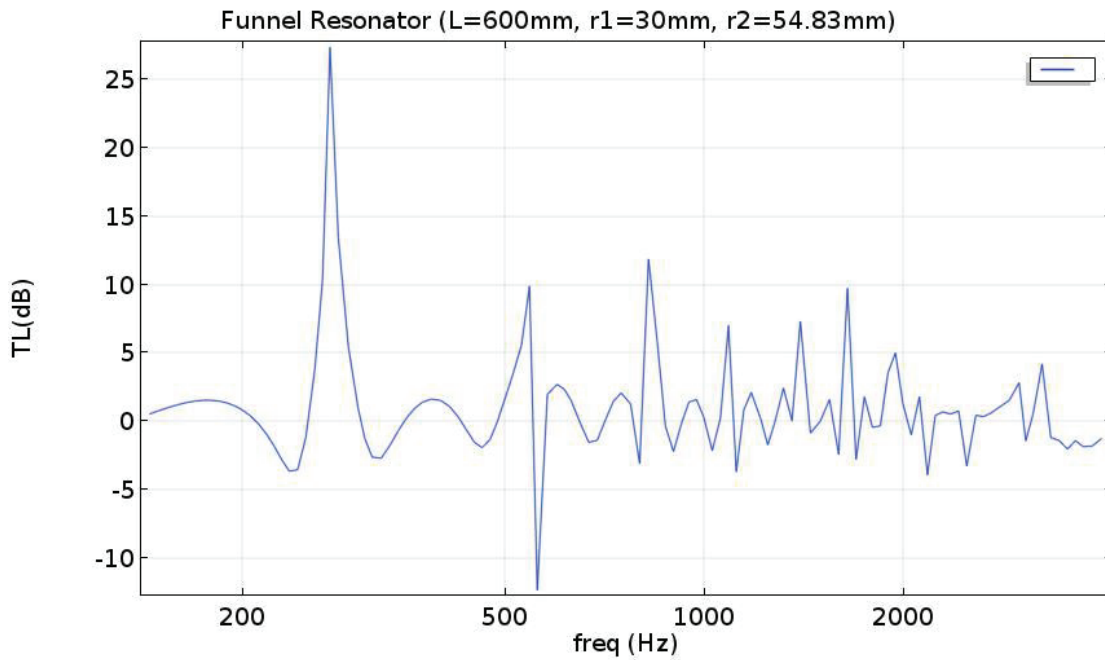
Figure 4.11: Transmission loss of the funnel resonator.

As can be seen in Fig. 4.11, the second and third eigen-frequencies, i.e., 553 Hz and 831 Hz are 2 and 3 times of the first one, 273 Hz,.

4.5 Spiral-Helicoidal Resonator

The combination of the spiral and helicoidal resonators will give lower eigen-frequencies in comparison with the helicoidal resonator. For instance, the acoustic pressure field of the SHR with 0.6 m length, 2 spiral turns, and 61° of helical turning is presented in Fig. 4.12 at its third eigen-frequency.
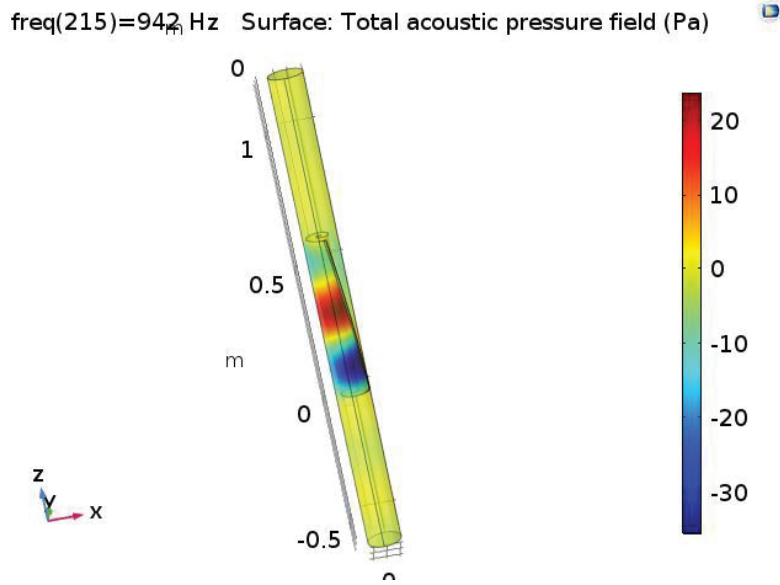
Figure 4.12: Acoustic pressure field of the spiral-helicoidal resonator at the third eigen-frequency.

Moreover, the transmission loss of this SHR is presented in Fig. 4.13:
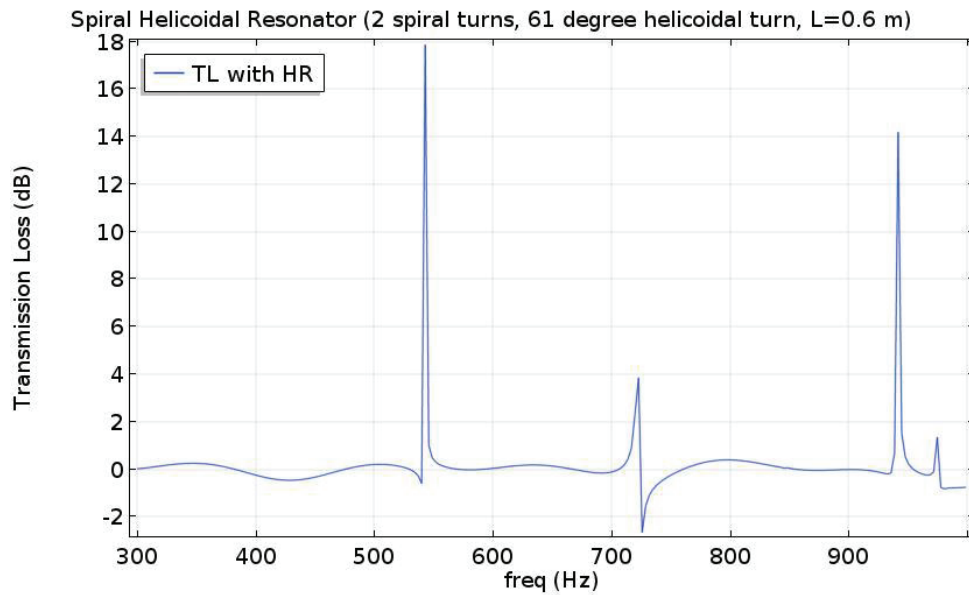
Figure 4.13: Transmission loss of the spiral_helicoidal resonator.

4.6 Funnel-Spiral-Helicoidal Resonator

The combination of these various resonators will give results which are better for broadband noise reduction while the fabrication process will become more complicated. For instance, the TL result of the FSHR is presented in Fig. 4.14 to show that the low frequency noises can be absorbed with only 0.45 m.
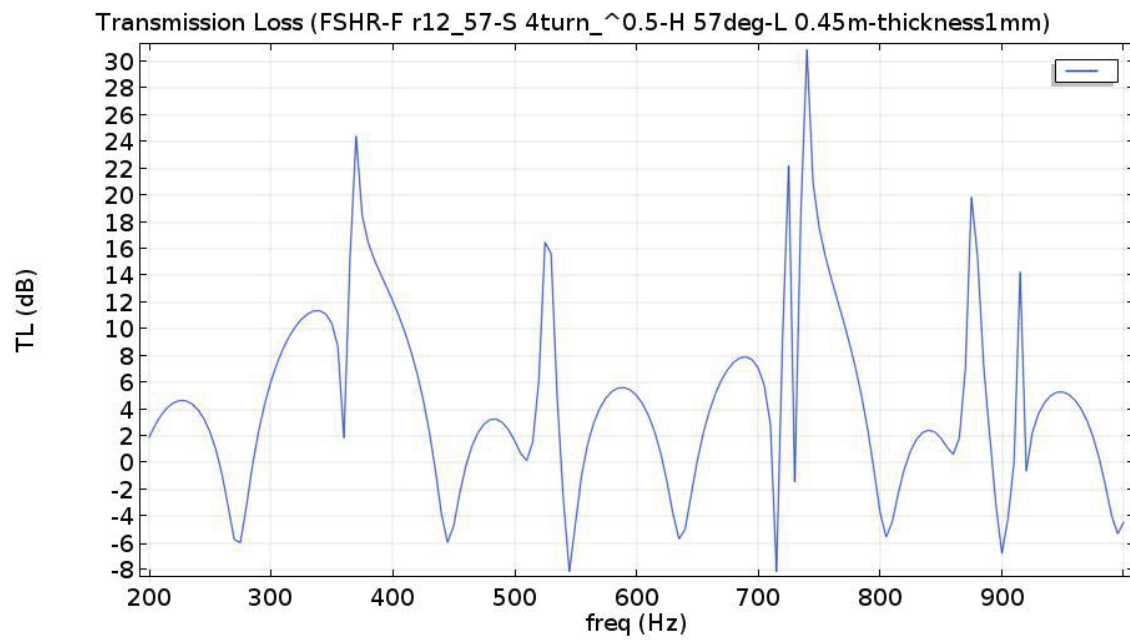

Figure 4.14. Transmission loss of the funnel_spiral_helicoidal resonator with 0.45 m length.

4.7 Acoustic Black Hole muffler

As mentioned in the previous chapter, the Acoustic Black Hole muffler can be installed inside the T-joint. For instance, the acoustic pressure field at 300 Hz is shown in Fig. 4.15:
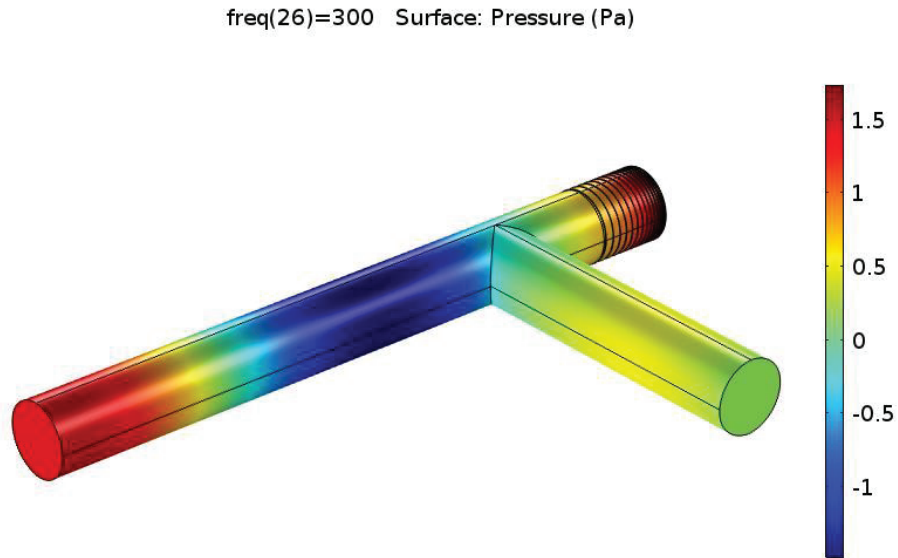
Figure 4.15. Acoustic pressure field of the ABH at 300 Hz.

This model is simulated similar to the real test setup that it will be discussed in Chapter 6, Section 5. The transmission loss of the ABH muffler with 135 mm length is shown in Fig. 4.16.
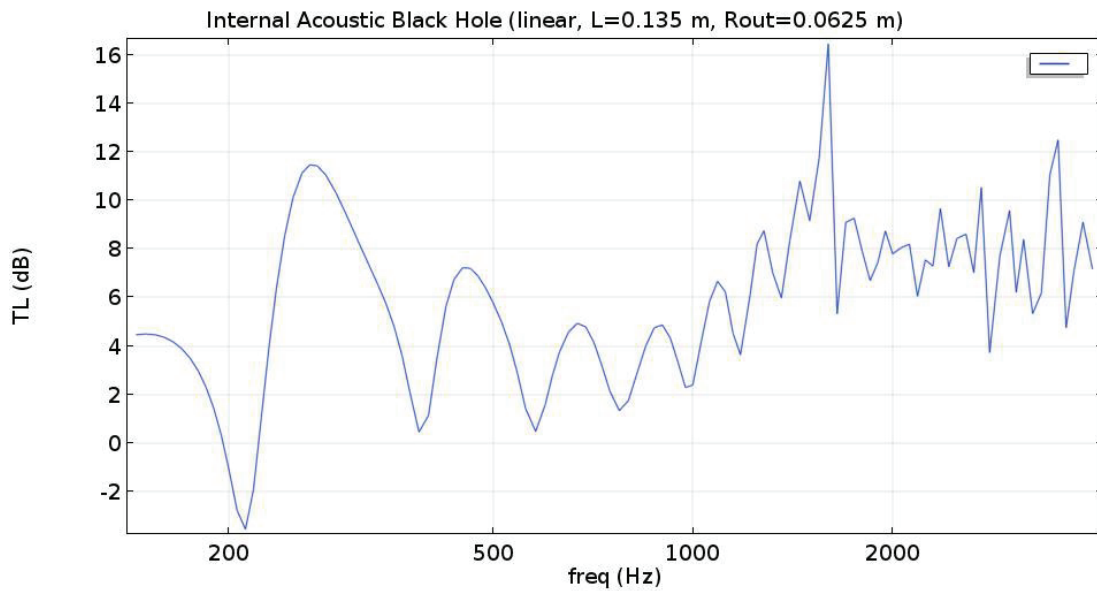

Figure 4.16. Transmission loss of the Acoustic Black Hole muffler.

As can be seen in Fig. 4.16, the ABH muffler can absorb broadband noise. The main noise reduction occurs between 230 Hz and 1700 Hz. The eigen-frequencies of this model are 285, 433, 609, 731, 834, 941, 1055, 1178, 1306, 1452, 1610, 1619, 1620, 1624, 1631, 1632… Hz.

4.8 External Acoustic Black Hole muffler

Due to the long channel needed to reduce the low frequency noise by the EABH muffler (see Fig. 3.16), the developed shape of external Acoustic Black Hole muffler should be used to achieve the desired goal in a short length. For instance, the front section view of half part of the EABH muffler is shown in Fig. 4.17 with 182 mm length, 62.5 mm, 127 mm inner and outer radiuses. The performance of this model is similar to the known External Acoustic Black Hole muffler.
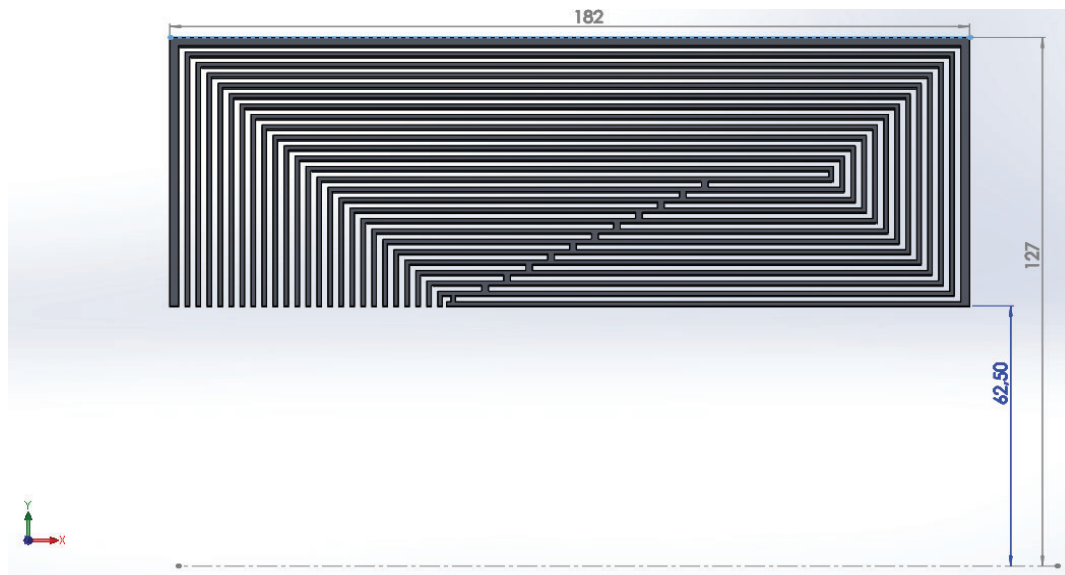
Figure 4.17. Front section view of the external Acoustic Black Hole muffler.

The transmission loss of the mentioned EABH muffler by considering Acoustic-Structure Interaction is depicted in Fig. 4.18:

EABH muffler (Outer diameter: 254 [mm], Inner diameter: 125 [mm], Length: 182 [mm]) considering Acoustic Structure Interaction
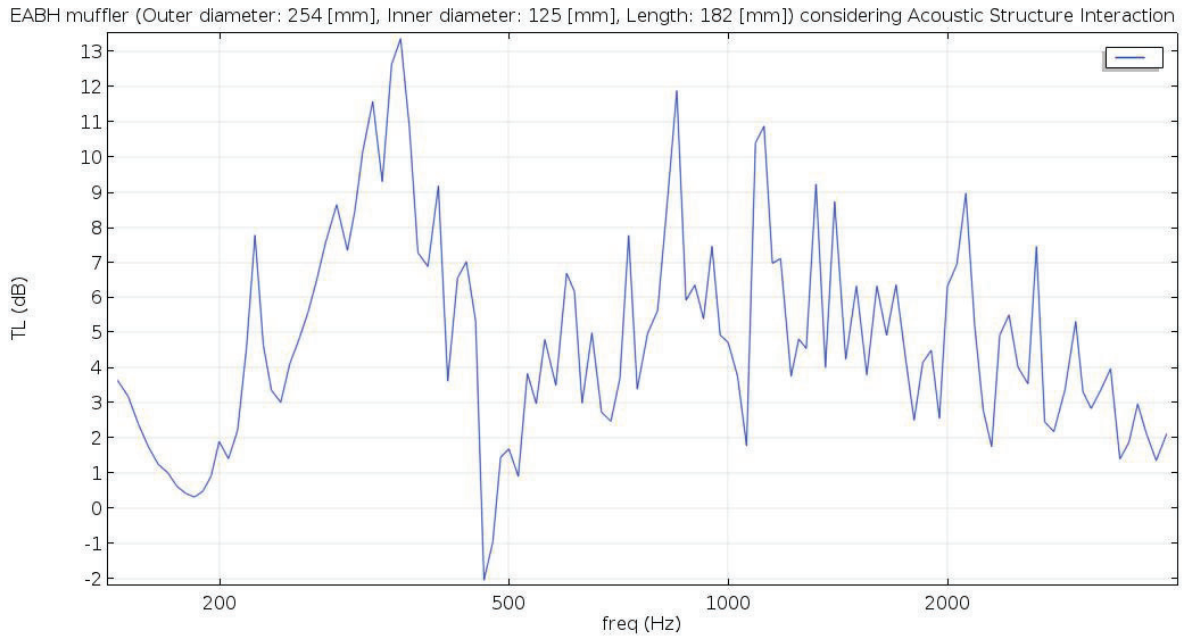

Figure 4.18: Transmission loss of the external Acoustic Black Hole muffler.

As can be seen in Fig. 4.18, this type of the muffler can be used as a broadband noise reduction system which can absorb even the noise at 270 Hz and even less. But to demonstrate the performance of this muffler, the power level of the fan at 325 m^3/h flowrate is considered then the EABH muffler is installed surrounding the duct in COMSOL simulation. The Insertion loss by considering Acoustic-Structure Interaction (ASI) is evaluated afterwards. The above EABH muffler could deduct 6.2 dB shown in Fig. 4.19:
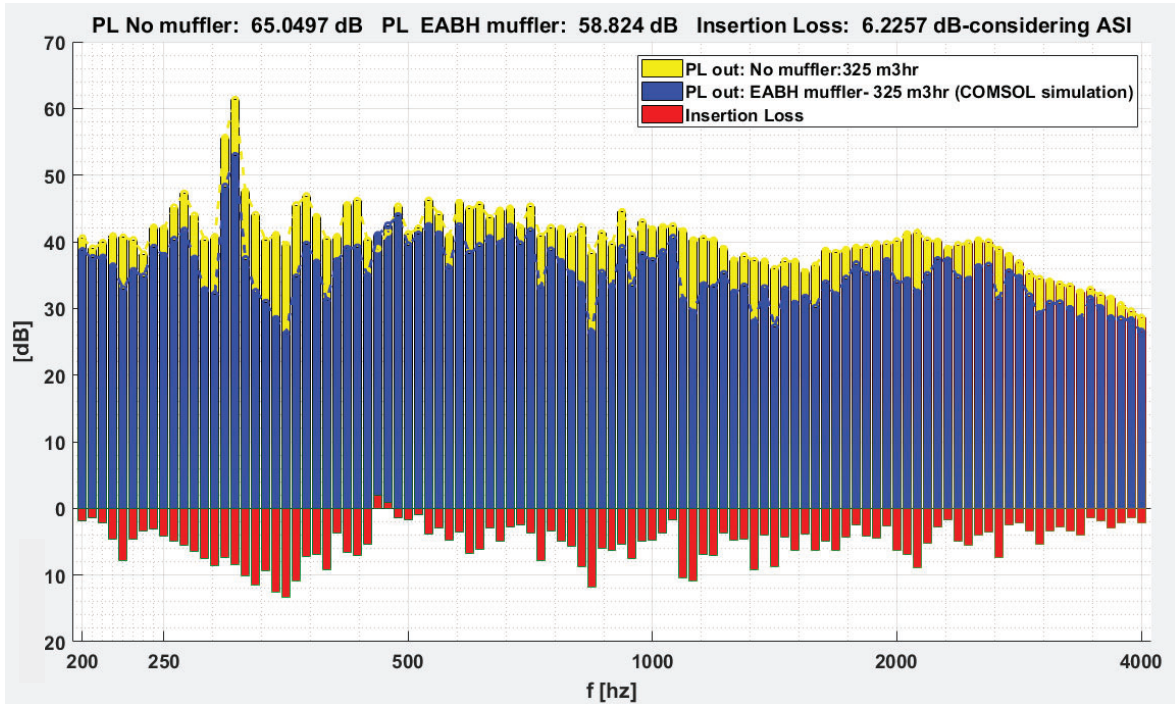
Figure 4.19: power level and Insertion Loss of the EABH muffler with considering ASI

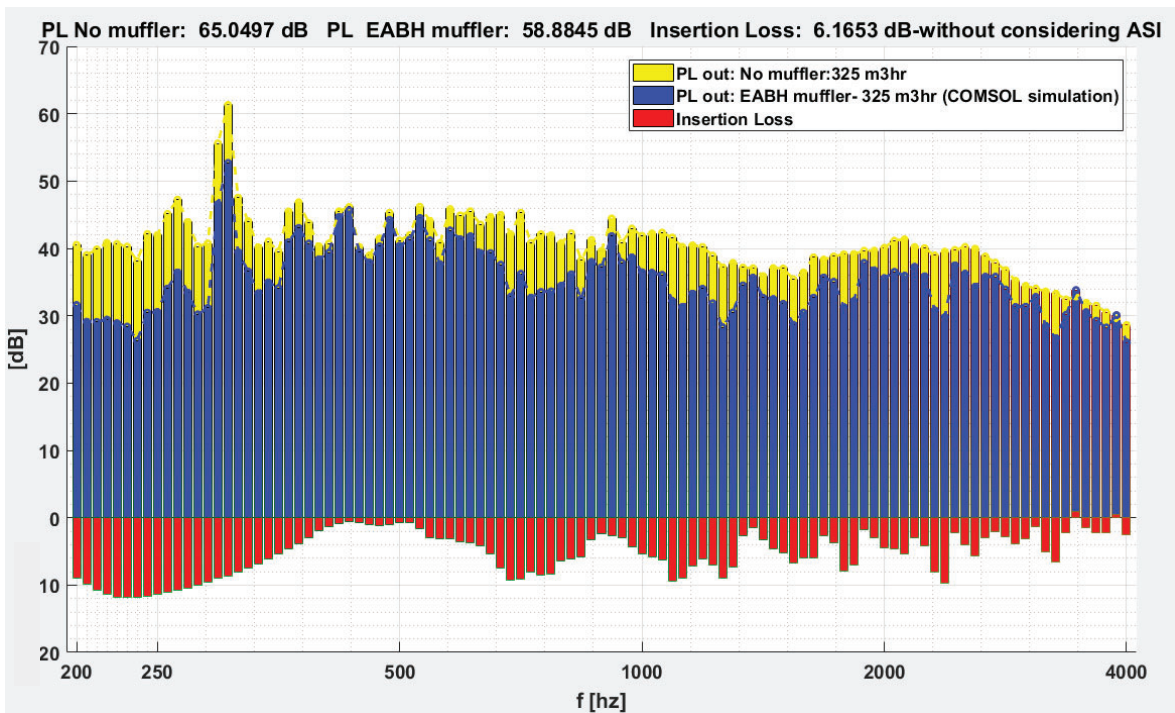If acoustic structure interaction is not considered, then the results will be like in Fig. 4.20:

Figure 4.20: Power level and transmission loss of the EABH muffler without considering ASI.

Comparing Fig. 4.19 and Fig. 4.20 reveals that a big differences is observed when ASI is not considered at low frequencies. Hence, it is recommended to use multi-physics module in IABH

and EABH simulation. Using three series EABH with 182 mm length, in total 546 mm, can be one of the best options to deduct the broadband noise more than 18 dB.

4.9 Cylindrical muffler

The new innovation termed Cylindrical Muffler (CM) is simulated to evaluate the performance of this muffler. For instance, the front section view of the CM with 25 compacted Loops is shown in Fig. 4.21.
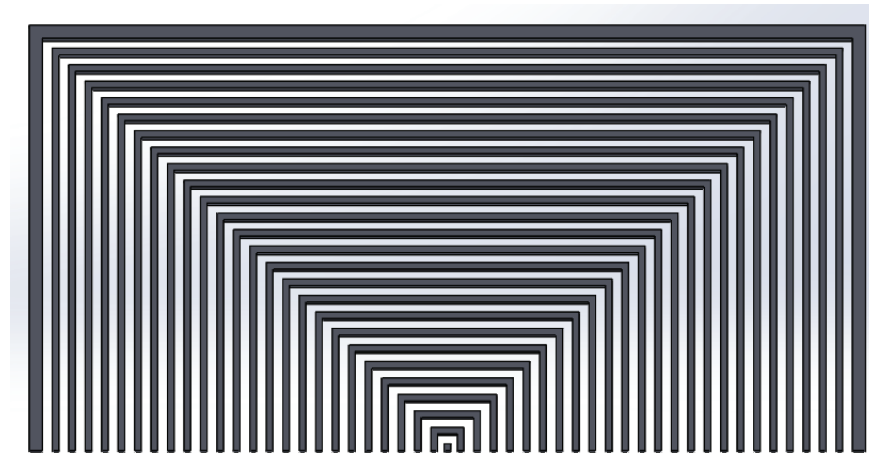

Figure 4.21: Front section view of the cylinder resonator with 25 compact Loops.

Moreover, in Fig. 4.22, the acoustic pressure field of the one loop CM with the outer radius 0.23 m, and 0.33 m length at the first eigen-frequency (248 Hz) is demonstrated.
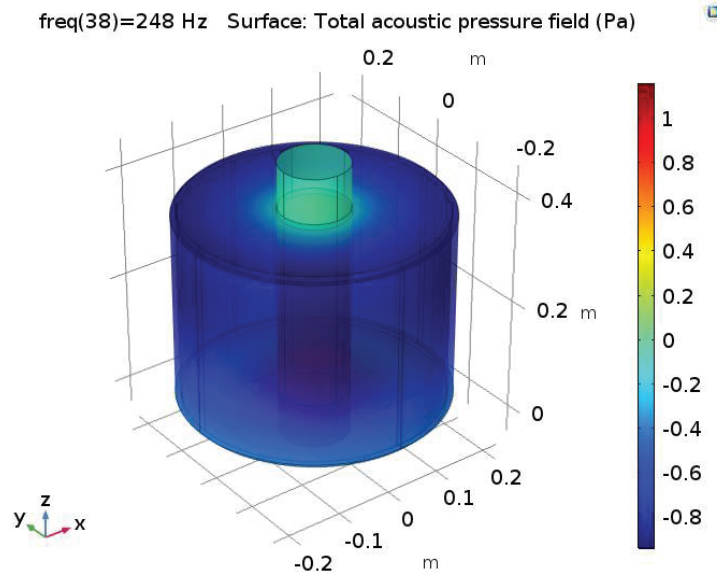

Figure 4.22: Acoustic pressure field of the one loop cylindrical muffler at the first eigen-frequency.

Transmission loss of the one loop cylindrical muffler is depicted in Fig. 4.23. As can be seen, the second and third eigen-frequencies are 2 and 3 times of the first one which is not possible to achieve with the known side resonators nor Acoustic Black Hole mufflers.
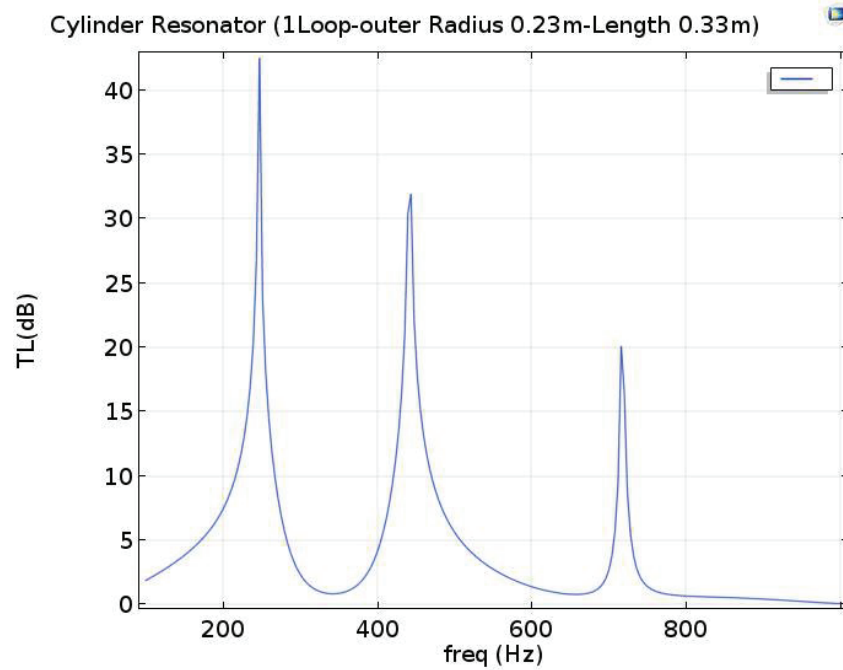

Figure 4.23: Transmission loss of the one loop cylindrical muffler.

Also, the acoustic pressure field of the two loops cylindrical muffler inside each other at the first and second eigen-frequencies are exposed in Fig. 4.24:
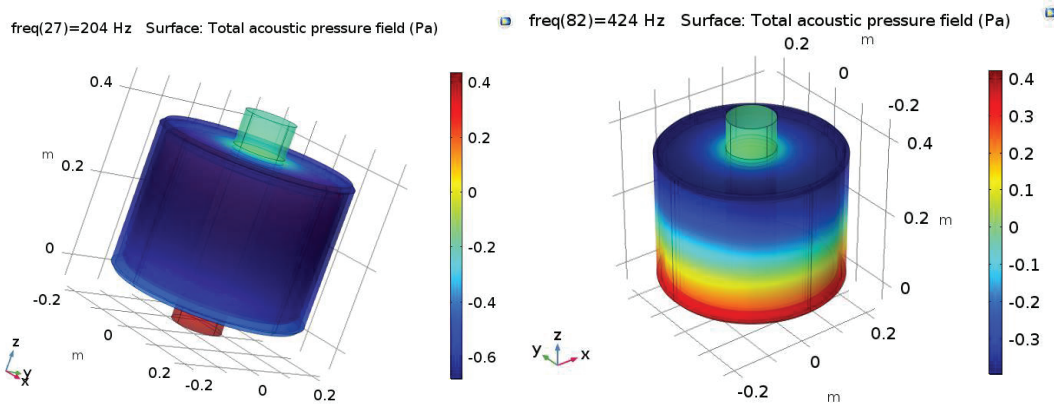

Figure 4.24: Acoustic pressure field of the two loops CM at the first and second eigen-frequencies.

The TL of the CM with 2 loops is presented in Fig. 4.25:

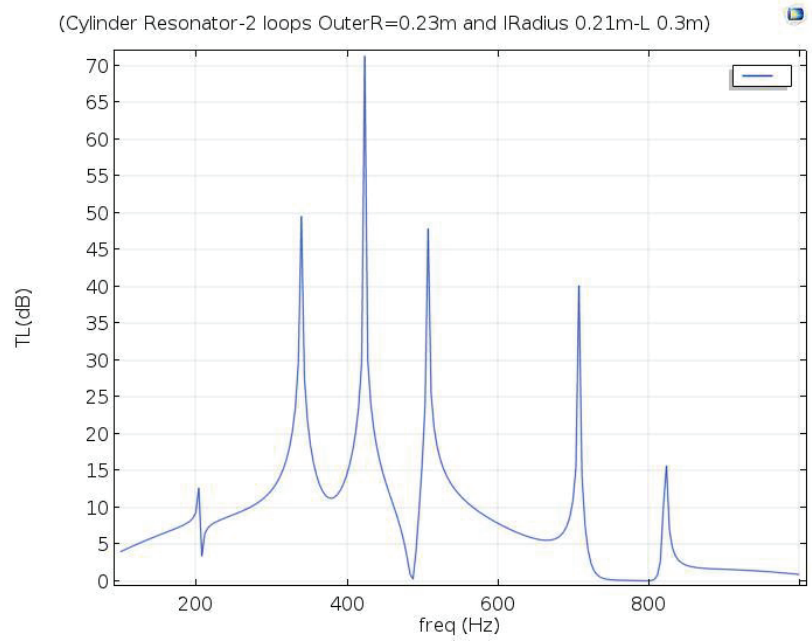(Cylinder Resonator-2 loops OuterR=0.23m and IRadius 0.21m-L 0.3m)

Figure 4.25: Transmission loss of the cylindrical muffler with 2 loops.

Better results could be achieved by increasing the number of loops. For instance, the transmission loss of the mentioned CM with 25 compacted Loops (see Fig. 4.21) is shown in Fig. 4.26. The thickness of the walls is 1 mm and the distance between walls is 1.5 mm. As can be seen in Fig. 4.26, the cylinder resonator with only 125 mm length can reduce the noise 9 dB. The point is that this resonator is useful for the frequencies more than 1000 Hz.
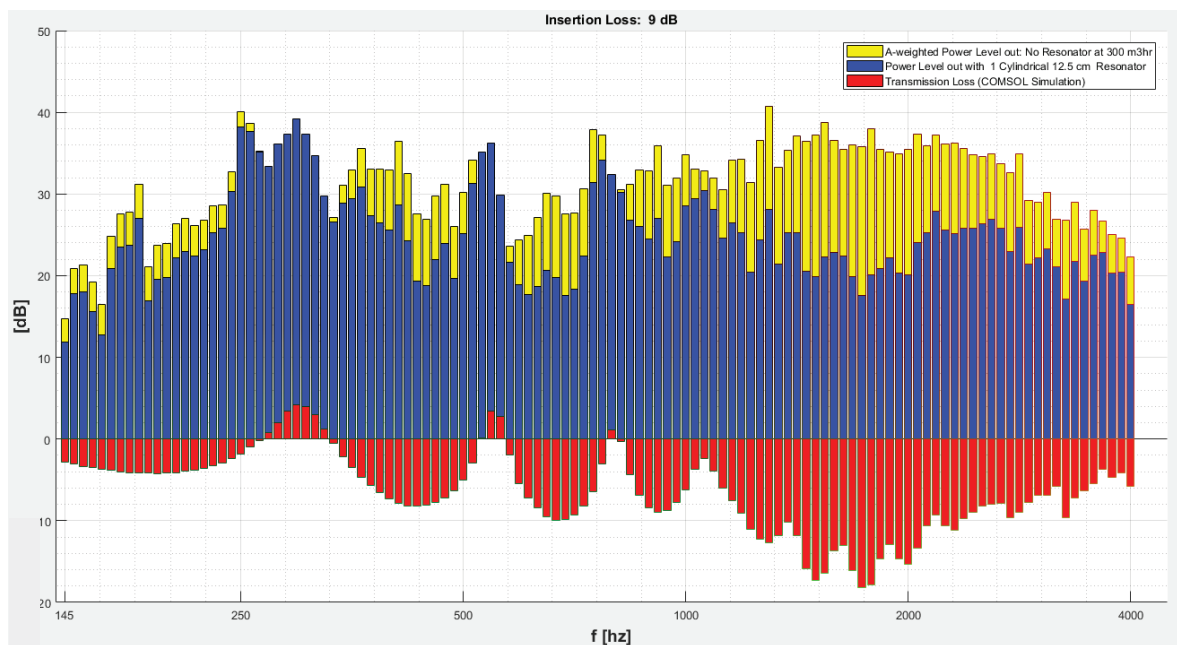

Figure 4.26: Transmission loss of the cylindrical muffler with 25 loops.

On the other hand by increasing the length of the CM, the low frequency noise can easily be absorbed. For instance, adding three long models of CM shown in Fig. 4.27 with 230 mm length, in total 690 mm, has a strong ability to remove the noises around 350 Hz. This result is depicted in Fig. 4.28:

Figure 4.27: Front section view of the long cylinder resonator with 12 Loops.
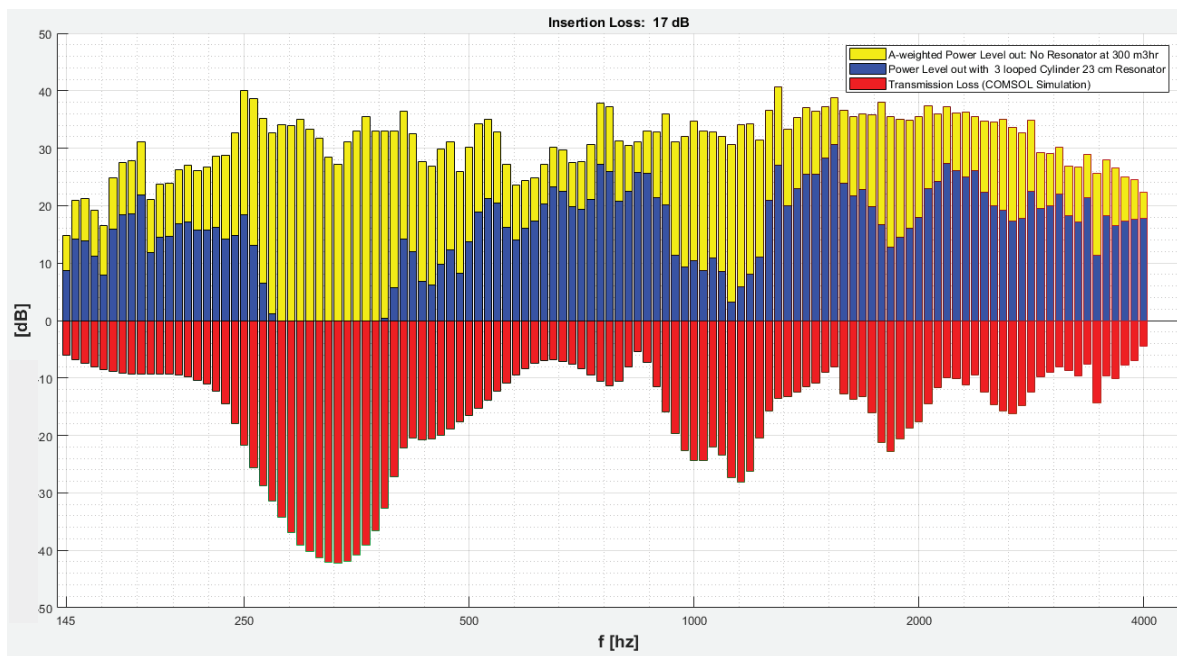

*Figure 4.28: Transmission loss of the three long cylindrical muffler (3*230 mm) with 12 loops.*

Based on the simulation result of the EABH and CM between 270 Hz and 400 Hz which are shown in Fig. 4.19 and Fig. 4.28, it can be concluded that the combination of the EABH muffler and cylindrical muffler could easily remove noises at any desired frequencies.

4.10   Internal Acoustic Black Hole muffler

The ventilation unit of the Brink Climate Systems is depicted in Fig. 4.29. This unit has two fans which transfer the airflow via two diffusers, shown in Fig 4.29, to the residential space and outside of the house. To hear less noise in residential space, two solutions can be implemented by applying external Acoustic Black Hole muffler. First the muffler can be considered as an accessory and installed outside the unit, second the muffler can be installed inside the unit in the diffuser. The second solution has more priority than the first one for the stakeholders, however it produces more pressure drop which means the fan needs more power to work and energy efficiency will drop a little bit.

Figure 4.29: Ventilation unit of the Brink Climate Systems.

The object is to design the internal Acoustic Black Hole muffler inside the diffuser. A part of the ventilation unit's model is demonstrated in Fig. 4.30 which involves the muffler inside the diffuser.
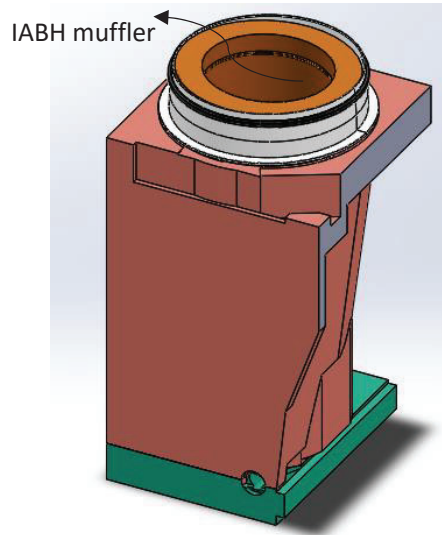
Figure 4.30: The diffuser part of the ventilation unit with the IABH muffler inside it.

As can be seen in Fig. 4.31, the cross section view of the diffuser, due to the unsymmetrical shape of the diffuser the size of the muffler has extra limits.
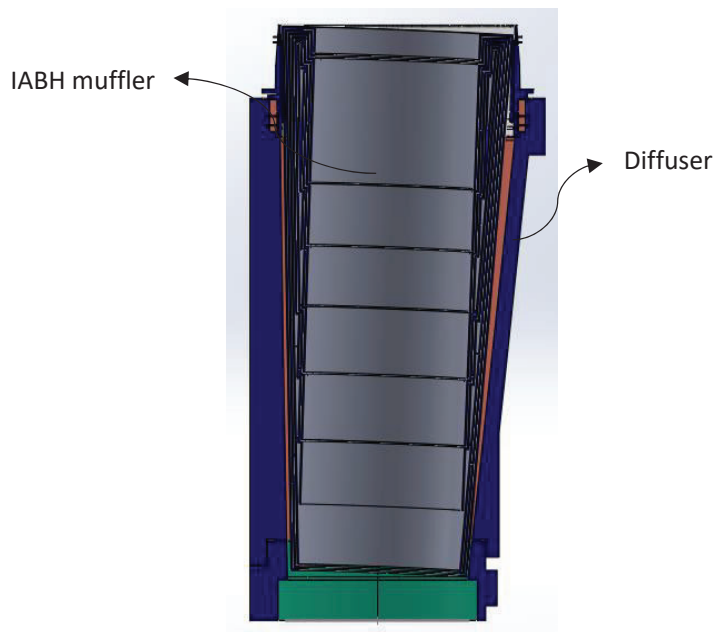

Figure 4.31: The cross section view of the diffuser and the muffler inside the ventilation unit.

The best possible dimension of the diffuser is depicted in Table 4.2. This muffler involves 10 channels to absorb the low frequency noise to high frequency noise based on the fan noise spectrum. To compact the muffler, the channels' width and wall thicknesses are considered

1 mm. The inlet of the channels are at the bottom side of the muffler that will be covered by a membrane to protect the muffler from the dust and bacteria growth.

Table 4.2: Dimension of the internal Acoustic Black Hole muffler inside the unit.

Internal Acoustic Black Hole muffler			
Length	335 mm	Blade thickness	1 mm
Outer diameter	118-152 mm	No. of channels	10
Inner diameter	108 mm		

To see the details of the muffler, the front section view of the muffler is plotted in Fig. 4.32. As can be seen in Fig. 4.32, the closed ends are demonstrated by black circles.
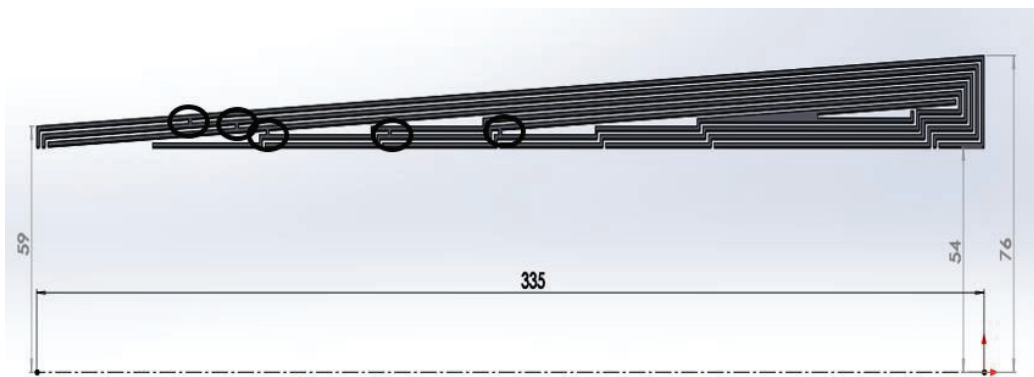

Figure 4.32: The front section view of the IABH muffler inside the ventilation unit.

To make this type of the muffler, one of the solutions is to divide the muffler into some segments like in Fig. 4.33.
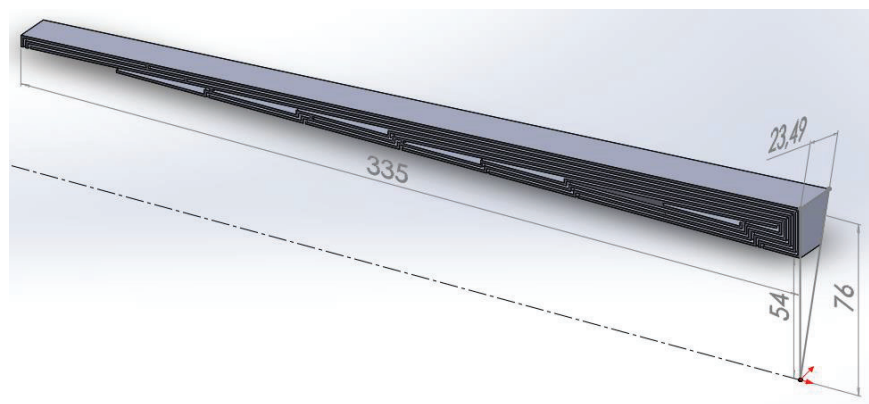

Figure 4.33: The segment of the internal Acoustic Black Hole muffler inside the Ventilation unit.

Assemble twenty pieces of this segment, will give the muffler shown in Fig. 4.34:
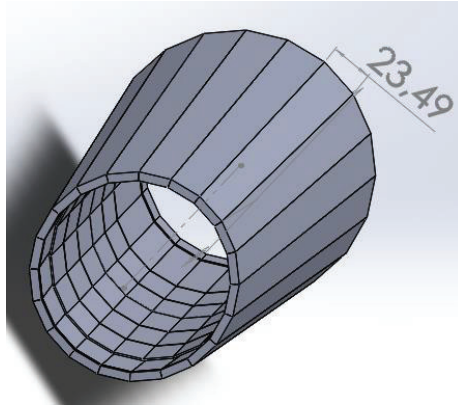
Figure 4.34: The assembly of segments of the internal Acoustic Black Hole muffler inside the unit.

Next, the model should be simulated by COMSOL software to find the acoustic performance of the muffler. Hence, the mesh model of the system is demonstrated in Fig 4.35.

Figure 4.35: The mesh of the internal Acoustic Black Hole muffler model inside the unit.

The maximum length of the mesh is calculated based on considering at least 6 points for the maximum desired frequency which in this case is 4000 Hz as $\dfrac{343[m/s]}{4000[1/s]*6} = 0.0143[m]$.
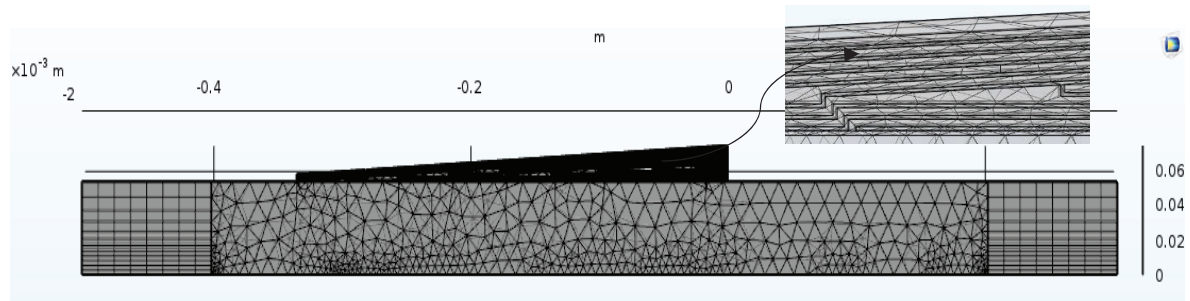
The transmission loss of the IABH muffler inside the unit is shown in Fig. 4.36.

65
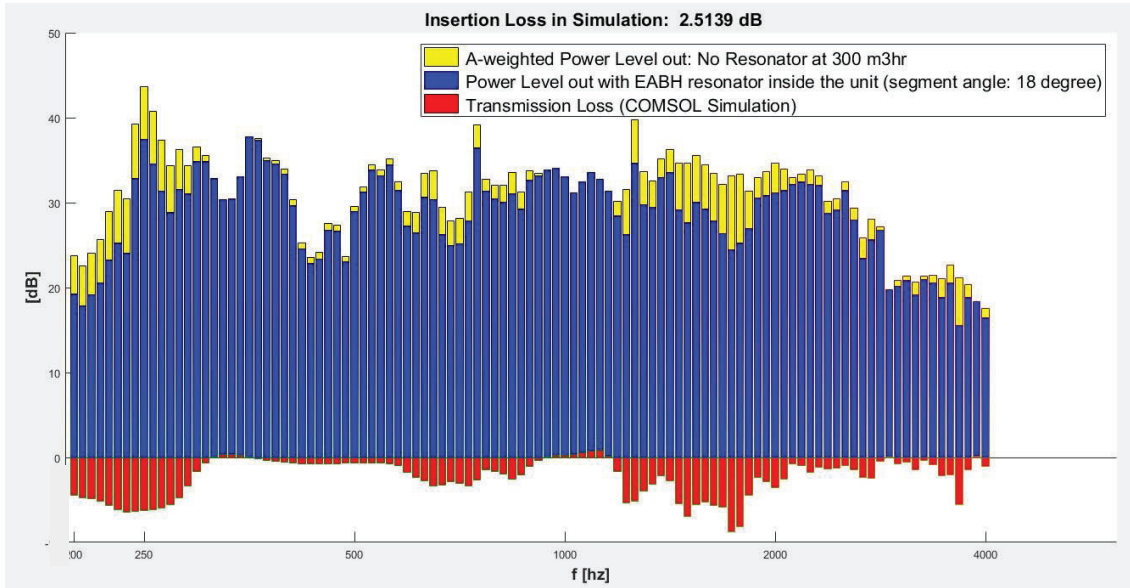
Figure 4.36: Transmission loss of the internal Acoustic Black Hole muffler inside the unit.

It should be noted that if the acoustic structure interaction is considered at the simulation, then the TL will become like in Fig. 4.37. In this model, polyamide is considered as a material of the muffler.

Figure 4.37: TL of the internal Acoustic Black Hole muffler inside the unit by considering ASI.

To present the differences of applying the ASI, the TL of the muffler with four various materials i.e. ABS, PP, and P.A. are compared with the TL of the model with rigid walls in Fig. 4.38:

66

Figure 4.38: TL of the internal Acoustic Black Hole muffler inside the unit.

Moreover, eigen-frequency analyses of the muffler is simulated to determine the first 15 eigen-frequencies for the each state and the results are written in Table. 4.3:

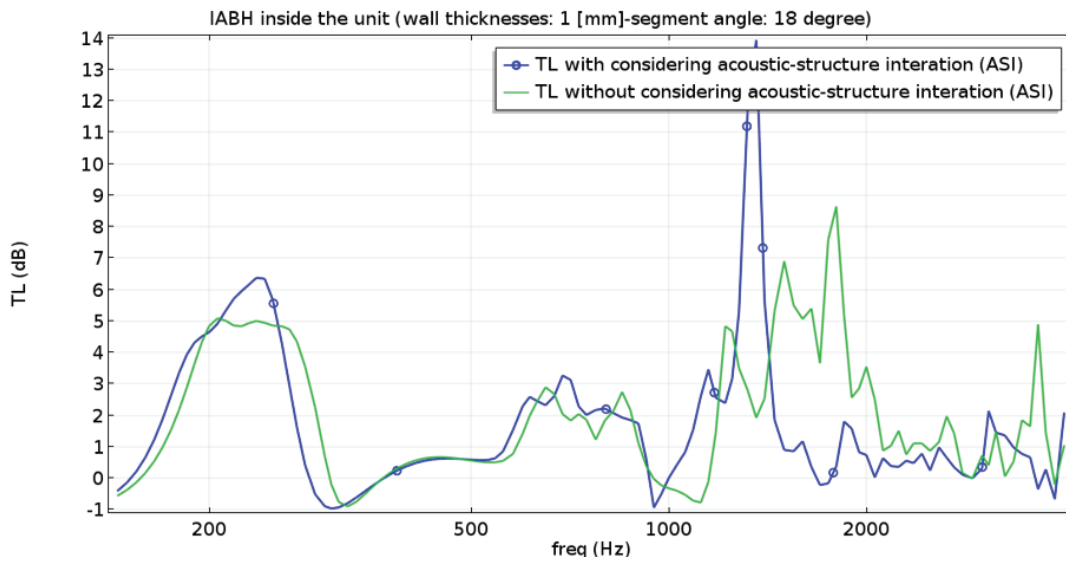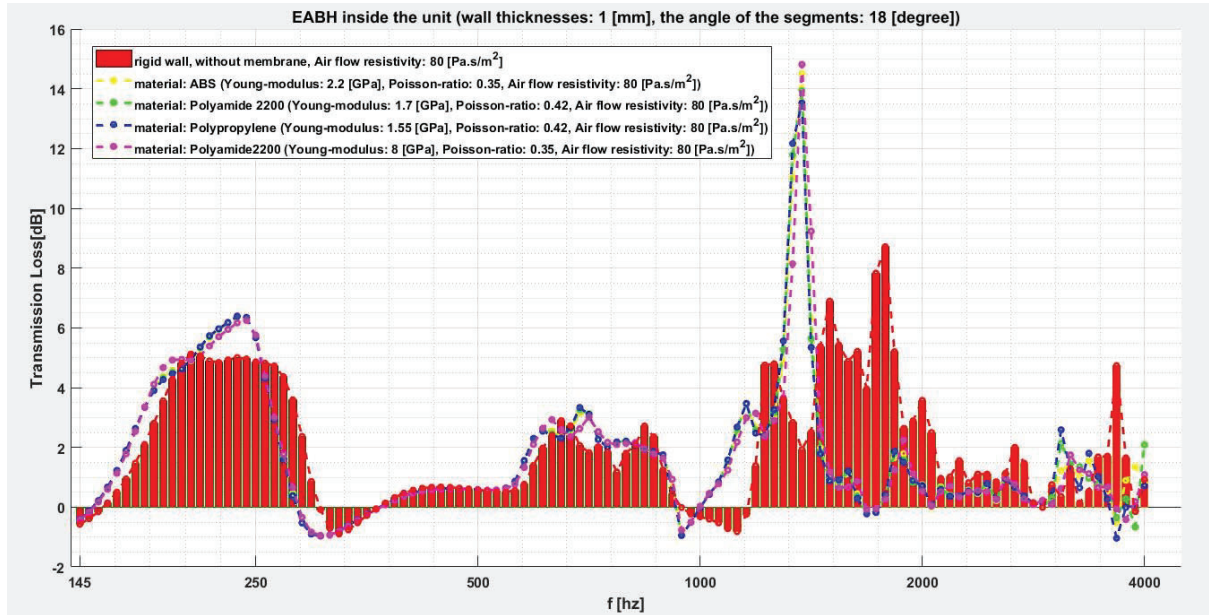Table 4.3: First to 15 eigen frequencies of the IABH muffler inside the unit.

No. Material	Pressure Acoustic module	Structure module (with considering a PVC membrane)			Acoustic-structure Interaction (with considering a PVC membrane)		
	air	ABS	PP	PA2200	ABS	PP	PA2200
1	111	2090	1883	1940	182	180	180
2	139	2223	2090	2090	182	181	181
3	179	3375	2850	2936	188	187	187
4	203	3527	3017	3109	190	189	190
5	207	3686	3146	3241	211	209	210
6	238	3818	3273	3372	212	210	211
7	271	3915	3376	3478	232	232	232
8	289	3941	3490	3596	237	234	235
9	295	4107	3518	3624	246	243	245
10	399	4181	3725	3838	248	246	247
11	498	4202	3750	3863	375	374	374
12	528	4357	3949	4068	375	375	375
13	586	4412	3955	4074	381	380	381
14	605	4446	3984	4104	383	382	382
15	609	4482	4004	4125	395	394	394

To sum up, various resonators and mufflers have been simulated in this chapter to validate the knowledge based designs. It can be concluded that it is possible to absorb low frequency noise via resonators and mufflers. Resonators can work in a specific range of the frequency which is useful for a narrow band treatments (see Fig. 3.2, Fig. 3.6, and Fig. 3.11) and the combination of resonators expand the effective frequency range (Fig. 3.13 and Fig. 3.14). However, mufflers can be considered as a broad band treatments (see Fig. 3.16, Fig. 3.18, Fig. 3.26, and Fig. 3.28). Moreover, mufflers simulations show that the combination of the EABH, IABH, and cylindrical mufflers can remove noises at any desired frequencies. The frequency noise reduction of the helicoidal resonator depends on the diameter of the duct, i.e. for the 125 mm duct the helicoidal resonator will effect on the frequencies more than 1100 Hz. On the other hand, spiral and funnel resonators can work in any range of the frequencies and it depends on the length and the other specification of the resonators.

Comparing the eigen-frequency of the system with and without considering acoustic-structure interaction reveals that mufflers' results are much more related to the ASI rather than resonators. Also, The result of the Fig. 4.38 and Table. 4.3 express that the differences of the eigen-frequencies with various materials are negligible however, it has a big difference with the rigid wall assumption.

Another advantage of the simulation phase is that system's optimizations is occurred. The results of this optimization are used in the next chapter to design details and develop each treatment.

Chapter 5

5. Detail design and development

5.1 Introduction

The performance of the numerical results lead to the development of the first sample. This will result to the detail design and development phase that prototypes are built and tested in the acoustic lab and the reverberation chamber to analyze the technical performance parameters such as the sound power level (PL) and the transmission loss. If TL is more than 3 dB, it means that the method is useful but it may need some optimization to reach the required values. Moreover, if TL is less than 10 dB, then a combination of the second method with the first will be attempted, and the tests will be performed again until it becomes more than 10 dB. The described procedure is demonstrated in Fig. 5.1 and it is presented in the following chapters 5 and 6.
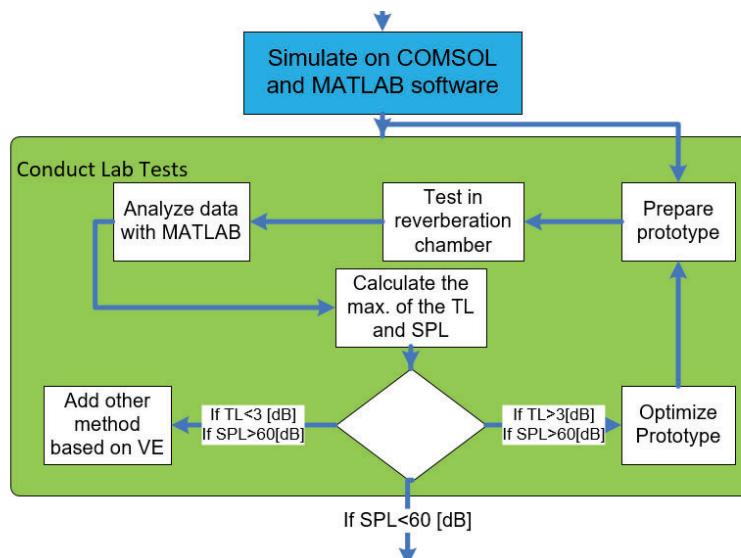

Figure 5.1: Procedure of the Detail Design and Development phase.

5.2 Helicoidal resonator

The nominal diameter of the duct of the ventilation system is 125 mm and the desired length of the resonator in this project is less than 35 cm. Hence, the helicoidal resonator with the specification in Table 5.1 is designed in SolidWorks software which is shown in Fig. 5.2:

Table 5.1: Specification of the helicoidal resonator.

Helicoidal resonator			
Length	250 mm	Blade thickness	5 mm
Outer diameter	125mm	Inner diameter	30 mm
Eigen-frequencies (numerical)	1195, 1255, 1361, 1570, 1665, 1714, 1756… Hz		
Acoustics eigen-frequencies considering ASI (numerical)	1196, 1255, 1360, 1570,1665,1714,1756 … Hz		

Also, the prototype of the helicoidal resonator which is made by a 3D printer at the University of Twente is exposed in Fig. 5.2:
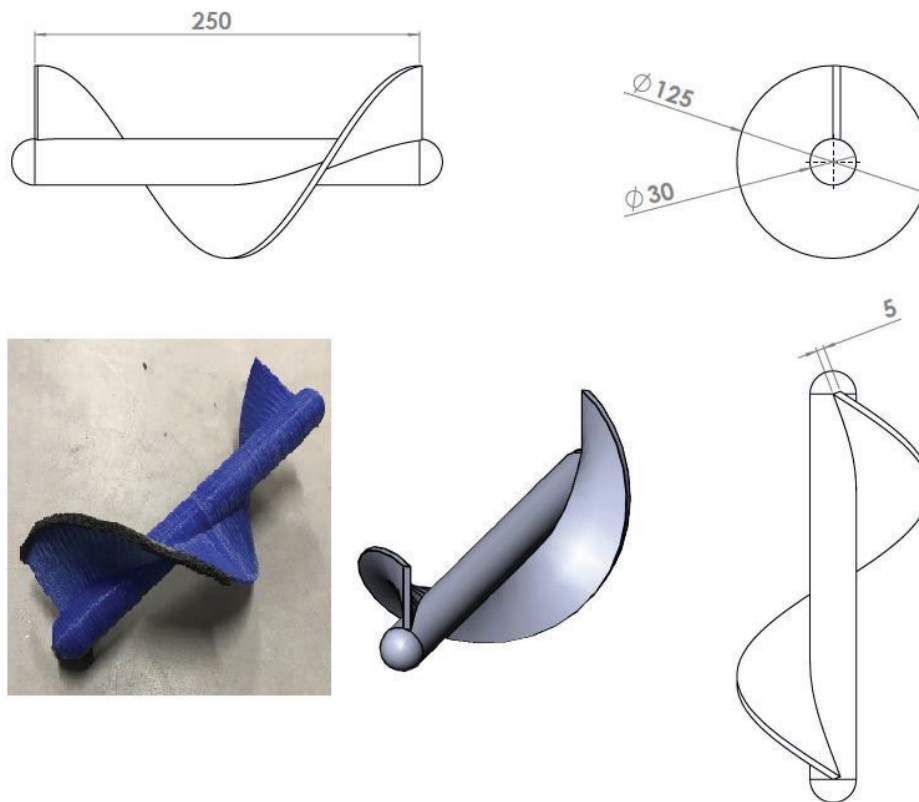

Figure 5.2: Detail design of the helicoidal resonator.

5.3 Spiral resonator

The spiral resonator with three turns and 500 mm length is considered for the prototype. The specification of the prototype is written in Table 5.2.

Table 5.2: Specification of the spiral resonator.

Spiral resonator			
Length	500 mm	Blade thickness	0.5 mm
Outer diameter	125mm	No. of spiral turns	3
Material	Stainless steel	Half-closed end	
Eigen-frequencies (numerical)	430, 629, 700, 826, 850, 978, 1012, 1028 Hz		

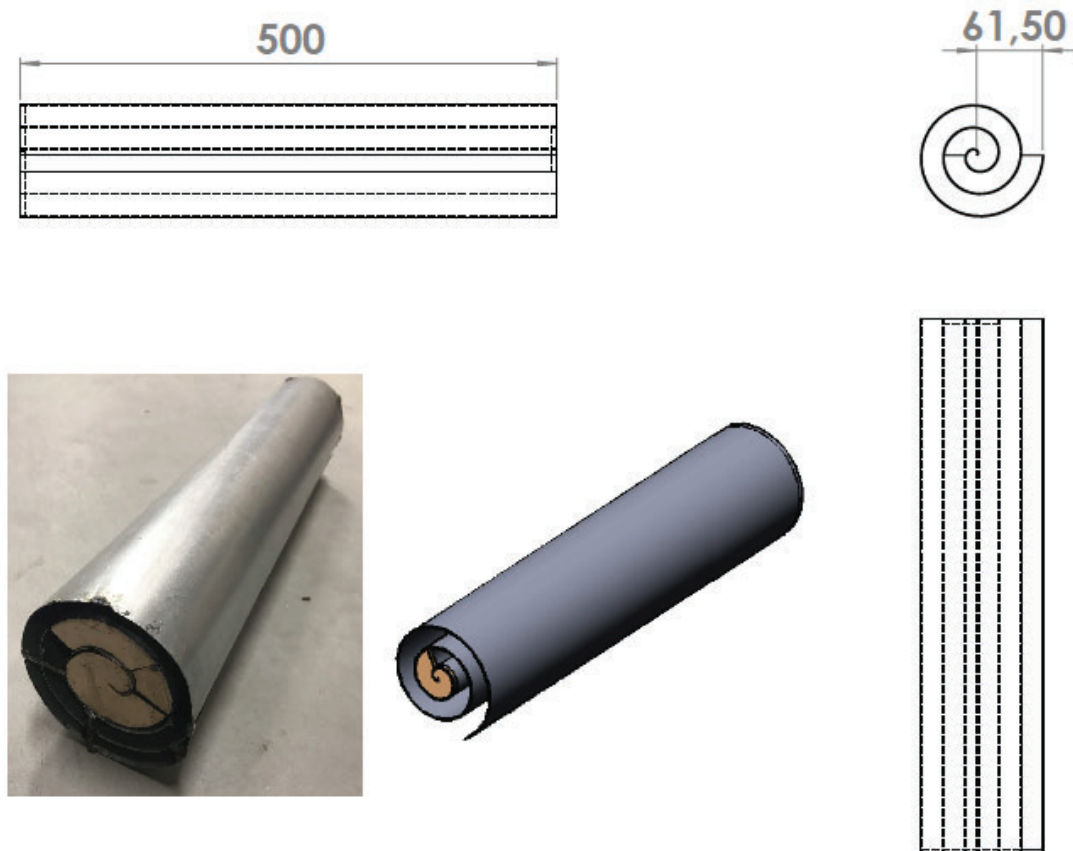The various views of the spiral resonator are plotted in Fig. 5.3.

Figure 5.3: Detail design of the spiral resonator.

5.4 Funnel resonator

The funnel resonator is useful for low-frequency noise reduction. The model with the written specification in Table 5.3, is made at Brink Climate Systems to evaluate the acoustic performance of the funnel resonator.

Table 5.3: Specification of the spiral resonator.

Funnel resonator			
Length	600 mm	Blade thickness	1 mm
Inlet diameter	60 mm	Outlet diameter	109.67 mm
Material	Stainless steel	Slope	4.1 %
Eigen-frequencies (analytical)	287, 578, 858, 1147… Hz		
Eigen-frequencies (numerical)	273, 553, 831, 1063, 1109 Hz		

The SolidWorks model and the prototype of the funnel resonator is shown in Fig. 5.4.
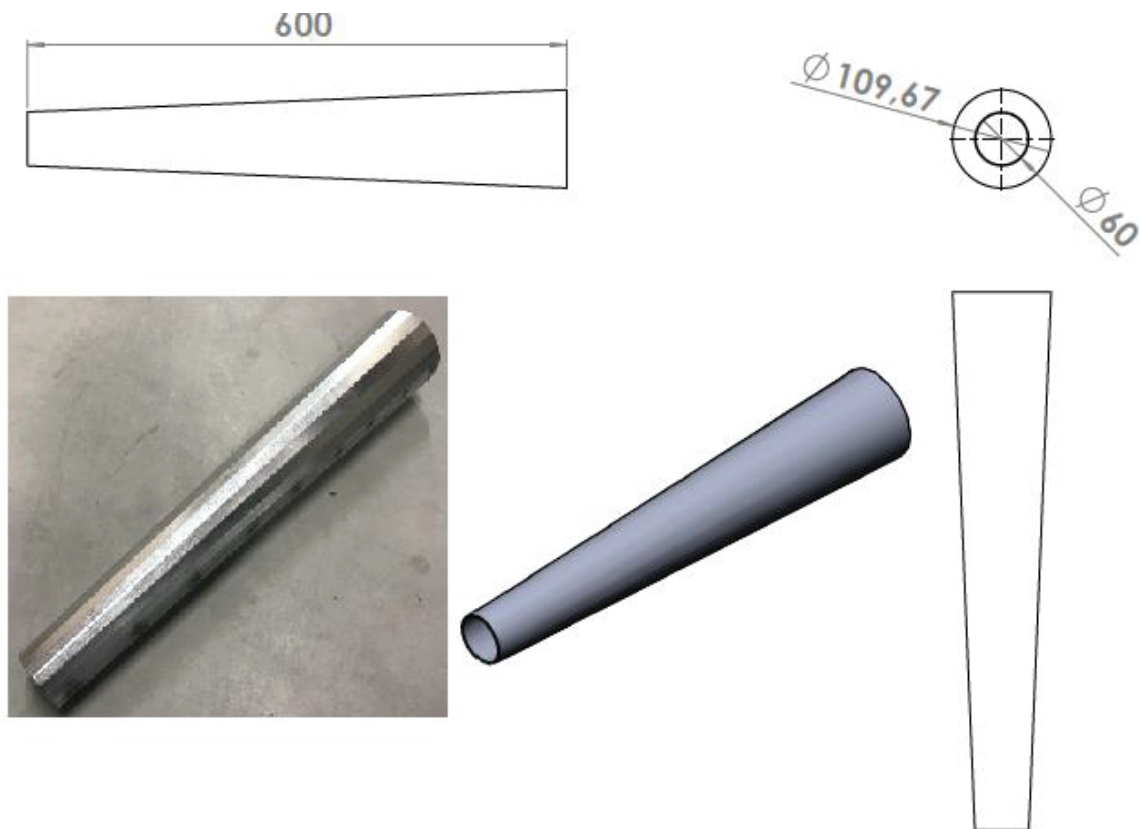

Figure 5.4: Detail design of the funnel resonator.

5.5 Acoustic Black Hole muffler

Because of the Acoustic Black Hole muffler should be installed inside the T-joint, then the outer diameter size is 125 mm. The model which is designed in this section has the written specifications mentioned in Table. 5.4.

Table 5.4: Specification of the Acoustic Black Hole muffler.

Acoustic Black Hole muffler			
Length	135 mm	Blade thickness	1 mm
No. of blades	18	Outlet diameter	125 mm
Material	ABS		
Eigen-frequencies (numerical)	285, 433, 609, 731, 834, 941, 1055, 1178, 1306, 1452, 1610, 1619, 1620, 1624, 1631, 1632… Hz		

The standard view of the model and the produced prototype is plotted in Fig. 5.5:
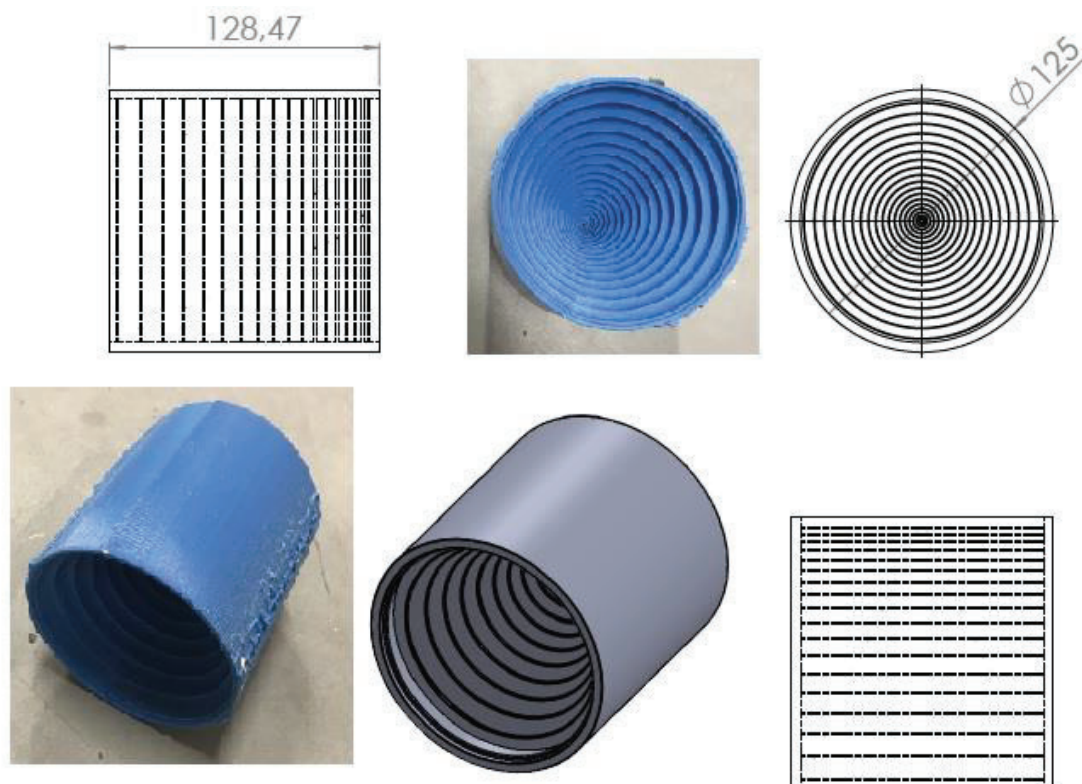

Figure 5.5: Detail design of the Acoustic Black Hole muffler.

5.6 External Acoustic Black Hole muffler

Based on the requirement, the outer diameter of the muffler size is selected to be 254 mm and the inner one should be the same as duct size which is 125 mm. By adding more channels inside the muffler, the transmission loss function will be smoother and higher. However, the smallest possible thickness to make is 0.4 mm and the channel width should be more than 1 mm to be possible to make it with 3D printer at University of Twente (model 'FORMIGA P101'). The specification of the EABH muffler outside the ventilation unit is written in Table 5.5:

Table 5.5: Specification of the external Acoustic Black Hole muffler.

External Acoustic Black Hole muffler			
Length	182 mm	Wall thickness	1 mm
No. of channels	24	Outer diameter	254 mm
Material	Polyamide 2200	Inner diameter	125 mm
Eigen-frequencies (numerical)	232, 242, 253, 264, 278, 294, 311, 327, 334, 361, 392, 432, 550, 607, 644, 681, 718, 723, 767, 786, 819, 866, 871, 941, 971, 978, 1015… Hz		

One of the best possible model as the external Acoustic Black Hole muffler is shown in Fig. 5.6.
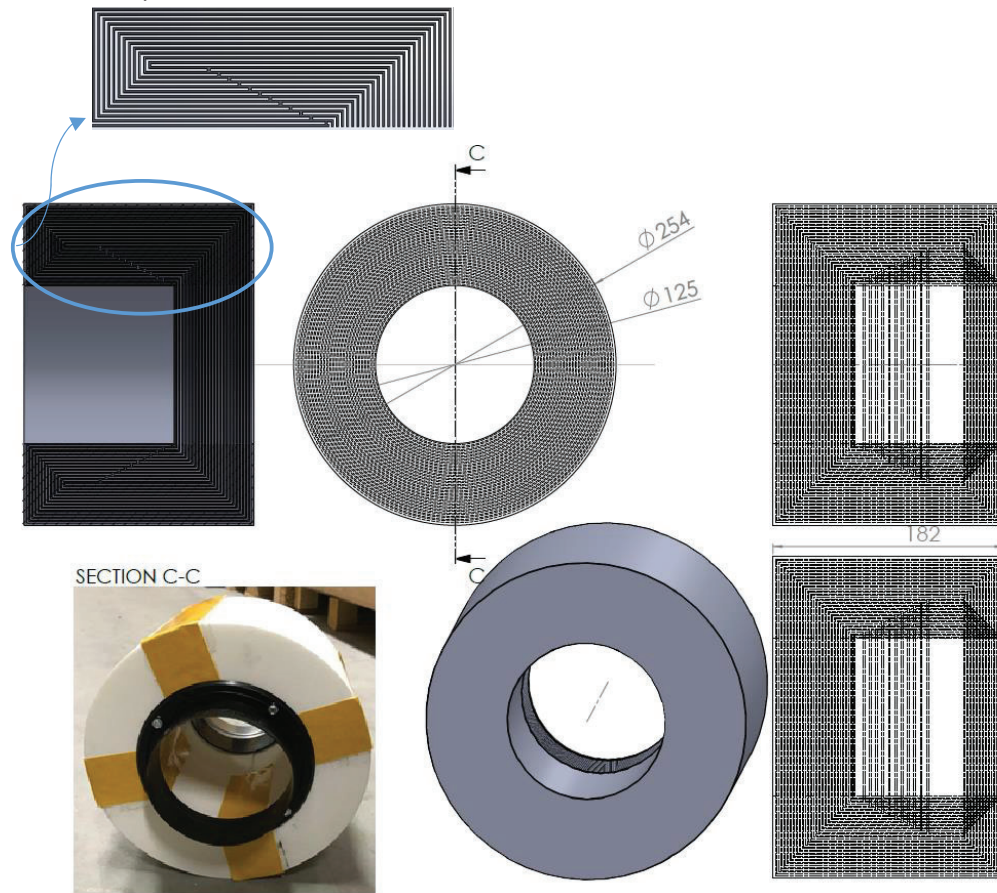

Figure 5.6: A detail design of the external Acoustic Black Hole outside the ventilation unit.

The muffler is divided into four segments, shown in Fig 5.7, which could be possible to make them with the mentioned 3D printer.
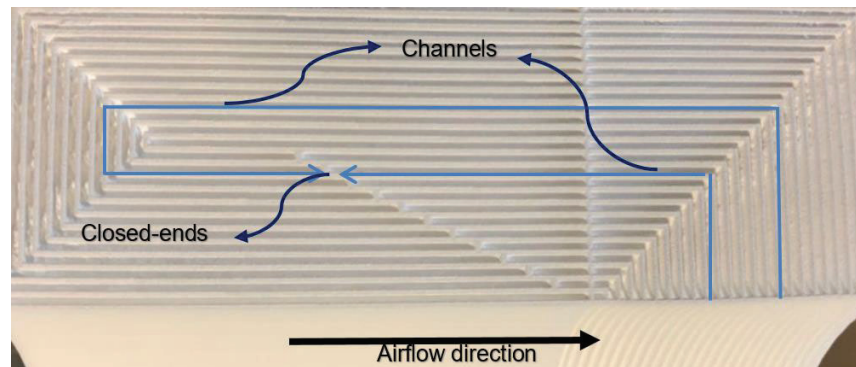

Figure 5.7: A segment of the external Acoustic Black Hole muffler outside the ventilation unit.

5.7 Internal Acoustic Black Hole muffler

As discussed before, to put the silencer inside the diffuser of the ventilation unit, it is needed to make some segments. These segments should have enough rigidity and should be possible to make by injection molding technique. Hence, a wall is inserted in the middle and the blade should be extruded with at least 1 ° draft. Also, it needs some pins which connect them together. Based on these characteristics, the designed segment is presented in Fig. 5.8:
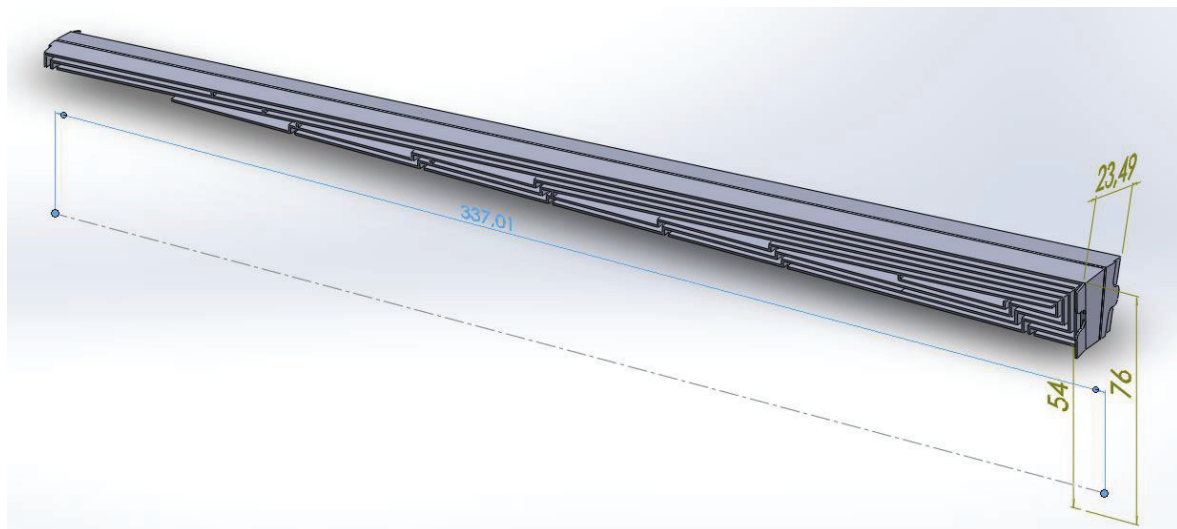

Figure 5.8: A segment of the internal Acoustic Black Hole inside the ventilation unit.

The specification of this design is depicted in Table 5.6:

Table 5.6: Specification of the internal Acoustic Black Hole muffler inside the unit.

Internal Acoustic Black Hole muffler			
Length	337 mm	Wall thickness	0.6-1 mm
No. of channels	10	Outer diameter	118-152 mm
Material	Polyamide 2200	Inner diameter	108 mm
Volume	41 dm^3	General draft	1 degree
Eigen-frequencies (numerical)	111, 139, 179, 203, 207, 238, 271, 289, 295, 399, 498, 528 Hz		
Acoustics Eigen-frequencies considering ASI (numerical)	180, 181, 187, 190, 210, 211, 232, 235, 245, 247, 374, 375, 381, 382, 394, 395, 397,399, 403 Hz		

The Cad-drawing of the segment to get an offer from the suppliers is shown in Fig. 5.9:
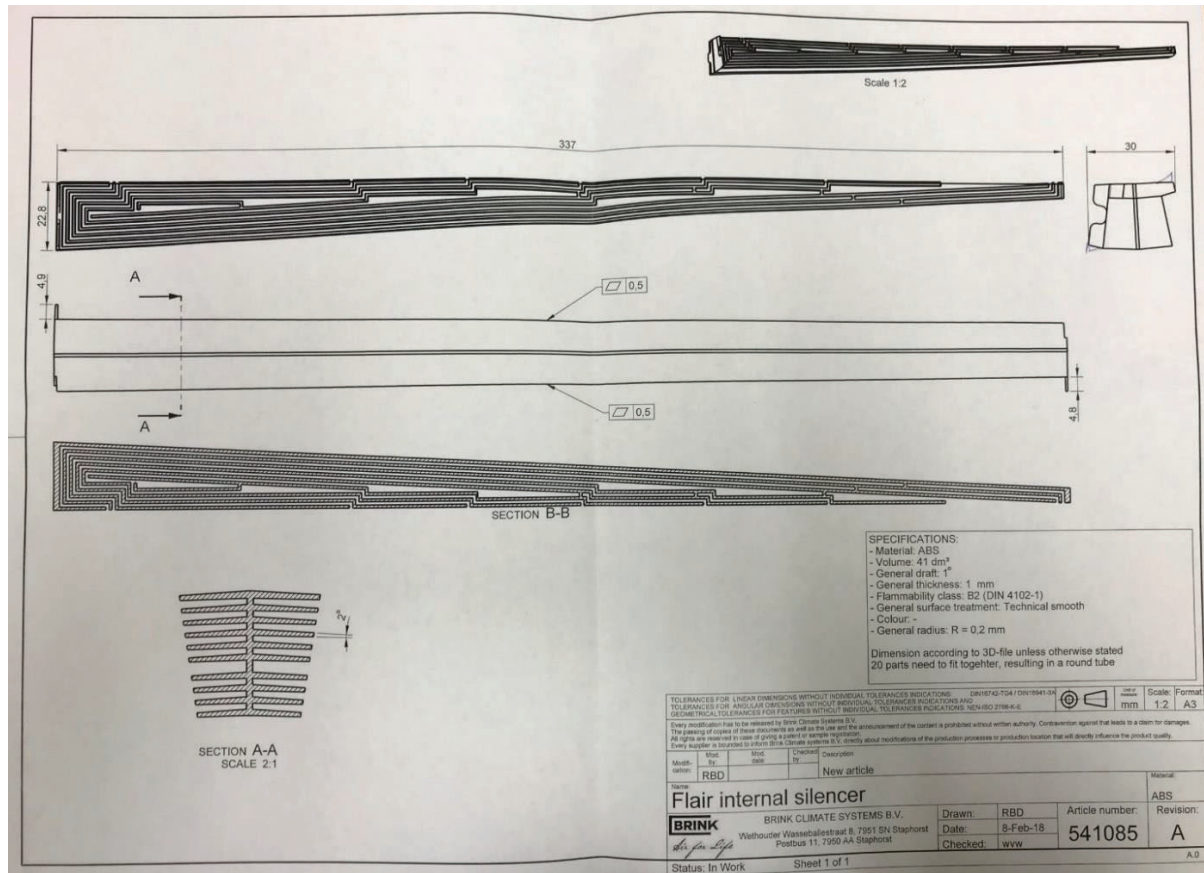
Figure 5.9: The Cad-drawing of a segment of the internal Acoustic Black Hole muffler.

The inserted pins help to assemble the segments like in Fig. 5.10:
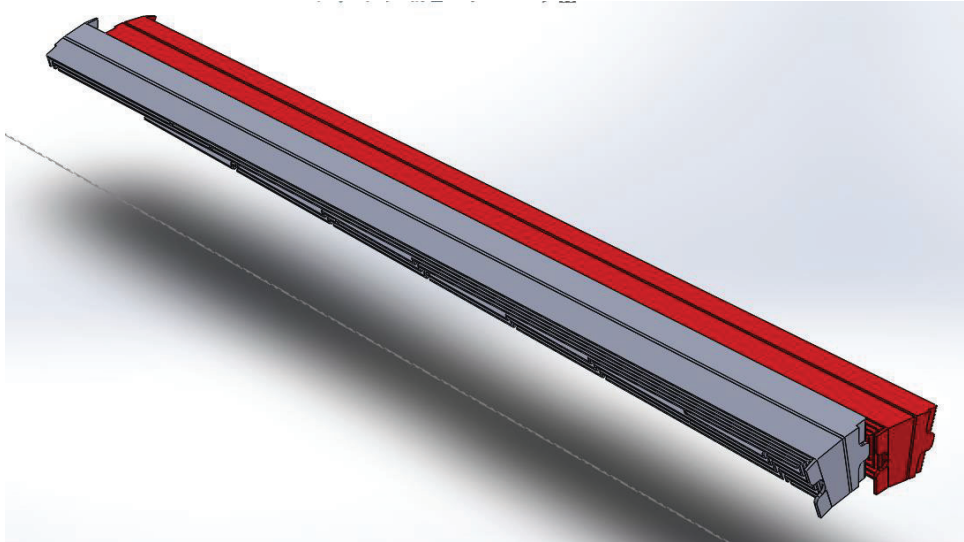
Figure 5.10: Assembly of segments of the internal Acoustic Black Hole muffler.

The final model of the muffler will become like in Fig. 5.11:
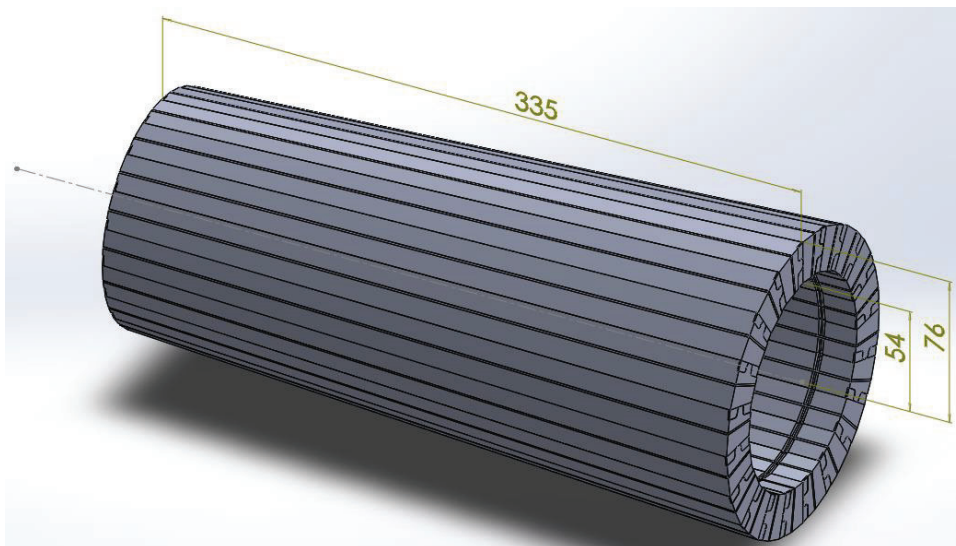
Figure 5.11: The internal Acoustic Black Hole muffler inside the ventilation unit.

Due to the maximum possible length of parts that 3D printer (*model: FORMIGA P101*) at the university could print, each segment is cut into two parts, then these parts are glued to become a segment like in Fig. 5.12:
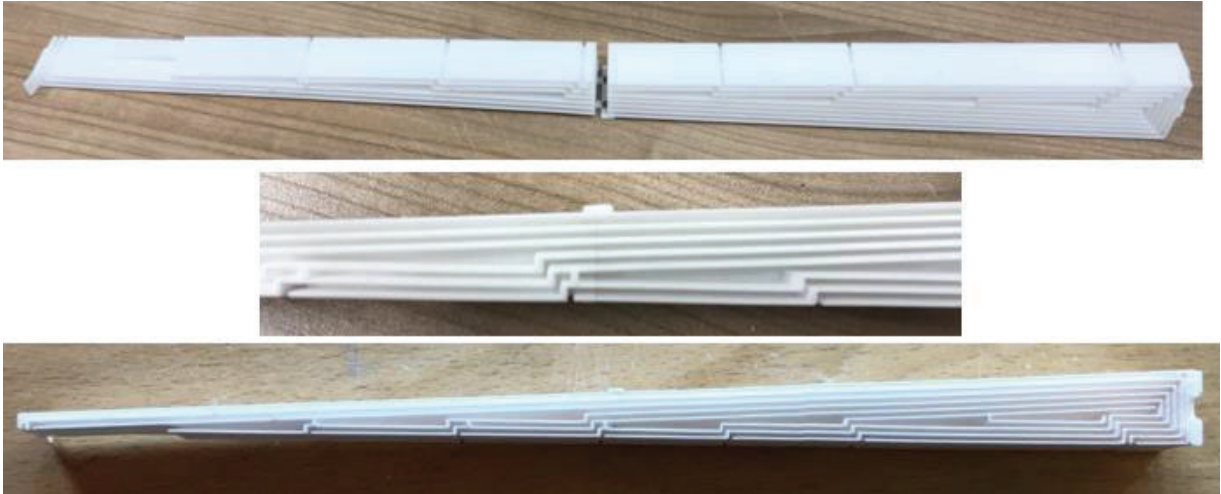
Figure 5.12: Making of each segments.

To assemble the muffler easily, two connectors are used like in Fig. 5.13 which gather the segments somehow they can be taped.

Figure 5.13: The prototype of the internal Acoustic Black Hole muffler.

In short, the detail of each treatments are presented in this chapter and prototypes are prepared to test them which is explained in the next chapter.

6. Treatment Implementation

6.1 Test setup

The test setups are made at the Brink Climate Systems. The company has a reverberation chamber to measure sound Power Level of the ventilation units. In this chamber, six microphones, *model: Bruel & Kjaer 2671,* are located to measure the acoustical pressure in 3 sets of 10 seconds based on ISO 3741 standard. In addition, it's equipped with a data acquisition system, *model: Bruel & Kjaer 3050-A-06,* to transfer the acoustic pressure data to the computer. Two test setups are prepared to evaluate the resonators and mufflers in a controlled environment and a real environment whether the requirement of the stakeholders are met.

The first test setup shown in Fig. 6.1, it involves the ventilation unit's fan as a noise source, *model: ebmpapst G3G190*, a flow meter to adjust the flowrate, *model: Flakt 125*, pitot tubes to measure the pressure drop, a micro-manometer, *model: RS232*, 6 microphones (5 located in the reverberation chamber and another one is placed before the resonator inside the tube) to measure the acoustic pressures.
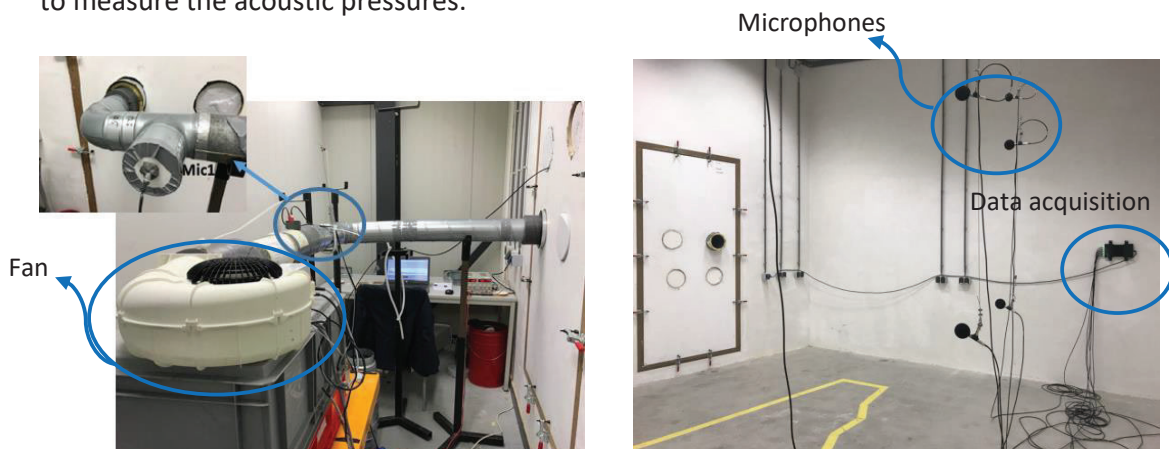
Figure 6.1: First test setup for testing in the controlled environment.

The second setup configuration is used for testing the resonators and mufflers inside and outside the ventilation unit in the real environment which is presented in Fig. 6.2 and sound power level is measured by six microphones inside the reverberation chamber.
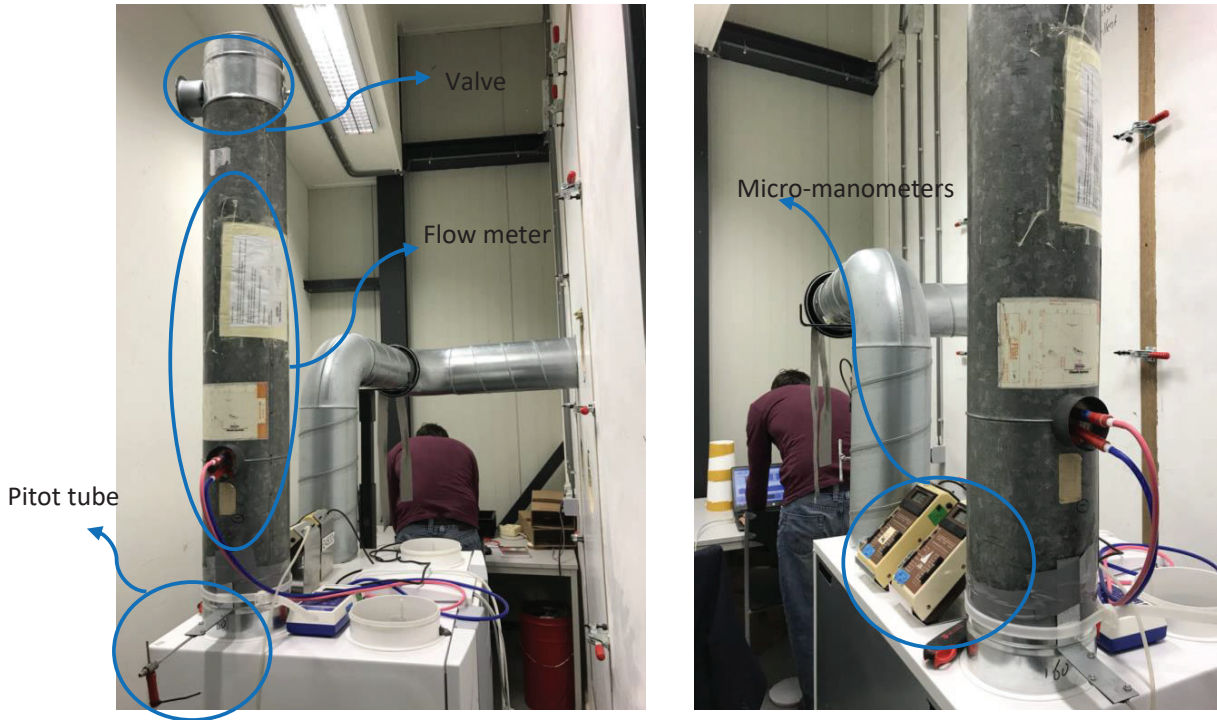
Figure 6.2: Second test setup for testing in the real environment.

The second test setup also involves the flow meter, three Pitot tubes to measure the pressure drop between the inlet and outlet ducts and pressure drop of the resonators, a power-meter, *model: Christ CLM1000*, a valve to adjust the pressure at the inlet duct, and the ventilation unit of Brink Climate Systems, *model: Flair 325*, shown in Fig. 6.3:

Figure 6.3: A ventilation unit of Brink Climate Systems model Flair 325.

Moreover, the internal resonators like the helicoidal resonator, decrease the cross section of the tube which is causing more pressure drop, then the fan needs to work harder and it makes more noise. In this case, the performance of the resonator cannot be evaluated well due to different noise sources. Hence, the co-axial duct, shown in Fig. 6.4, is used and the insertion loss is calculated between the situation that the resonator has been installed inside the co-axial duct and the situation without the resonator.

Figure 6.4: The co-axial duct (outer diameter: 160 mm, inner diameter: 125 mm).

For instance, the 1/1 and 1/3 octave band sound power level spectrum of the Flair 325 without any resonator at 325 m³/h flowrate and 150 Pa pressure differences between the inlet and outlet ducts is plotted in Fig. 6.5. The weather conditions during the test were: temperature 19.9 °C, atmosphere pressure 1013.4 Pa, and relative humidity 39%.
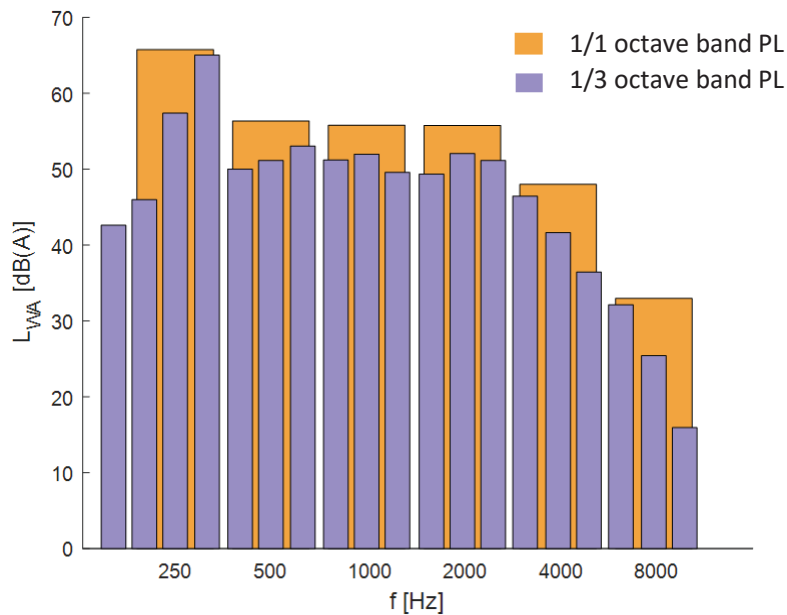
Figure 6.5: 1/1 and 1/3 octave band sound power level spectrum of the unit (model: Flair 325).

To have better analysis the result, the 1/24 octave band PL spectrum is also considered. Fig. 6.6 shows the 1/24 octave band sound power level spectrum of the Flair 325 without any resonator at 325 m³/h flowrate and 150 Pa pressure differences between the inlet and outlet ducts. Also, the frequency range is considered from 145 Hz to 12000 Hz.
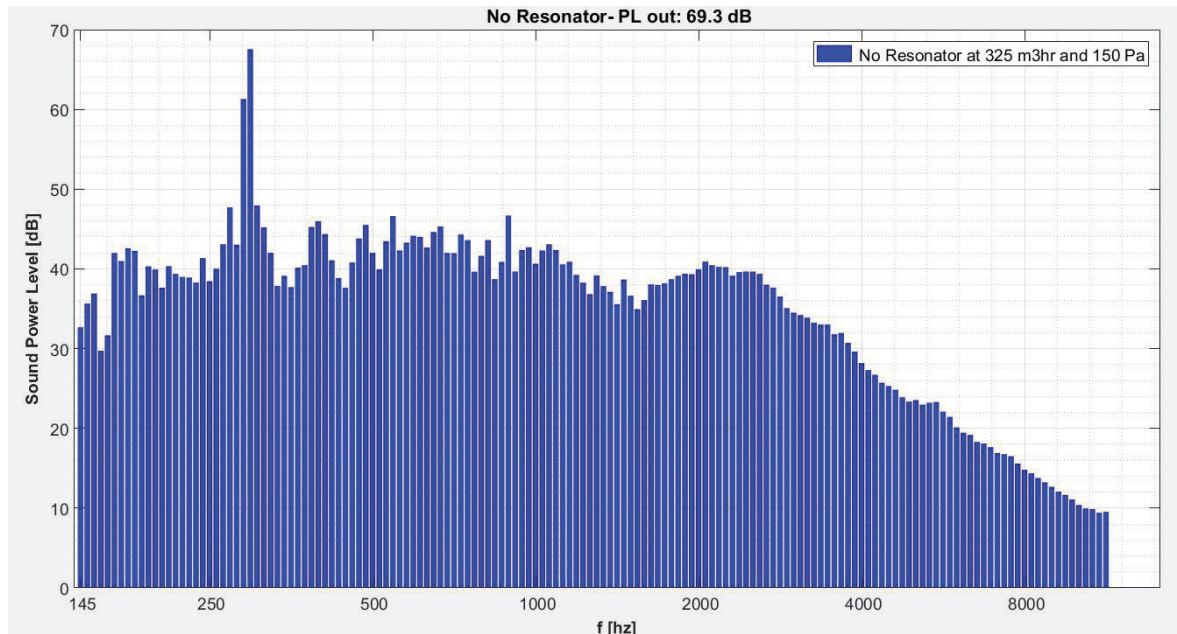

Figure 6.6: 1/24 octave band sound power level spectrum of the ventilation unit (model: Flair 325).

6.2 Helicoidal resonator

Fig. 6.7 presents the helicoidal resonator inside the co-axial ducts to install among the ventilation duct size 160 mm.
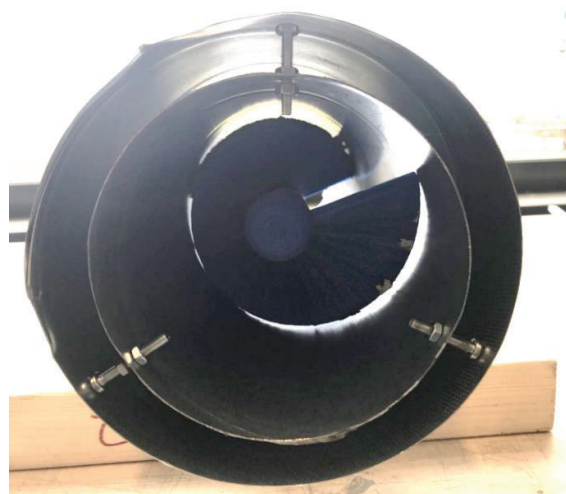
Figure 6.7. The helicoidal resonator inside the co-axial duct.

The sound power level of the system by applying the helicoidal resonator inside the co-axial duct in the second test setup at 325 m³/h flowrate and 150 Pa pressure differences between the inlet and outlet ducts is shown in Fig. 6.8:
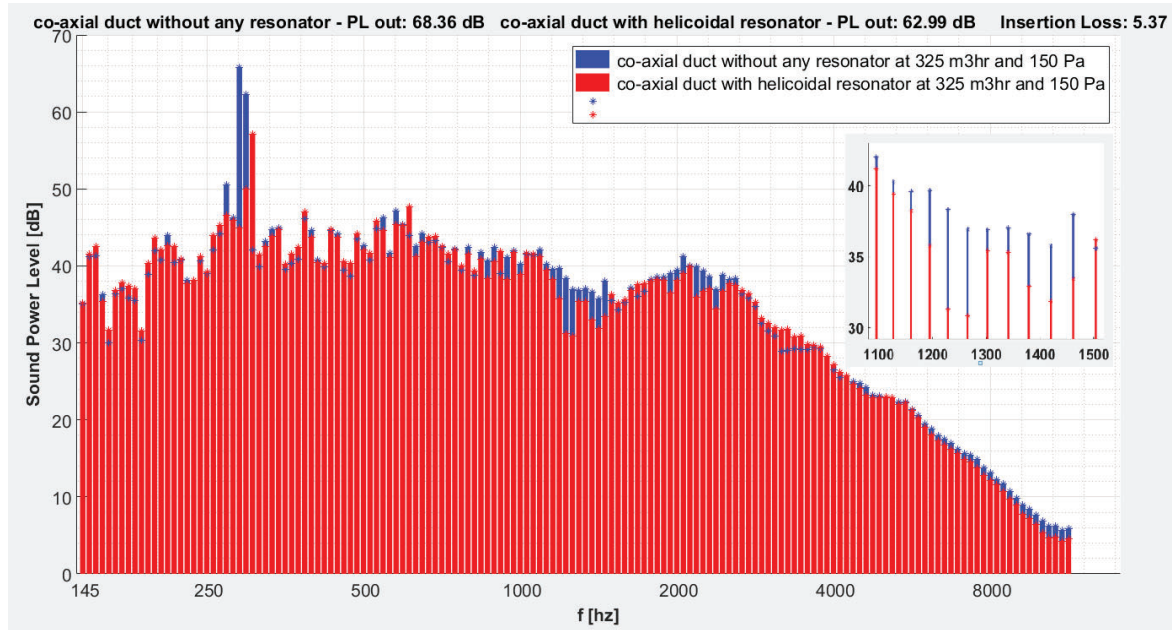
Figure 6.8: Sound power level of applying the helicoidal resonator at 325 m³/h and 150 Pa.

As can be seen in Fig. 6.8, the noise reduction at the desired eigen-frequencies (1180 Hz, 1300 Hz, 1615 Hz, 1709 Hz, etc.) are achieved. In addition, another analysis has been done at Brink to determine the sound power level of the unit at various frequencies and the result is written in Table. 6.1:

Table 6.1: measured Sound power level of the unit Flair 325.

	Lw dB	Lw dB	Lw dB	Lw dB	Lw dB	Lw dB	Lwa dB(A)
	250 Hz	500 Hz	1000 Hz	2000 Hz	4000 Hz	8000 Hz	overall
co-axial 160mm no silencer 325 m³/h, 150 Pa	72.1	59.6	55.9	53.7	44.7	33.1	66.2
co-axial 160mm helicoidal resonator 325 m³/h, 150 Pa	66.2	59.7	55.2	52.7	45.5	32.5	62.6
Insertion Loss	5.9	-0.1	0.7	1	-0.8	-1.4	3.6

6.3 Spiral resonator

The test setup configuration for the spiral resonator is the same as for the helicoidal resonator, the spiral resonator inside the co-axial duct is shown in Fig. 6.9:

Figure 6.9. The spiral resonator inside the co-axial duct.

The sound power level of the spiral resonator at 325 m^3/h flowrate and 150 Pa pressure over the unit is plotted in Fig. 6.10:
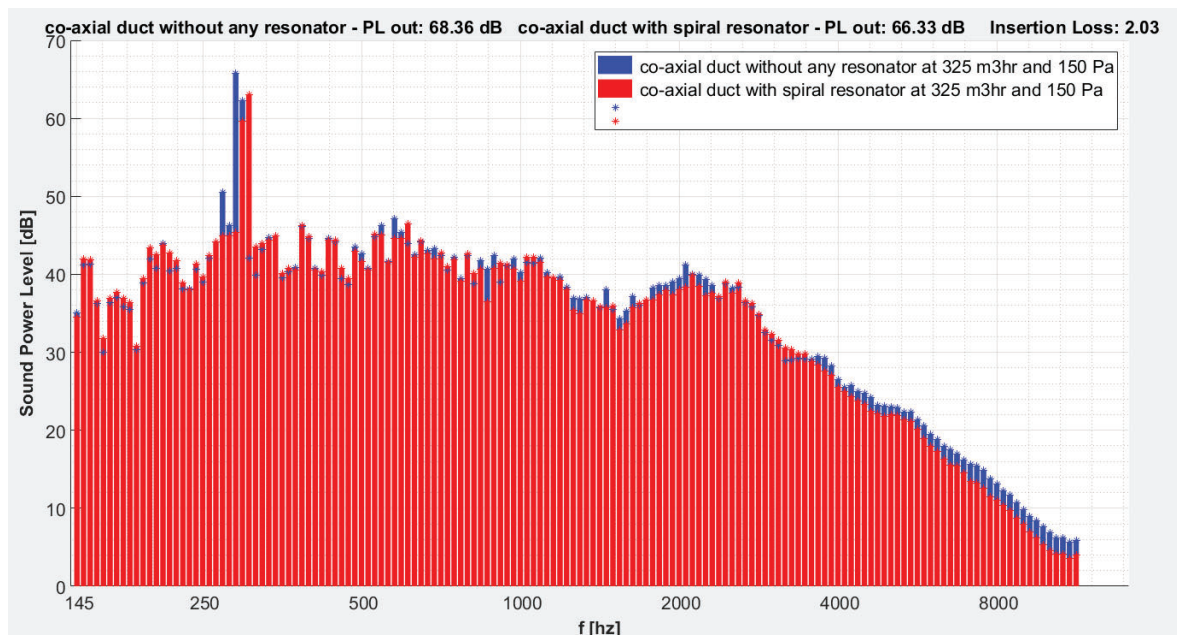
Figure 6.10: Sound power level of applying the spiral resonator at 325 m^3/h and 150 Pa.

The insertion loss of the spiral resonator in the real environment is 2.03 dB but in Fig. 6.10 the eigen-frequencies are not clear, so the first test setup is used to demonstrate the effect of the spiral resonator. The sound power level and the insertion loss for the spiral resonator in the first test setup at 300 m³/h flowrate is presented in Fig. 6.11:
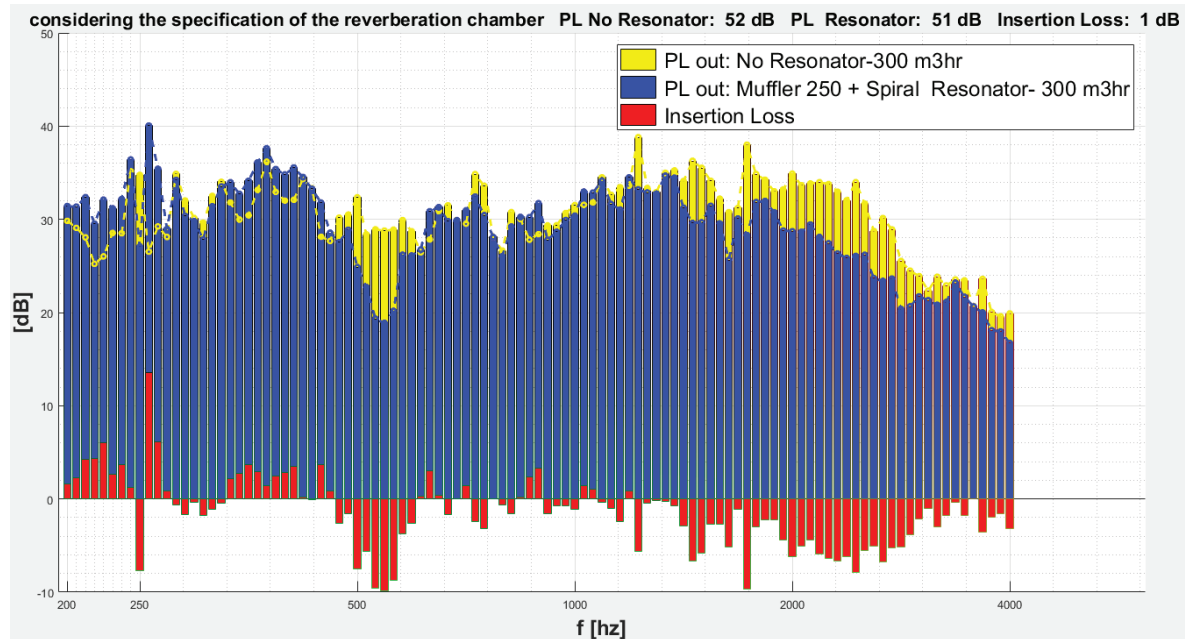
Figure 6.11: Sound power level and Insertion loss of applying the spiral resonator at 300 m³/h.

As the same to the helicoidal resonator, reducing the noise at the desired eigen-frequencies, i.e., 421Hz, 656Hz, 705Hz, 876 Hz, etc. based on analytical and simulation are achieved however, due to the uncontrolled inlet air pressure, the fan is working harder which causes more noise specially at the critical frequency of the fan, 270 Hz, and the total performance of the resonator becomes lower.

6.4 Funnel resonator

Like the other internal resonators, the funnel resonator shown in Fig. 6.12 is placed inside the co-axial duct before implementing inside the tube.
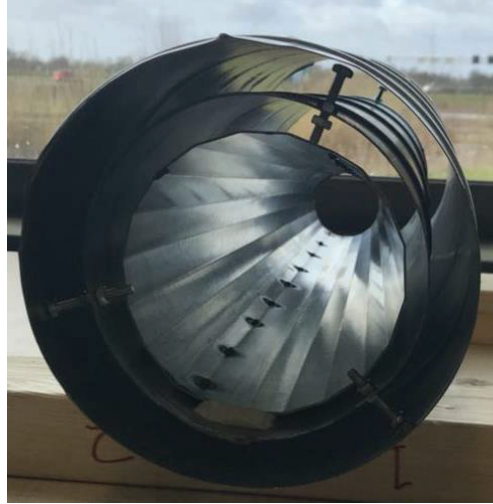
Figure 6.12. The funnel resonator inside the co-axial duct.

The 1/24 octave band sound power level spectrum of the unit by applying the funnel resonator at 325 m³/h flowrate and 150 Pa pressure differences between the inlet and outlet ducts is depicted in Fig. 6.13:
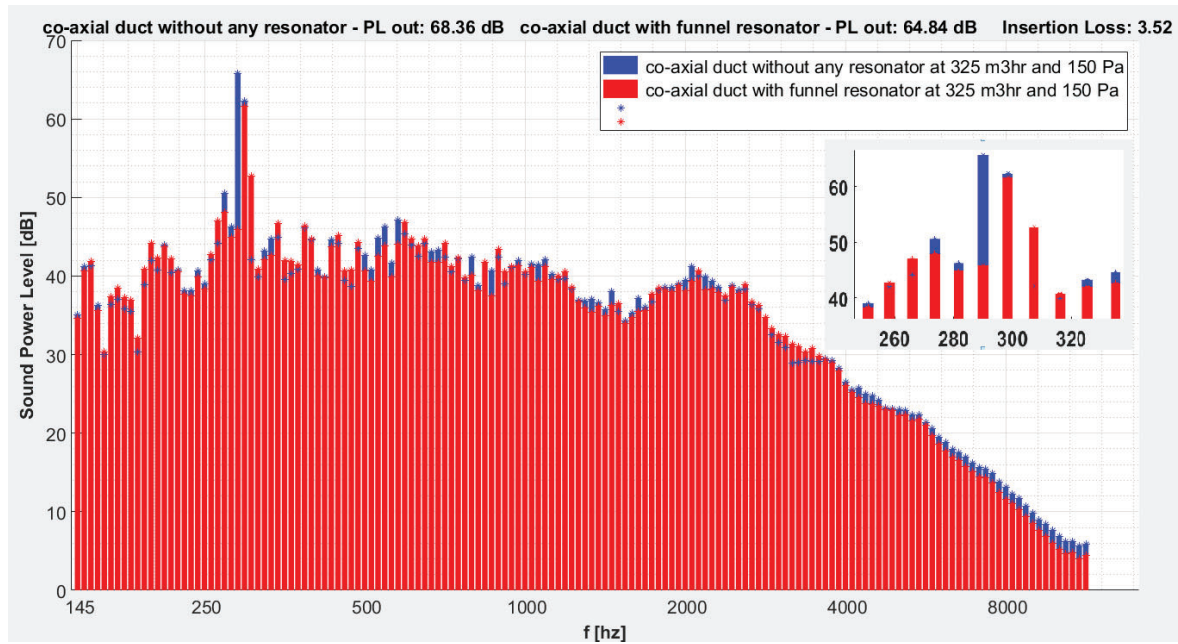
Figure 6.13: Sound power level of applying the funnel resonator at 325 m³/h and 150 Pa.

The measured sound power level at various frequencies is written in Table 6.2 which shows the noise reduction at the desired eigen-frequencies, i.e., 272, 540, 810 Hz is achieved.

Table 6.2: measured Sound power level of the unit Flair 325.

	Lw dB	Lw dB	Lw dB	Lw dB	Lw dB	Lw dB	Lwa dB(A)
	250 Hz	500 Hz	1000 Hz	2000 Hz	4000 Hz	8000 Hz	overall
co-axial 160mm no silencer 325 m³/h, 150 Pa	72.1	59.6	55.9	53.7	44.7	33.1	66.2
co-axial 160mm funnel resonator 325 m³/h, 150 Pa	67.6	59.3	55.7	53.3	45.3	32.1	63.3
Insertion Loss	4.5	0.3	0.2	0.4	-0.6	1	2.9

6.5 Acoustic Black Hole muffler

The first test setup is changed such that the Acoustic Black Hole muffler can be applied at the T-joint which is displayed in Fig. 6.14.
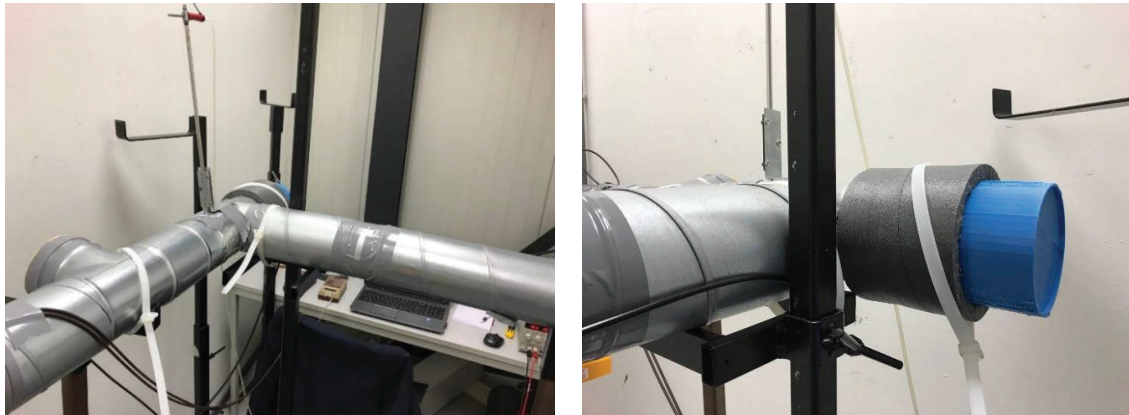
Figure 6.14. Installing the Acoustic Black Hole muffler in the T-joint.

The sound power level and the insertion loss for the Acoustic Black Hole muffler at 300 m³/h flowrate is plotted in Fig. 6.15:
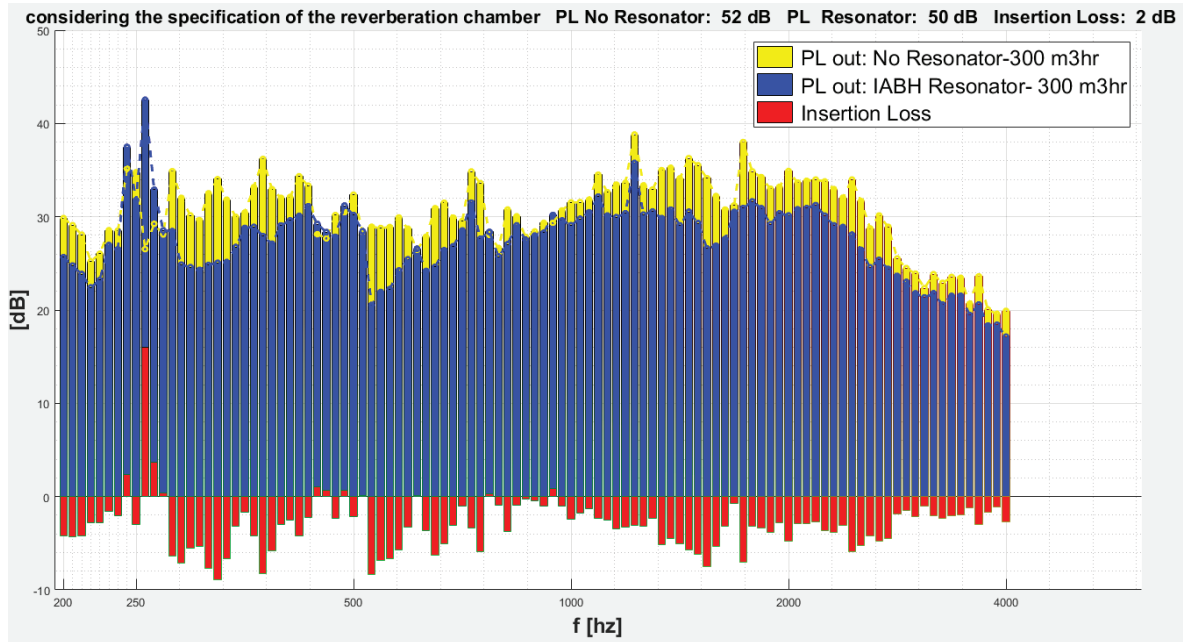
Figure 6.15: Sound power level and Insertion loss of applying the ABH muffler at 300 m^3/h.

As can be seen in Fig. 6.15, the Acoustic Black Hole muffler can be considered as the broadband noise reduction system and it can be installed at each 90 degree elbow to absorb the noise. It should be noted that by modifying the first test setup, the noise at critical frequency will not increase and the total result will be 5 dB instead of 2 dB.

6.6 External Acoustic Black Hole muffler

The first test setup is used to test the external Acoustic Black Hole muffler, shown in Fig. 6.16, in the controlled environment.
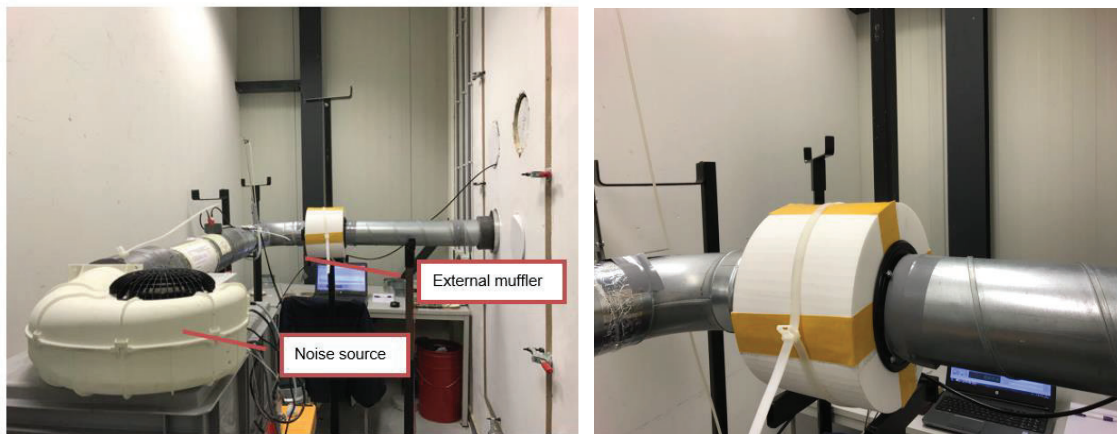
Figure 6.16: The first test setup for testing the external Acoustic Black Hole muffler.

The sound power level and the insertion loss of the external Acoustic Black Hole muffler at 300 m³/h flowrate is plotted in Fig. 6.17.
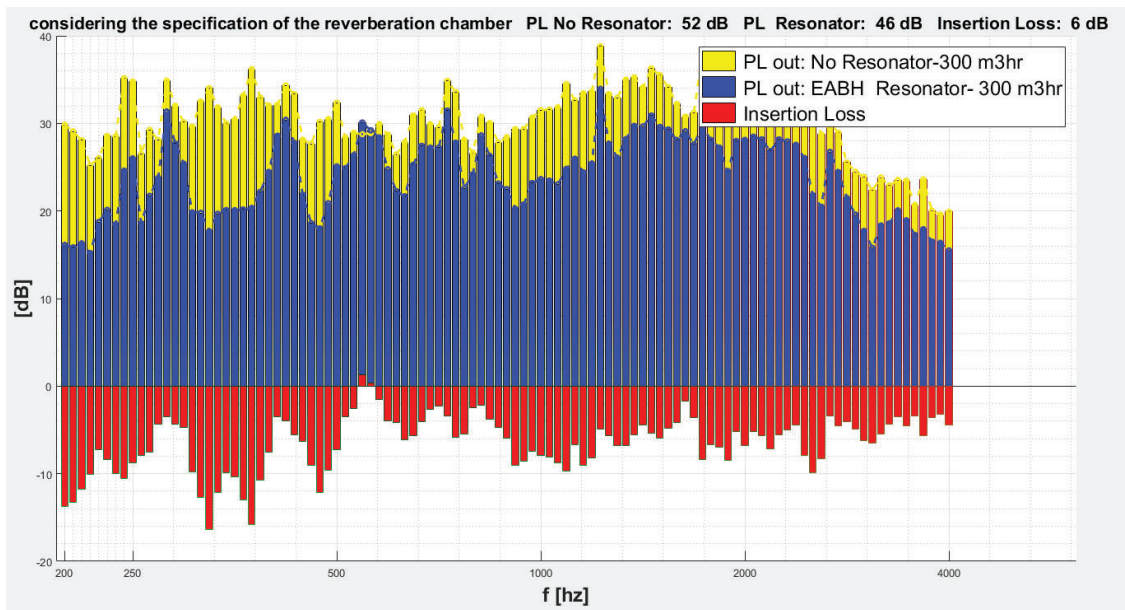
Figure 6.17: Sound power level and Insertion loss of applying the EABH muffler at 300 m³/h.

The insertion loss of the system is more than 6 dB which is a big achievement for this project, then the second test setup is prepared to test it in the real environment shown in Fig. 6.18:
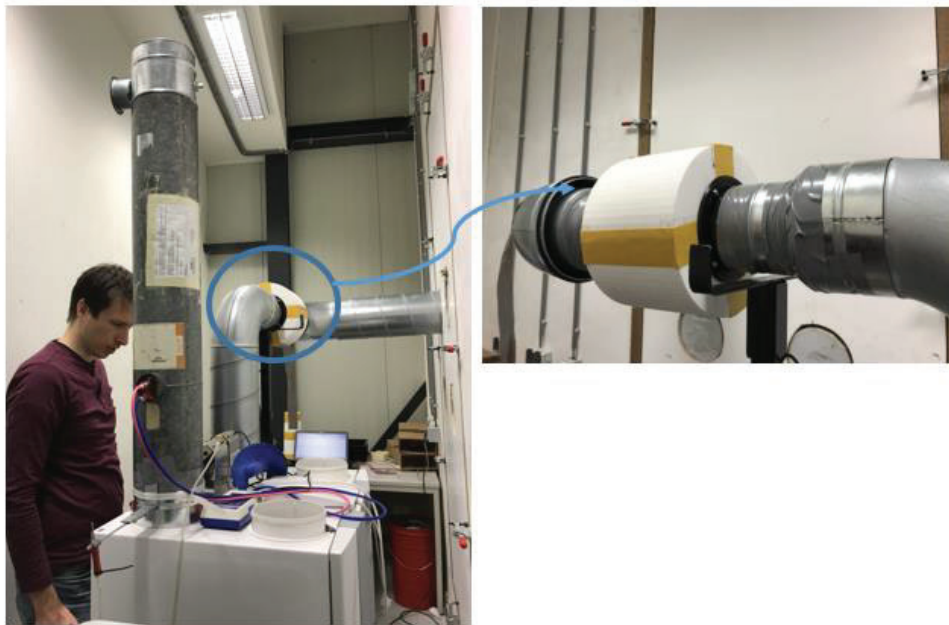
Figure 6.17: The second test setup for testing the EABH muffler in the real environment.

The sound power level of the external Acoustic Black Hole muffler at 325 m³/h flowrate and 150 Pa pressure differences between the inlet and outlet ducts is shown in Fig. 6.18:

Figure 6.18: PL of applying the EABH muffler at 325 m³/h and 150 Pa in the real environment.

The measured sound power level at various frequencies is written in Table 6.3.

Table 6.3: measured Sound power level of the unit Flair 325.

	Lw dB	Lw dB	Lw dB	Lw dB	Lw dB	Lw dB	Lwa dB(A)
	250 Hz	500 Hz	1000 Hz	2000 Hz	4000 Hz	8000 Hz	overall
no silencer 325 m³/h 150 Pa	69.2	60.6	56.8	54.9	47.6	34.8	64.9
external ABH 325 m³/h 150 Pa	57.6	54.5	51.3	46.3	38.8	27.8	56.3
Insertion Loss	11.6	6.1	5.5	8.6	8.8	7	8.6

The results of Fig. 6.18 and Table. 6.3 reveal that the external Acoustic Black Hole muffler is one of the best mufflers to absorb the broadband noise. To compare the simulation result vs the practical result, the power level and the insertion loss of the system are plotted in Fig. 6.19:

90
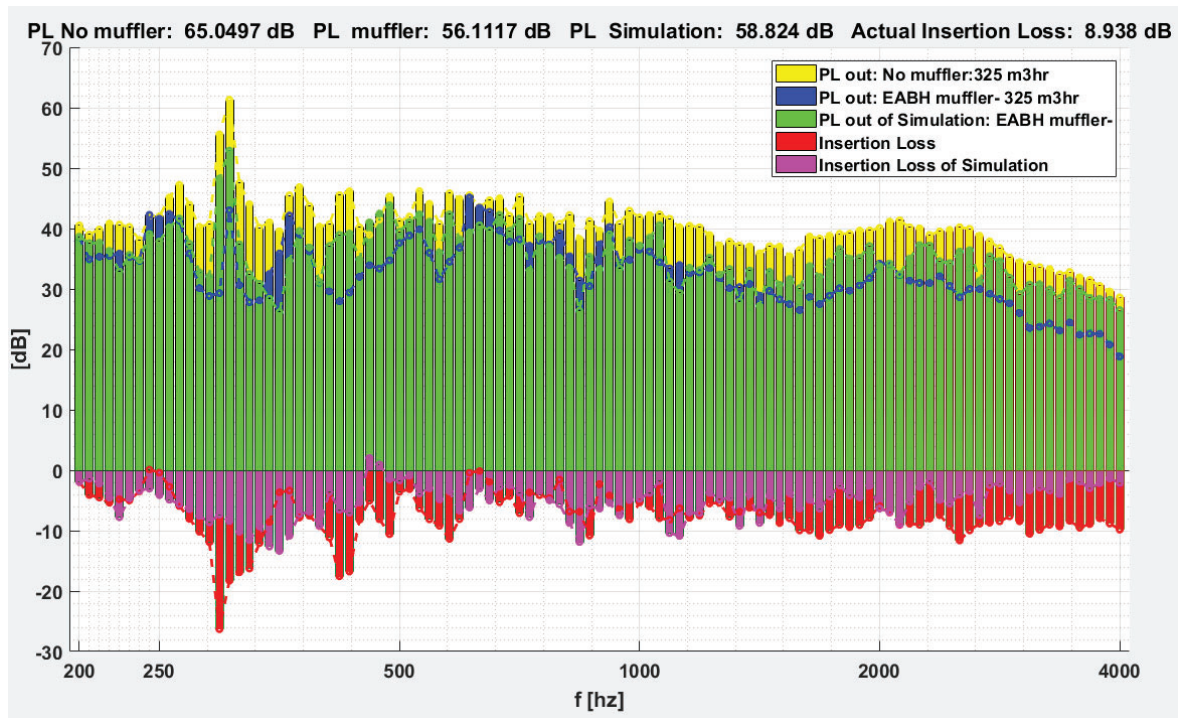
Figure 6.19: PL and IL of applying the EABH muffler at 325 m³/h and 150 Pa.

Fig. 6.19 displays a good agreement between the simulation result and practical one however, it could be better by controlling more parameters in the simulation and test.

6.7 The combination of the External and internal Acoustic Black Hole resonators

One of the combinations of the mufflers is shown in Fig 6.20, which involves ABH muffler and EABH muffler.
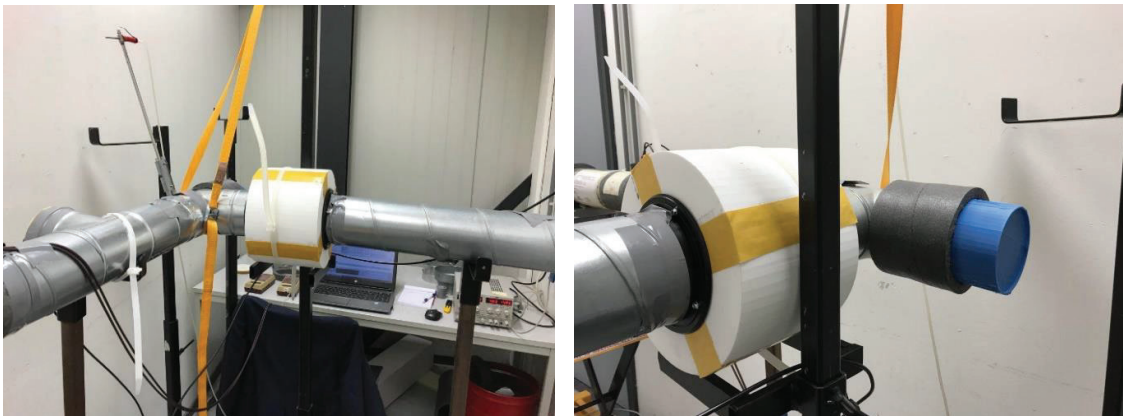
Figure 6.20: Test setup of the combination of the ABH and EABH mufflers.

The sound power level and the insertion loss of the combination of the ABH muffler with EABH muffler at the first test setup at 300 m³/h flowrate is shown in Fig. 6.21.
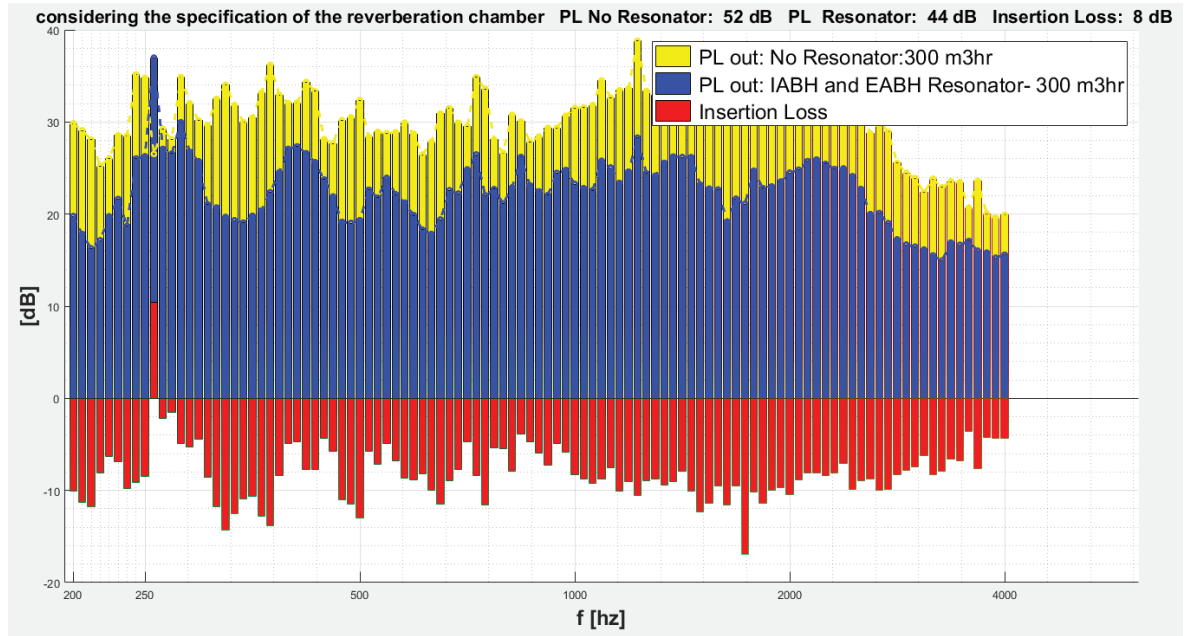
Figure 6.21: Sound power level and Insertion loss of the ABH and EABH mufflers at 300 m³/h.

6.8 The internal Acoustic Black Hole muffler

The second test setup is prepared to test the IABH muffler, put inside the ventilation unit, shown in Fig. 6.22.

Figure 6.22: The internal Acoustic Black Hole muffler inside the ventilation unit.

The sound power level of the noise measured in the reverberation chamber in two situations, with and without internal Acoustic Black Hole muffler inside the unit, at 325 m³/h flowrate and 150 Pa pressure differences between the inlet and outlet ducts is plotted in Fig. 6.23:
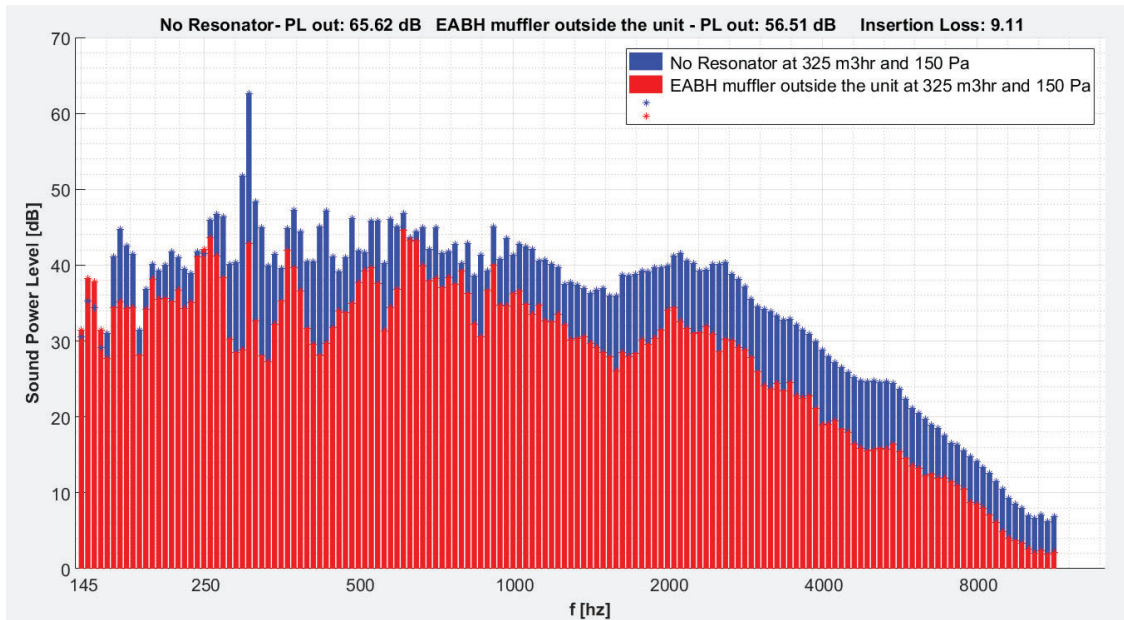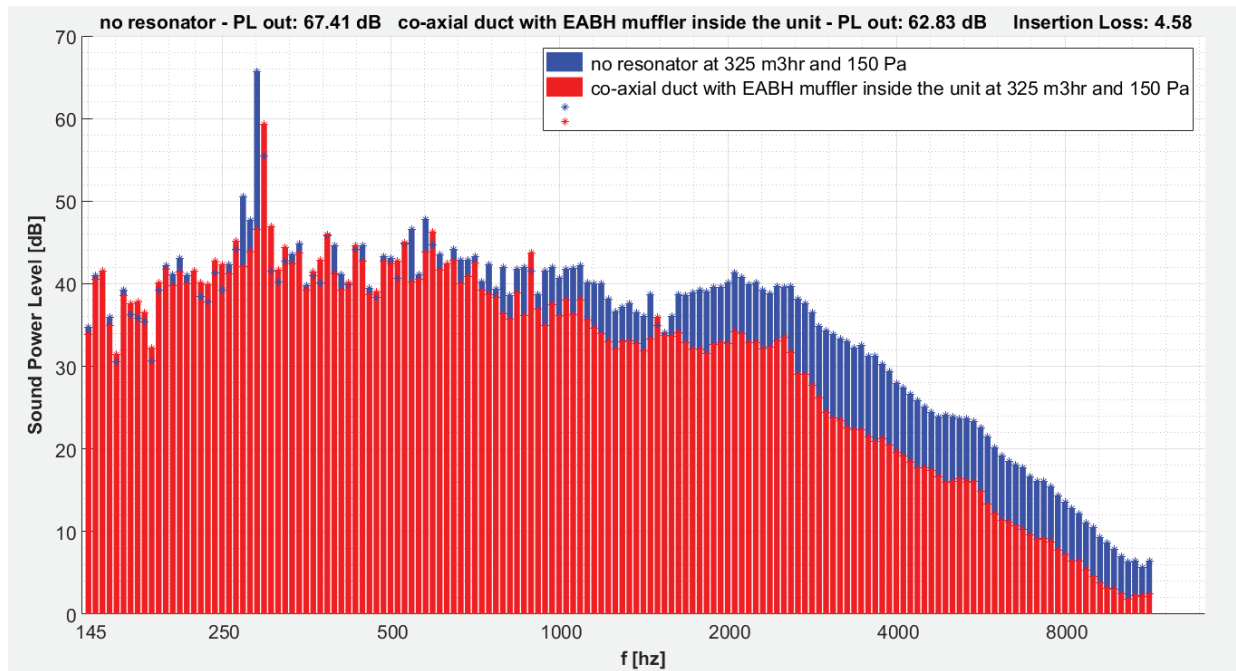
Figure 6.23: Sound power level of the IABH muffler inside the unit at 325 m³/h and 150 Pa.

The measured sound power level at various frequencies are depicted in Table 6.4.

Table 6.4: measured Sound power level of the unit Flair 325.

	Lw dB	Lw dB	Lw dB	Lw dB	Lw dB	Lw dB	Lwa dB(A)
	250 Hz	500 Hz	1000 Hz	2000 Hz	4000 Hz	8000 Hz	overall
160mm no silencer 325 m³/h 150 Pa	73.1	59.5	56	54.6	46.9	33.8	67
duct 160mm internal ABH 325 m³/h 150 Pa	67.2	58.5	52.8	48.5	37.8	26.1	62
Insertion Loss	5.9	1	3.2	6.1	9.1	7.7	5

In this chapter, 6 prototypes are tested and acoustic performance of each resonator and muffler are obtained. The implementation evaluation of the resonators and mufflers are discussed in the next chapter.

Chapter 7

7. Implementation evaluation and conclusion

7.1 Acoustics performance

To evaluate the acoustical performance of each resonator and muffler, the best TPM value is the insertion loss of the system. The insertion loss of each resonator and muffler is depicted in Table. 7.1:

Table 7.1: measured Insertion Loss of the noise reduction systems.

Resonator/muffler	Flowrate m3/h	Pressure difference of inlet and outlet ducts Pa	Insertion Loss dB
Helicoidal resonator	325	150	5.37
Spiral resonator	325	150	2.03
Funnel resonator	325	150	3.52
External Acoustic Black Hole muffler	325	150	9.11
Internal Acoustic Black Hole muffler	325	150	5.58

7.2 Pressure drop and energy efficiency

To define the energy efficiency for each of the noise reduction systems, pressure drop of the resonator or muffler, input power of the ventilation unit and specific power input ratio are suitable TPMs to measure. The results are written in Table. 7.2:

Table 7.2: measured energy TPMs values of the noise reduction systems.

	Flowrate m3/h	Pressure drop over unit Pa	Pressure drop over silencer Pa	Input power of the unit	Specific power input
No silencer L=0.8 m	327	152	12	75 [W]-224 [V]	0.229
co-axial duct -160-125 mm	326	153	12	75 [W]-224 [V]	0.230
Helicoidal resonator	324	153	33	79 [W]-223 [V]	0.244
Spiral resonator	326	153	24	78 [W]-225 [V]	0.240
Funnel resonator	326	152	27	78 [W]-224 [V]	0.240
External Acoustic Black Hole muffler	323	152	22	80 [W]-224 [V]	0.247
Internal Acoustic Black Hole muffler	322	153	-	76 [W]-226 [V]	0.236

7.3 Conclusion

System engineering guided the structuring of this project. Starting from the problem investigation the design process algorithm was drawn. The next step was treatment design, which involved finding analytical solutions based on solving the wave equation, followed by a knowledge-based preliminary design phase to design the proper treatments. Then, the treatments were validated by numerical simulation. The results guided us to do the next step, comprising the detail designing and development phase. The prototypes were made and tested in controlled and real environments. Finally the treatment implementations were evaluated.

The main outcome of the project is the design and production of six resonators and mufflers, i.e., three internal resonators (helicoidal, spiral, and funnel resonators) to put inside the ventilation ducts, an Acoustic Black Hole muffler that is possible to add in each 90° elbow by placing it to the T-joint, and two external/internal Acoustic Black Hole mufflers to put outside/inside the ventilation unit. It should be noted that resonators are mainly considered as a narrow band treatments while the mufflers are broadband treatments.

Generally speaking, the analytical and numerical results do match well. Also, the achieved practical eigen-frequencies are almost similar to the derived eigen-frequencies in theory and simulation while the desired performances, IL and PL, are not achieved completely. More time and tests are needed to know how these resonators should be implemented so that the desired noise reduction values will be obtained.

The stakeholder's needs and requirements are met in this project in terms of acoustical performance, space limitations, energy efficiency, and health issues which are explained in detail as follows.

> **External acoustic black hole muffler**

In terms of the space limitation, the length of the muffler is less than 1 meter (0.182 m), the outer diameter of the external muffler is 254 mm which is less than 300 mm, and the inner diameter is similar to the normal duct size of 125 mm. The insertion loss of the system is 9.1 dB which is near to the desired 10 dB. However, by combining three of these mufflers, the insertion loss will be more than 20 dB. Also by increasing the length of the muffler the transmission loss at lower frequencies can be increased. In terms of energy efficiency, this

muffler is installed surrounding the pipe and generally it does not have any pressure drop, but due to the connections needed in this model the input power of the fan is increased from 75 W to 80 W. Moreover, this treatment is a passive noise reduction technique. Possible health issues can be prevented by adding a membrane at the inner side of the muffler so that air cannot flow directly into the muffler. Hence the health issue regarding growing the bacteria inside the muffler will not happen.

> **Internal acoustic black hole muffler**

In terms of the space limitation, the muffler is fitted exactly inside the diffuser of the ventilation system (model: Flair 325). The insertion loss of the system is 5.58 dB which is more than expected in simulation, 2.3 dB. It may result from the sensitivity of the system to the pressure differences between the inlet and outlet ducts of the unit, i.e., by increasing even 1 Pa more, the noise level at the critical frequency will increase extremely. In terms of energy efficiency, this muffler is installed inside the unit and it produces more pressure drop over the unit; the input power of the fan is increased from 75 W to 76 W. In terms of health issues, this resonator is similar to the EABH muffler and it does not have any problem in this regard.

> **Helicoidal resonator**

In terms of the space limitation, it is installed inside a duct with a diameter more than 125mm and it does not have any problem, however it could be possible to incorporate it inside the unit due to the length of the resonator being less than 35 cm. The insertion loss of the system is 5.37 dB which is a good achievement for this type of the resonator, since it can only tune the noise at specific frequency (more than 1180 Hz). In terms of energy efficiency, this muffler should be installed inside the co-axial duct to not increase the pressure drop over the resonator dramatically which causes the production of more noise from the fan. In case of installation inside a co-axial duct, the input power of the unit is increased from 75 W to 79 W. Also, this treatment like the previous treatments does not have health issues.

> **Spiral resonator**

In terms of the space limitation, it is installed inside ducts, whereas the length and number of turns give more opportunity to tune the noise at desired frequencies. The insertion loss of the system is 2 dB, which means that more time is needed to find out how it should be implemented to get the desired result. It is obvious that this resonator is much more effective than a helicoidal resonator at low frequencies. In terms of energy efficiency, this muffler

should be installed inside the co-axial duct. The input power of the unit is increased from 75 W to 78 W. Also, this treatment like the previous treatments does not have health issues.

> ➢ **Funnel resonator**

In terms of the space limitation, it should be installed inside the co-axial duct. The insertion loss of the system is 3.52 dB which mainly happens at the designed frequency, 287 Hz. In terms of energy efficiency, the input power of the unit is increased from 75 W to 78 W. Moreover, this treatment like the previous treatments does not have health issues.

An additional solution could be obtained by inserting the spiral-helicoidal resonator and funnel-spiral-helicoidal resonator inside the duct, which makes it possible to absorb the noise at any desired low frequency.

7.4 Future work

For various types of the ventilation units at Brink Climate Systems, one or a combination of these developed resonators and mufflers could be the best choice due to the use limitations, advantages and disadvantages of each method. Therefore, developing an analysis and design tool to support the designer in choosing the right methodology for the problem at hand could be the next project for the near future.

By analyzing the noise spectrum of the unit (see Fig. 6.6) it can be seen that the critical frequency is between 250 to 300 Hz. One of the main reasons for high noise power level at this frequency range is a propeller flowmeter installed inside the fan shown in Fig. 7.1. The fan optimization was not considered in this project, but it could be considered to change this type of flowmeter with another one. For instance, a new invented acoustical flowmeter or ultrasonic flowmeter could be good solutions in this respect.

A propeller flowmeter
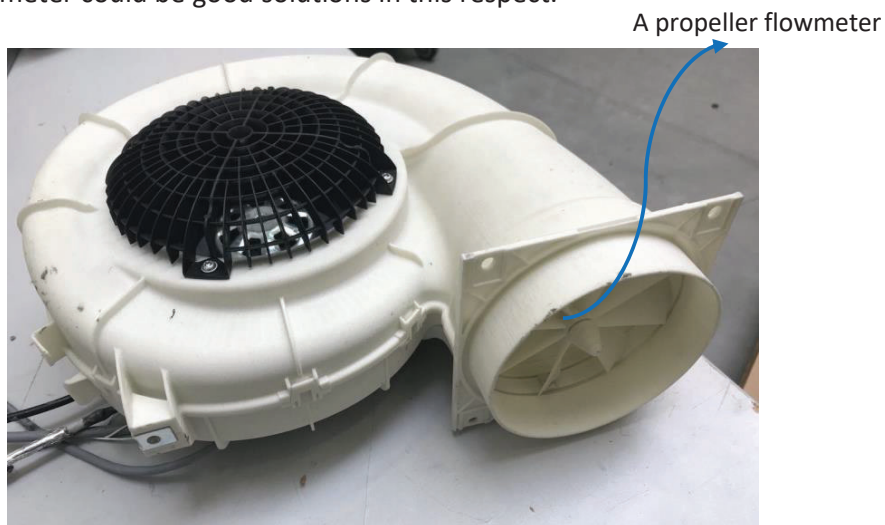
Figure 7.1: The fan of the ventilation unit with a propeller flowmeter inside.

To get good correlation between analytical, numerical, and practical results, it is needed to consider more parameters in equations and simulations. Somehow, the simulated models become more similar to the system in the real environment. Analyzing this type of the complicated models takes more time and energy, so it could be another future topic.

Finally, an improvement of each of the mentioned resonators and mufflers could be undertaken to get still better acoustical performance and energy efficiency.

Appendix A.

- The pressure gradient in cylindrical coordinate could be written as:

$$\nabla \vec{P} = \frac{\partial R}{\partial r}\vec{e}_r + \frac{1}{r}\frac{\partial \Phi}{\partial \varphi}\vec{e}_\varphi + \frac{\partial Z}{\partial z}\vec{e}_z \quad , \vec{e}_r = \begin{pmatrix} \cos(\varphi) \\ \sin(\varphi) \\ 0 \end{pmatrix}, \vec{e}_\varphi = \begin{pmatrix} -\sin(\varphi) \\ \cos(\varphi) \\ 0 \end{pmatrix}, \vec{e}_z = \begin{pmatrix} 0 \\ 0 \\ 1 \end{pmatrix}$$

$$\Rightarrow \nabla \vec{P} = \begin{pmatrix} \dfrac{\partial R}{\partial r}\cos(\varphi) - \dfrac{1}{r}\dfrac{\partial \Phi}{\partial \varphi}\sin(\varphi) \\ \dfrac{\partial R}{\partial r}\sin(\varphi) + \dfrac{1}{r}\dfrac{\partial \Phi}{\partial \varphi}\cos(\varphi) \\ \dfrac{\partial Z}{\partial z} \end{pmatrix}$$. (a.1)

The helicoid surface could be expressed:

$$Helicoid\ Surface = \begin{pmatrix} r\cos(\dfrac{2\pi}{L}z) \\ r\sin(\dfrac{2\pi}{L}z) \\ z \end{pmatrix} \quad , \varphi = \frac{2\pi}{L}z \ .$$ (a.2)

To find the normal vector of the surface, the derivation with respect to the *r* and *z* is needed:

$$\vec{S}_r = \begin{pmatrix} \cos(\dfrac{2\pi}{L}z) \\ \sin(\dfrac{2\pi}{L}z) \\ 0 \end{pmatrix}, \vec{S}_z = \begin{pmatrix} -\dfrac{2\pi r}{L}\sin(\dfrac{2\pi}{L}z) \\ \dfrac{2\pi r}{L}\cos(\dfrac{2\pi}{L}z) \\ 1 \end{pmatrix}.$$ (a.3)

The normal vector of the surface could be found by the cross product of the above vectors:

$$\hat{n} = \vec{S}_r \times \vec{S}_z = \begin{pmatrix} \sin(\dfrac{2\pi}{L}z) \\ -\cos(\dfrac{2\pi}{L}z) \\ \dfrac{2\pi r}{L} \end{pmatrix}.$$ (a.4)

- Function and normal vector of the spiral surface could be expressed:

$$Spiral\ Surface = \begin{pmatrix} \dfrac{r_2\varphi}{2n\pi}\cos(\varphi) \\ \dfrac{r_2\varphi}{2n\pi}\sin(\varphi) \\ z \end{pmatrix} \vec{S}_\varphi = \begin{pmatrix} \dfrac{r_2}{2n\pi}\cos(\varphi) - \dfrac{r_2\varphi}{2n\pi}\sin(\varphi) \\ \dfrac{r_2}{2n\pi}\sin(\varphi) + \dfrac{r_2\varphi}{2n\pi}\cos(\varphi) \\ 0 \end{pmatrix}, \vec{S}_z = \begin{pmatrix} 0 \\ 0 \\ 1 \end{pmatrix}$$

$$\hat{n} = \vec{S}_\varphi \times \vec{S}_z = \begin{pmatrix} \dfrac{r_2}{2n\pi}\sin(\varphi) + \dfrac{r_2\varphi}{2n\pi}\cos(\varphi) \\ -\dfrac{r_2}{2n\pi}\cos(\varphi) + \dfrac{r_2\varphi}{2n\pi}\sin(\varphi) \\ 0 \end{pmatrix}$$

. (a.5)

- For the regions, 2 and 3, in spiral resonator (see Fig. 3.8) we have:

$$\begin{cases} A_{m1}J'_m(k_r r_1) = [A_{m2}J'_m(k_r r_1) + B_{m2}Y'_m(k_r r_1)] \\ r_1\varphi_1 A_{m1}J'_m(k_r r_1) = r_2\varphi_2[A_{m2}J'_m(k_r r_2) + B_{m2}Y'_m(k_r r_2)] \end{cases} \Rightarrow$$

$$\begin{cases} A_{m2}(r) = A_{m1}(r) * [\dfrac{r_1\varphi_1 J'_m(k_r r_1)}{r_2\varphi_2 J'_m(k_r r_2)} - \dfrac{J'_m(k_r r_1)}{Y'_m(k_r r_1)}\dfrac{Y'_m(k_r r_2)}{J'_m(k_r r_2)}]/[1 - \dfrac{J'_m(k_r r_1)}{Y'_m(k_r r_1)}\dfrac{Y'_m(k_r r_2)}{J'_m(k_r r_2)}] \\ B_{m2}(r) = [A_{m1}(r) - A_{m2}(r)] * \dfrac{J'_m(k_r r_1)}{Y'_m(k_r r_1)} \end{cases}$$ (a.6)

For the last region, Re. 4, unknown parameters will be derived as:

$$\begin{cases} r_1\varphi_1 A_{m1}J'_m(k_r r_1) = r_2\varphi_2[A_{m3}J'_m(k_r r_2) + B_{m3}Y'_m(k_r r_2)] \\ A_{m3}J'_m(k_r r_3) + B_{m3}Y'_m(k_r r_3) = 0 \end{cases} \Rightarrow$$

$$\begin{cases} A_{m3}(r) = A_{m1}(r) * [\dfrac{r_1\varphi_1}{r_2\varphi_2}J'_m(k_r r_1)]/[J'_m(k_r r_2) - \dfrac{J'_m(k_r r_3)}{Y'_m(k_r r_3)}Y'_m(k_r r_2)] \\ B_{m3}(r) = -A_{m3}(r) * \dfrac{J'_m(k_r r_3)}{Y'_m(k_r r_3)} \end{cases}$$ (a.7)

- The funnel surface can be expressed:

$$Funnel\ Surface = \begin{pmatrix} (r_1 + \dfrac{r_2 - r_1}{L}z)\cos(\varphi) \\ (r_1 + \dfrac{r_2 - r_1}{L}z)\sin(\varphi) \\ z \end{pmatrix}.$$ (a.8)

To find the normal vector of the funnel surface, the derivation respect to the *r* and *z* is needed:

$$\vec{S}_\phi = \begin{pmatrix} -(r_1 + \dfrac{r_2 - r_1}{L}z)\sin(\phi) \\[2mm] (r_1 + \dfrac{r_2 - r_1}{L}z)\cos(\phi) \\[2mm] 0 \end{pmatrix}, \vec{S}_f = \begin{pmatrix} \dfrac{r_2 - r_1}{L}\mathrm{Cos}(\phi) \\[2mm] \dfrac{r_2 - r_1}{L}\mathrm{Sin}(\phi) \\[2mm] 1 \end{pmatrix} * \dfrac{L}{r_2 - r_1}.$$ (a.9)

The normal vector of the surface can be found by the cross product of the above vectors:

$$\hat{n} = \vec{S}_\phi \times \vec{S}_z = \begin{pmatrix} (\dfrac{L}{r_2 - r_1}r_1 + z)\cos(\phi) \\[2mm] (\dfrac{L}{r_2 - r_1}r_1 + z)\sin(\phi) \\[2mm] -(\dfrac{L}{r_2 - r_1}r_1 + z) \end{pmatrix}.$$ (a.10)

- The approximate of the first and second kinds of Bessel functions are:

$$J_m(x) = \begin{cases} \displaystyle\sum_{l=0}^{\infty} \dfrac{(-1)^l}{2^{2l+|m|}\, l!\,(|m|+l)!}\, x^{2l+|m|} & \text{for } |m| \neq \frac{1}{2} \\[4mm] \sqrt{\dfrac{2}{\pi x}}\cos x & \text{for } m = -\frac{1}{2} \\[4mm] \sqrt{\dfrac{2}{\pi x}}\sin x & \text{for } m = \frac{1}{2}. \end{cases}$$

$$Y_m(x) \sim \begin{cases} \dfrac{2}{\pi}\left[\ln\left(\frac{1}{2}x\right) + \gamma\right] & m = 0,\, x \ll 1 \\[4mm] -\dfrac{\Gamma(m)}{\pi}\left(\dfrac{2}{x}\right)^m & m \neq 0,\, x \ll 1 \end{cases}$$

$$Y_m(x) \sim \sqrt{\dfrac{2}{\pi x}}\sin\left(x - \dfrac{m\pi}{2} - \dfrac{\pi}{4}\right) \quad x \gg 1,$$ (a.11)

Based on the approximate of the first and second kinds of Bessel functions, the Taylor's expansions for $m = 0$ are:

$$J_0(x) = 1 - \dfrac{1}{2^2}x^2 + \dfrac{1}{2^4(2!)^2}x^4 - \ldots$$

$$J_0'(x) = -\dfrac{2}{2^2}x + \dfrac{4}{2^4(2!)^2}x^3 - \ldots$$

$$Y_0(x) = \begin{cases} \dfrac{2}{\pi}[Ln(\dfrac{x}{2}) + 0.57721] & x \ll 1 \\[4mm] \sqrt{\dfrac{2}{\pi x}}\,Sin(x - \dfrac{\pi}{4}) & x \gg 1 \end{cases}.$$ (a.12)

$$Y_0'(x) = \begin{cases} \dfrac{1}{x\pi} & x \ll 1 \\[4mm] \sqrt{\dfrac{2}{\pi x}}\,Cos(x - \dfrac{\pi}{4}) - \sqrt{\dfrac{2}{\pi}}\dfrac{1}{2x^{1.5}}Sin(x - \dfrac{\pi}{4}) & x \gg 1 \end{cases}$$

References

[1]   Brink, "About Brink," 2018. [Online]. Available:

        https://www.brinkclimatesystems.nl/en-us/international/home.

[2]   R. Wieringa, *Design Science Methodology for Information Systems and Software Engineering*. 2014.

[3]   K. Visscher and J. I. A. Visscher-Voerman, "Organizational design approaches in management consulting," *Manag. Decis.*, vol. 48, no. 5, pp. 713–731, 2010.

[4]   M. Kojourimanesh, "Literature Study for PDEng- Noise reduction for ventilation systems with heat exchangers," 2016.

[5]   G. M. Bonnema, T. Veenvliet, and J. F. Broenink, *systems design and engineering*. 2013.

[6]   Brink, *Installation & Regulations of Flair 325*. 2017.

[7]   W. O. Schotborgh, C. Mcmahon, and F. J. A. M. Van Houten, "A knowledge acquisition method to model parametric engineering design processes," vol. 4, 2012.

[8]   J. M. J. Becker and W. W. Wits, "A Template for Design for eXcellence (DfX) Methods," *Smart Prod. Eng.*, vol. 5, pp. 33–42, 2013.

[9]   W. Lapka, "Numerical study of acoustic-structure interaction of selected helicoidal resonator with flexible helicoidal profile," 2016.

[10]   M. Schroeder, *Springer Handbook of Acoustics*. 2007.

[11]   L. E. Kinsler, A. R. Frey, A. . Coppens, and J. V. Sanders, *Fundamentals of Acoustics*. New York: John Wiley &Sons, Inc, 2000.

[12]   *ISO 3741: Preview Acoustics -- Determination of sound power levels and sound energy levels of noise sources using sound pressure -- Precision methods for reverberation test rooms*. 2010.

[13]   M. L. Munjal, *Acoustics of Ducts and Mufflers*. John Wiley &Sons, Inc, 1987.

[14]   S. Errede, "Mathematical Musical Physics of the Wave Equation – Part 2," pp. 1–26, 2017.

[15]   F. Jacobsen, "Propagation of sound waves in ducts," *Lect. notes*, no. 31260, p. 71, 2011.

[16]   Comsol, "Comsol Multiphysics," *User Guid.*, pp. 630–645, 2012.

[17]   A. Bayliss, M. Gunzburger, and E. Turkel, "Boundary Conditions for the Numerical Solution of Elliptic Equations in Exterior Regions," *SIAM J. Appl. Math.*, vol. 42, no. 2, pp. 430–451, 1982.

[18]   D. Givoli and B. Neta, "High-order non-reflecting boundary scheme for time-dependent waves," *J. Comput. Phys.*, vol. 186, no. 1, pp. 24–26, 2003.

[19]   M. A. Mironov and V. V Pislyakov, " One-Dimensional Acoustic Waves in Retarding Structures with Propagation Velocity Tending to Zero," *Acoustical Physics,* vol. 48, no. 3, pp. 347–352, 2002.

[20] S. Marburg and H. J. Hardtke, "Study on the acoustic boundary admittance. Determination, results and consequences," *Eng. Anal. Bound. Elem.*, vol. 23, no. 9, pp. 737–744, 1999.

[21] A. T. Moorhouse, "Analysis of Low Frequency Muffler based on ' Acoustic Black Hole Effect,'" no. September, 2016.

[22] W. Lapka, "Acoustic attenuation performance of selected helicoidal resonators lined with an absorbent materials of different thickness and density," *Arch. Acoust.*, vol. 32, no. 4, pp. 247–252, 2007.